12 p.

2061278
Columbia University in the City of New York
@ Lamont Geological Observatory
Palisades, New York

T Nondestructive Neutron-Activation Analysis of Small Particles

T@ Six-month Status Report, March, 1963 - August, 1963

(NASA Grant NsG-232-62)

Research on Quantities and Concentrations of Extra-terrestrial Matter through Samplings of Ocean Bottoms.

Principal Investigator: W. A. Cassidy

[1963] 121 p refs

Nondestructive Neutron-Activation Analysis of Small Particles

W. A. Cassidy
Lamont Geological Observatory
of Columbia University

Introduction

An intensive program for the collection of a large number of natural magnetic spherules has been in progress at Lamont Geological Observatory for about two years. The collection now consists of over one thousand spherules varying in size from 50-650 μ in diameter. The source of spherules has been "flow-in" samples from Lamont's ocean-bottom core library. Flow-in material is that section of the core that has flowed into the sampler after it has stopped its descent. After being driven into the ocean floor as far as it will go, the sampler is extracted by a cable attached to a piston inside the core tube. At the moment the core tube stops its descent the piston is at the sediment-water interface. It must be pulled to the top of the core tube before it can pull the tube free of the ocean floor, and in rising up the tube it draws the whole core sample after it. The disturbed material sucked into the bottom of the core tube during this process is the flow-in mud. This mud has the great advantage that it is known to

come from well below the modern ocean floor and, except for the small chance of contamination by spherules carried d down by the coring tube, can be assumed to be free of modern technological contamination. Any spherules found in this flow-in sample are assumed to be natural in origin. The spherules considered in this paper are of four types: (1) undoubted natural spherules, (2) spherules of unknown origin collected in plankton nets, (3) spherules from smoke and soot, and (4) welding beads. All except three or four individuals are magnetic. The nonmagnetic ones are undoubted natural spherules collected over a period of years by D. Ericson, of Lamont Geological Observatory, while making micropaleontological studies on ocean cores. Fig. 1 shows a group of undoubted natural spherules collected from flow-in samples derived from well below the modern ocean floor. Fig. 2 shows a group of spherules of unknown origin collected at the ocean surface in plankton nets. Fig. 3 shows a group of spherules found in soot from the smoke-stack of the Lamont Geological Observatory's research vessel, VEMA. Fig. 4 shows a group of welding beads picked up with a magnet in the Lamont Geological Observatory welding shop.

The work reported here describes procedures and results in the nondestructive neutron-activation analysis of the four types of particles listed above.

Fig. 1

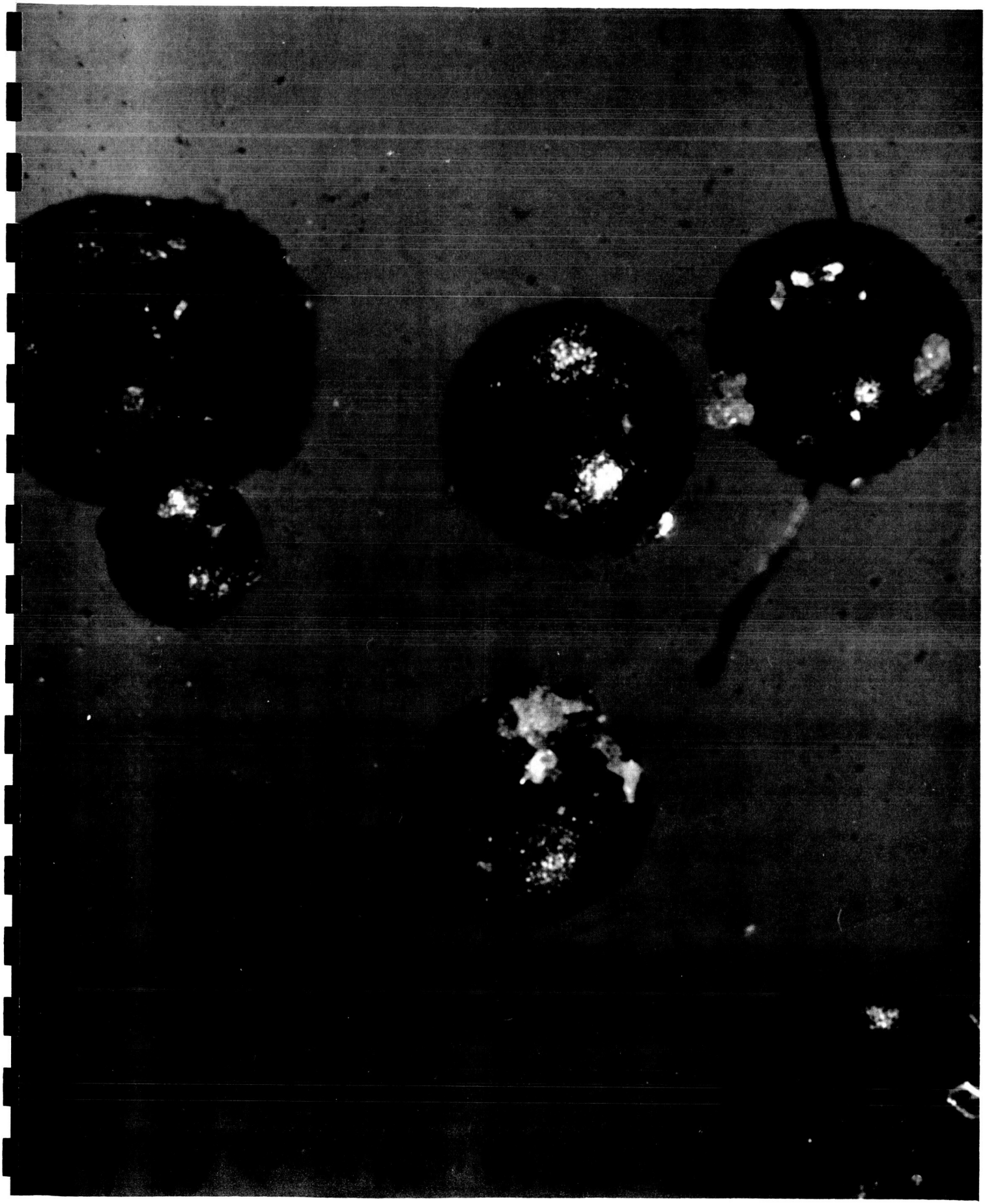

Fig. 2

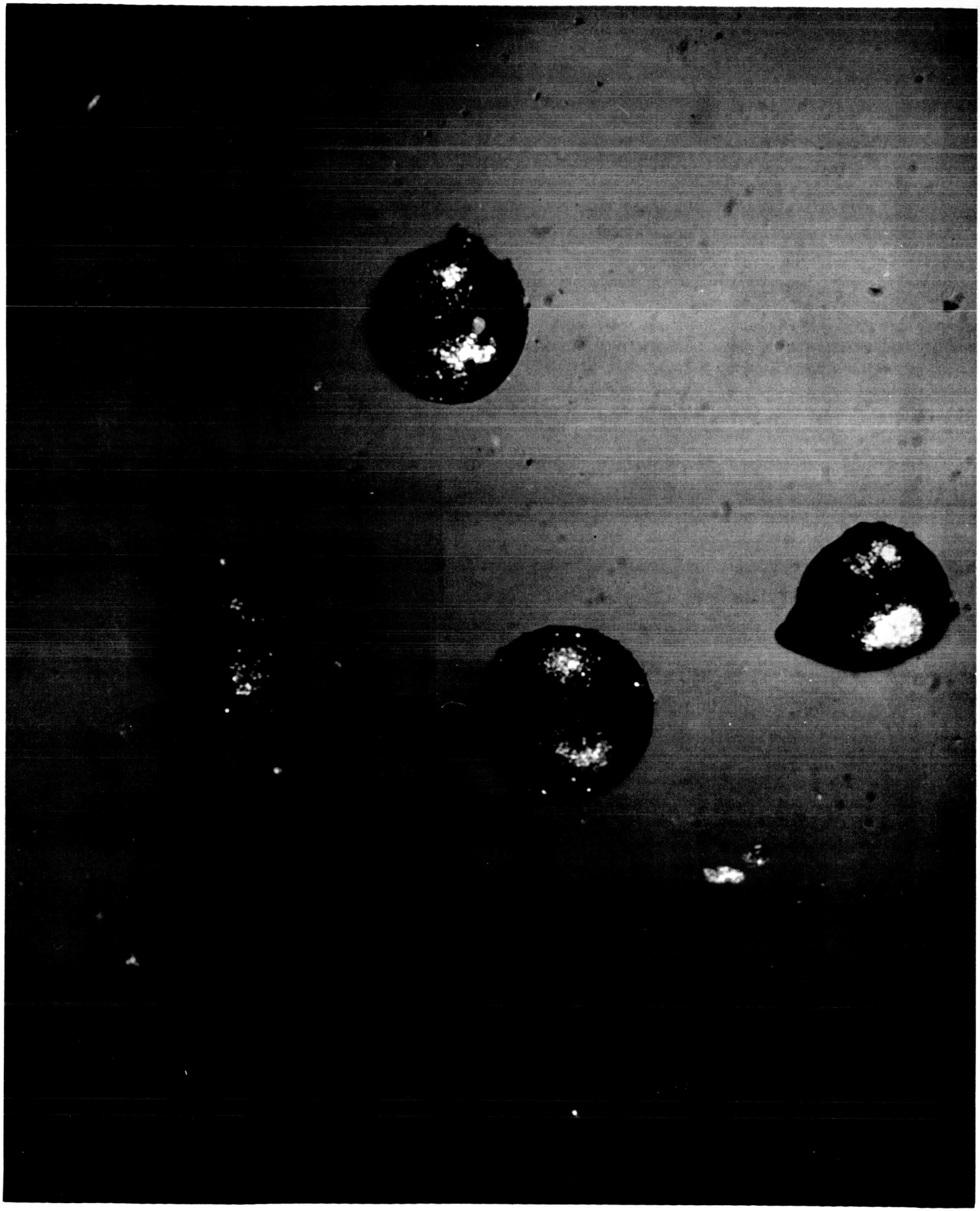

Fig. 3

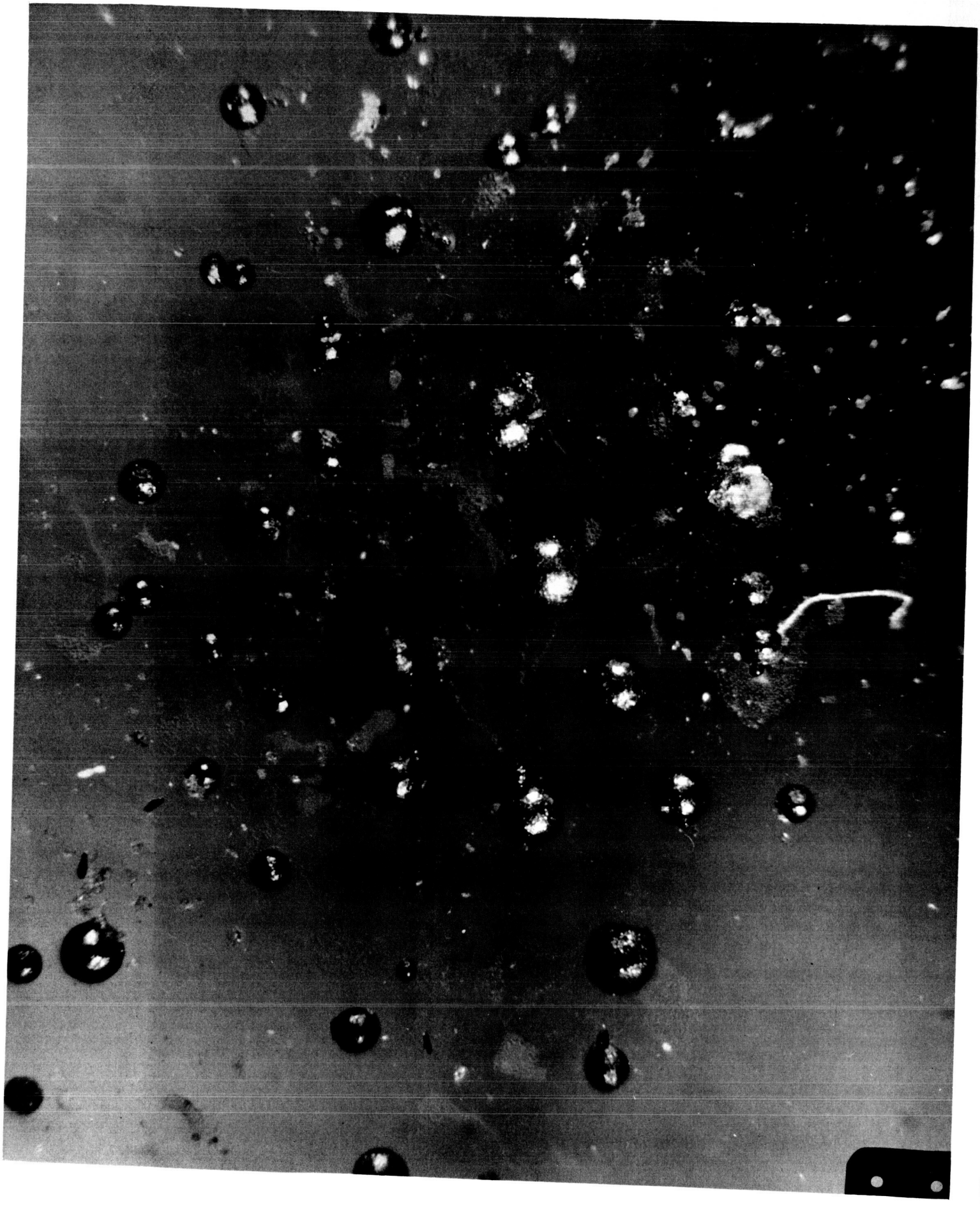

Fig. 4

The Problem

Because of the production of vast quantitites of microscopic spherules in industrial and technological processes, it is important to be able to tell the difference between natural spherules and artificial spherules. In many cases, contemporary collections of microscopic spherules can be contaminated by artificial products, and data based on these collections will be misleading. It is desired, therefore, to try to establish a method by which a microscopic spherule is known to be artificial or natural in origin. The method must be nondestructive if further data are required from those spherules that prove to be natural. The first problem considered, then, was whether nondestructive neutron-activation analysis could be used to establish criteria for the natural or artificial origin of a given microscopic spherul

When the natural origin of a spherule has been establishe it will be of great interest to get metallographic, petrographic, and chemical data on its composition. If there are any nondestructive methods of obtaining this information, they should be used first. Therefore, the second problem considered was whether useful compositional data could be obtained by nondestructive neutron-activation analysis of natural spherules.

Experimental Procedures

Facilities of the Industrial Reactor Laboratories, Plainsboro, New Jersey, were used for this work. The reactor is a swimming-pool type, with quick access to the core by means of beam tubes, vertical tubes, pneumatic tubes, and thermal column. Maximum available neutron-flux density is around 10^{14} $n/cm^2/sec$ in the core. The pneumatic tube facility, which was used almost exclusively in this study, provides a maximum flux of 10^{13} thermal $n/cm^2/sec$ and 2×10^{12} fast $n/cm^2/sec$.

The spherule to be irradiated was first inserted into a gelatin capsule. The capsule was then mounted inside a 1 x 7.5 cm polyethylene tube, which was mounted inside a polyethylene pneumatic-tube messenger capsule, called a rabbit.

To carry out the irradiation the rabbit was inserted into the pneumatic tube at the outside face of the swimming pool. It was carried to a position next to the reactor core for a 10-second or 30-second interval, then returned to the reactor face. The radiation level of the rabbit was checked by a health-physics employee as shown in Fig. 5, and if found to be safe the rabbit was opened as shown in Fig. 6. The gelatin capsule containing the spherule was removed and carried to the low-level counting room. There,

Fig. 5

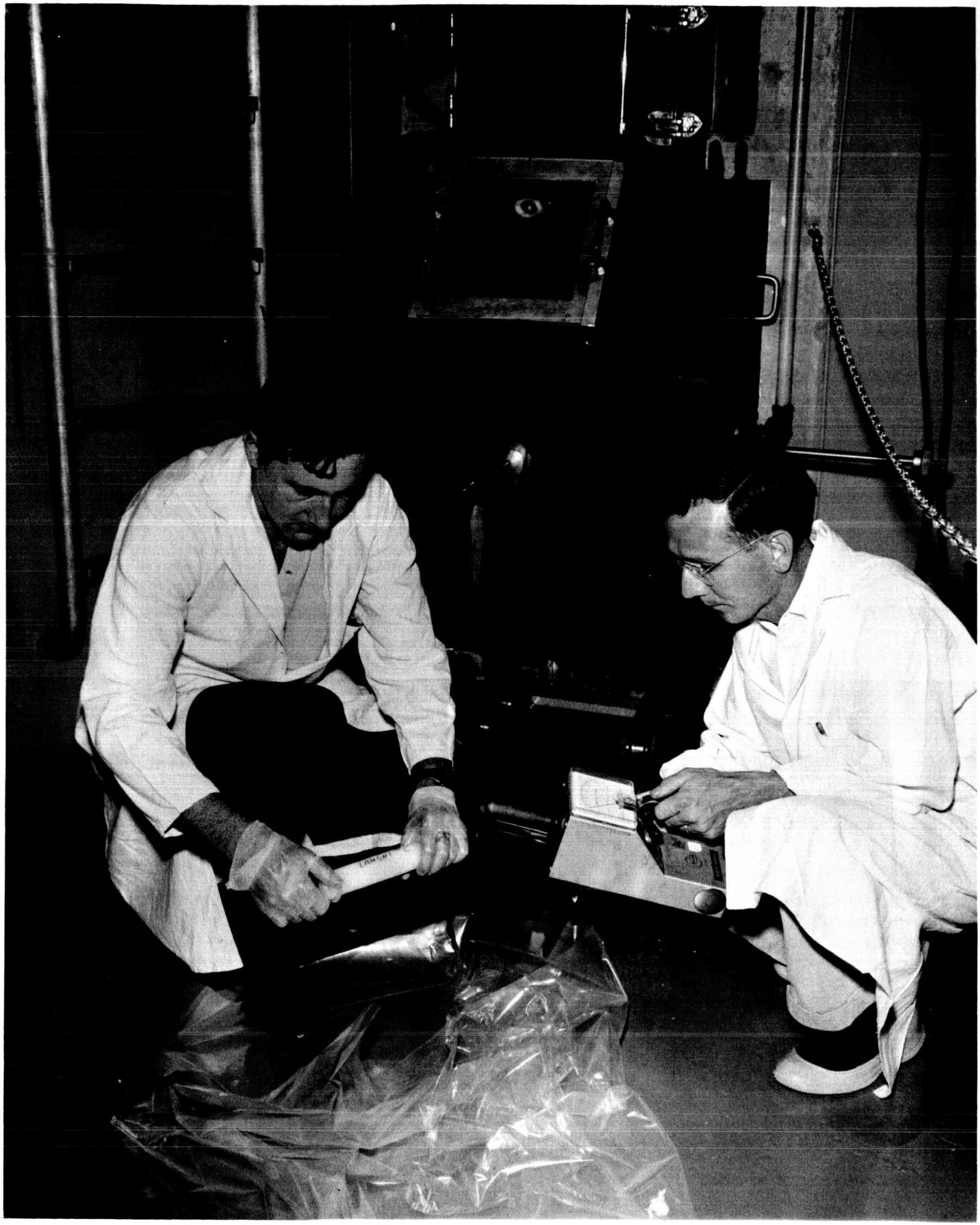

Fig. 6

using a binocular microscope, the spherule was transferred to an unirradiated gelatin capsule as shown in Fig. 7. It was then ready to count. The whole procedure from the end of irradiation to beginning of counting took from four to eight minutes, so in most cases it was possible to study the decay of Al^{28}, with a 2.4 minute half-life, as well as unstable nuclides with longer half-lives. The reactions found to be important in this study are shown in Table I.

Examination of Table I discloses some of the problems encountered in this type of study. For example, Al^{27} and Si^{28} can produce the same daughter, Al^{28}, if the neutron flux has a wide energy spectrum. There are two ways to avoid this difficulty. One is by using the second Al^{27} reaction. This produces Mg^{27} which decays with a different $t_{1/2}$ and ~~units~~ emits gamma-radiation of different energies. Unfortunately the major peak from Mg^{27} is coincident with the major peak from Mn^{56}, and the reaction $Mg^{26}(n,\gamma)Mg^{27}$ also interferes. The other way around the difficulty is to screen out the thermal neutron radiation from the core by surrounding the sample with Cd metal, 0.030" of which will cut the thermal flux by about 10^3. Two irradiations are then necessary: one with 0.060" of Cd shielding, to cut the thermal-neutron flux by 10^6, and one with no shielding. The first allows only the $Si^{28}(n,p)Al^{28}$ reaction, while the second allows

Table I[1]

Nuclear Reactions Pertinent To This Study

No.	Isotope Reaction	σ (barns) Thermal	14 Mev[2]	$t_{1/2}$	Abundance of Stable Isotope	Gamma Decay (Mev)
1.	$Al^{27}(n,\gamma)Al^{28}$	0.23		2.4m	1.0	1.78
2.	$Al^{27}(n,p)Mg^{27}$	2.8×10^{-3}	0.07	10.2m	1.0	0.84, 1.02
3.	$Fe^{56}(n,p)Mn^{56}$	0.44×10^{-3}	0.11	2.58h	0.916	0.845, 1.81, 2.13
4.	$Mg^{26}(n,\gamma)Mg^{27}$	0.027		10.2m	0.1129	0.84, 1.02
5.	$Mg^{24}(n,p)Na^{24}$	1.0×10^{-3}	0.19	15.0h	0.786	1.37, 2.75
6.	$Na^{23}(n,\gamma)Na^{24}$	0.53		15.0h	1.0	1.37, 2.75
7.	$Si^{28}(n,p)Al^{28}$	4×10^{-3}	0.22	2.4m	0.9218	1.78
8.	$V^{51}(n,\gamma)V^{52}$	5.1		3.76	0.997	1.44

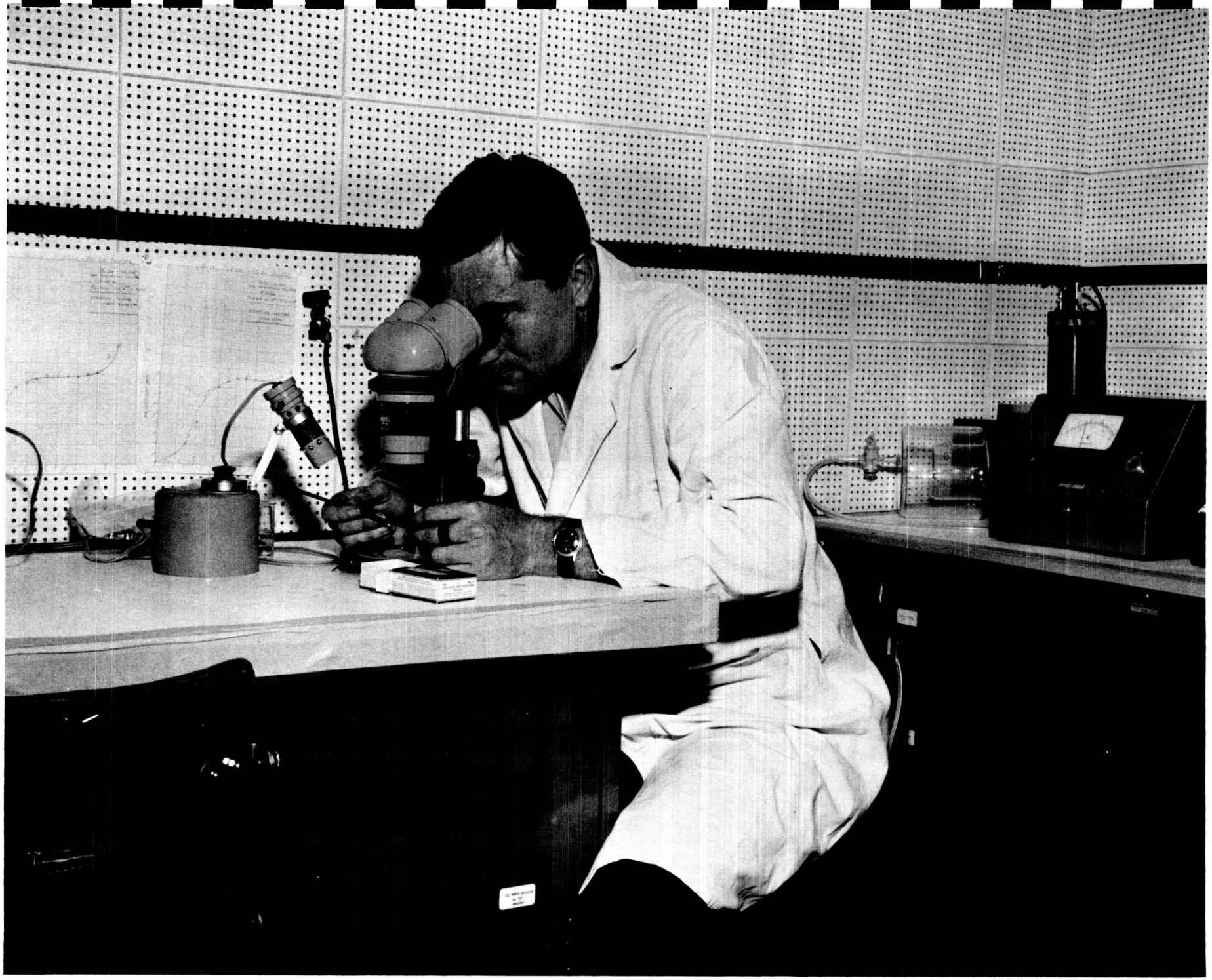

Fig. 7

both. After calibration against standards of known composition, the amount of Si^{28} becomes known and is used to calculate the amount of Al^{27} by discounting an appropriate fraction of the unshielded Al^{28} peak.

The RIDL 400-channel analyser used in this work was equipped with a typewriter print-out. The data were recorded using one hundred channels during a one-minute counting period. Printing-out took one minute and twenty-two seconds, so a new one-minute count was begun every two minutes and twenty-two seconds. Accumulation of one-minute counts during the first twenty to thirty minutes after irradiat can show the decay of short-lived daughter neuclides such as Al^{28}, if present, and may allow identification by means of their half-lives.

Results

Figures 8 through 78 are a compilation of results in the form of a catalogue of spherule spectra and associated decay curves. All spherules were irradiated in the rabbit tube facility for ten or thirty seconds, then counted periodically during decay of induced radiation. In most cases only one spectrum, out of the many recorded, is given for each specimen. This spectrum is that one that best shows the features by means of which it is hoped to assign the specimen to the natural or artificial categories. Eight spectra are given of one green, transparent natural spherule.

Fig. 9 Natural spherule NS 1. Very shiny, black, non-magnetic spherule 180μ diam. from Lamont core A 167-1. 30 sec irrad'n, one-minute count. Δt = 5m 20s.

No identifiable peaks. Very low count indicates spherule is hollow.

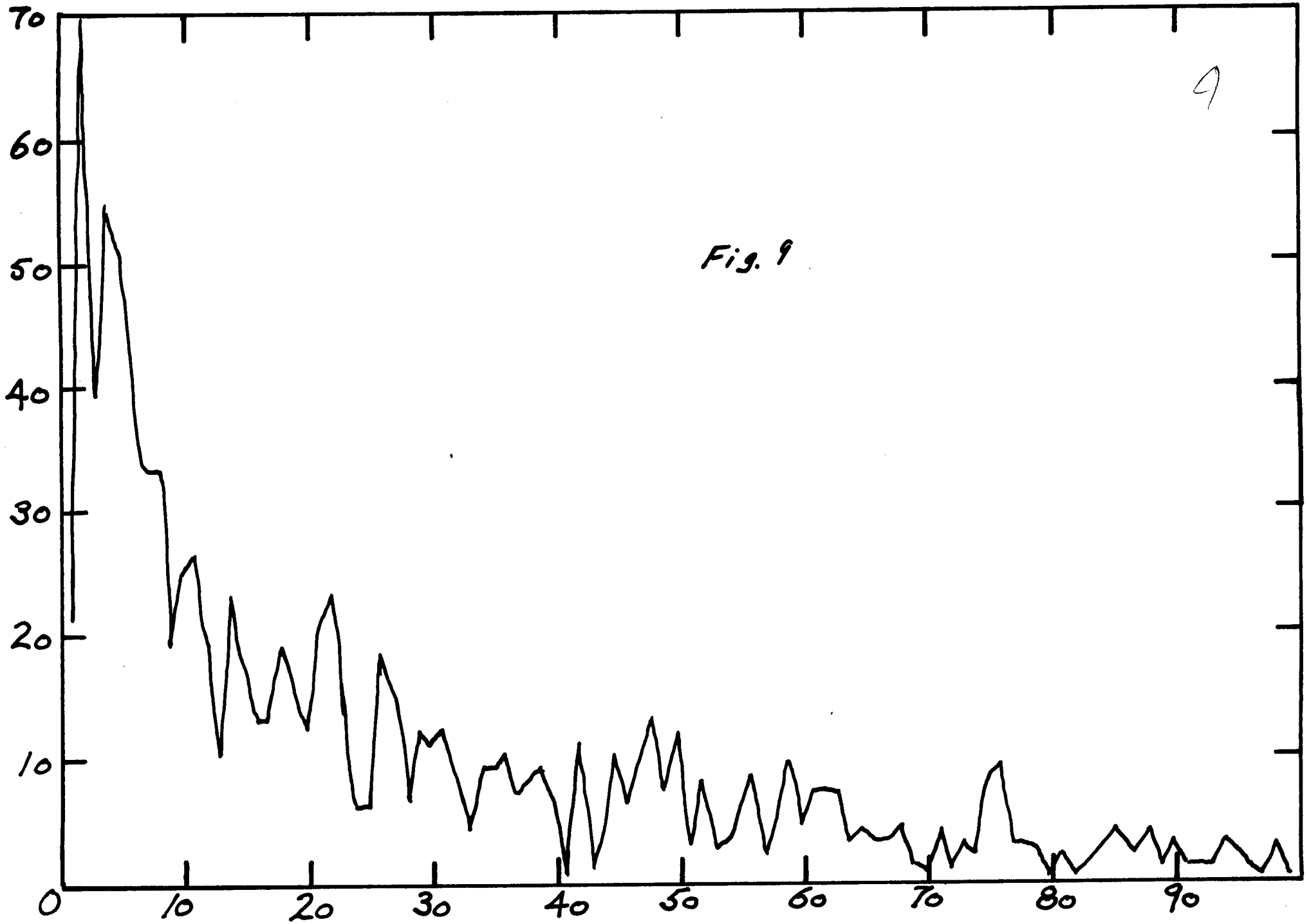

Fig. 9

Fig. 10 Natural spherule NS 2. Black magnetic spherule 100μ diam. from Lamont core V 16-30. 10-sec irradiation, one-minute count. Δt=5m20s. No identifiable peaks with possible exception of 0.84 Mev Mn^{56} at channel 28.

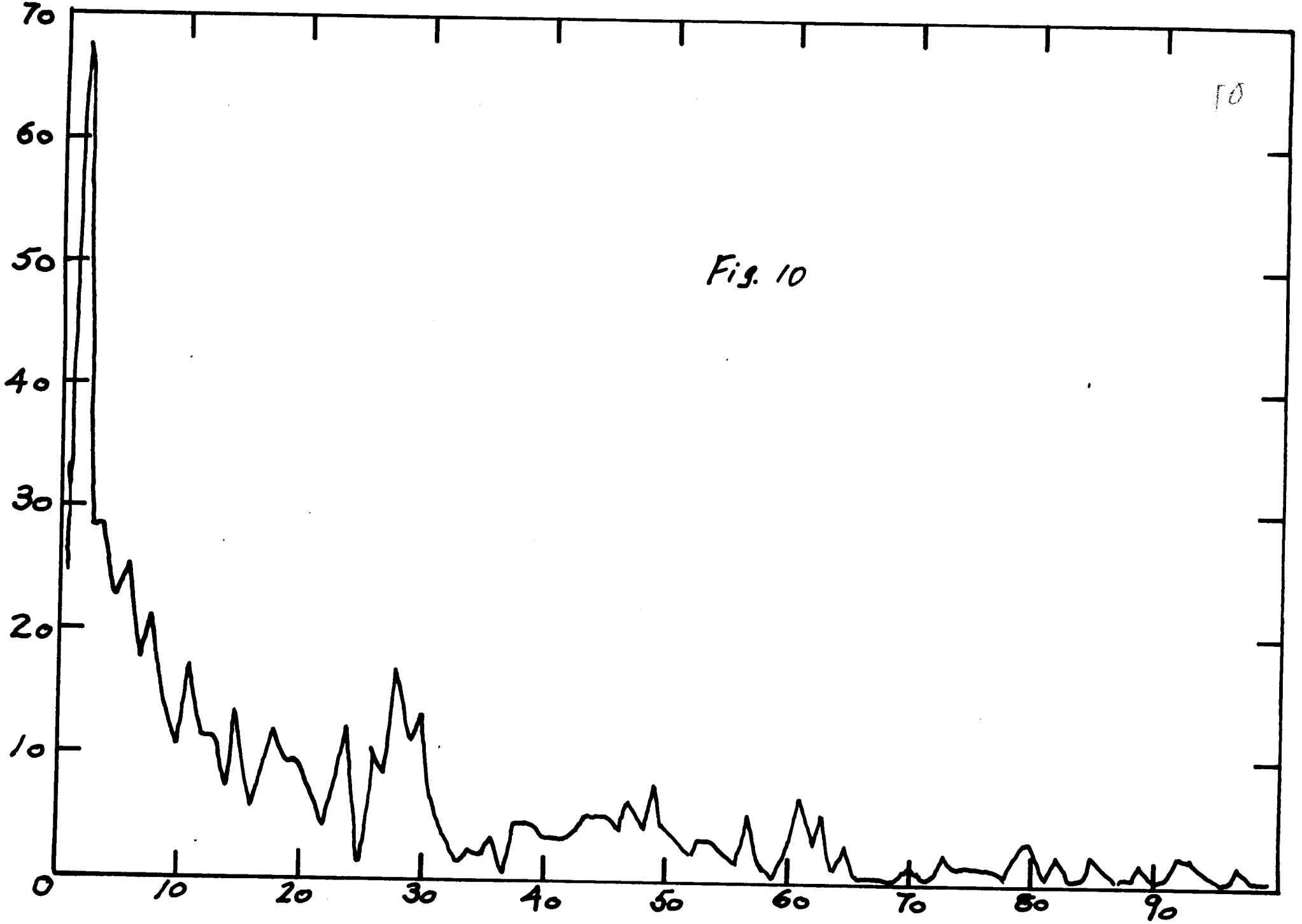

Fig. 10

Fig. 11 Natural spherule NS 3. Black, magnetic spherule 150μ diam. from Lamont core V 16-30. 30 sec. irradiation, one-minute count. $_{\Delta}t$=4m53s. Peaks at 0.52 Mev channel 17 (annihilation); 0.84 Mev channel 30 (Mn^{56}); 144 Mev channel 49 (V^{52}); 1.78 Mev channel 61 (Al^{28} or Mn^{56}).

Fig. 12 NS 3 decay curve, Mn^{56}

Fig. 13 NS 3 decay curve, V^{52}

Fig. 14 NS 3 decay curve, Al^{28}

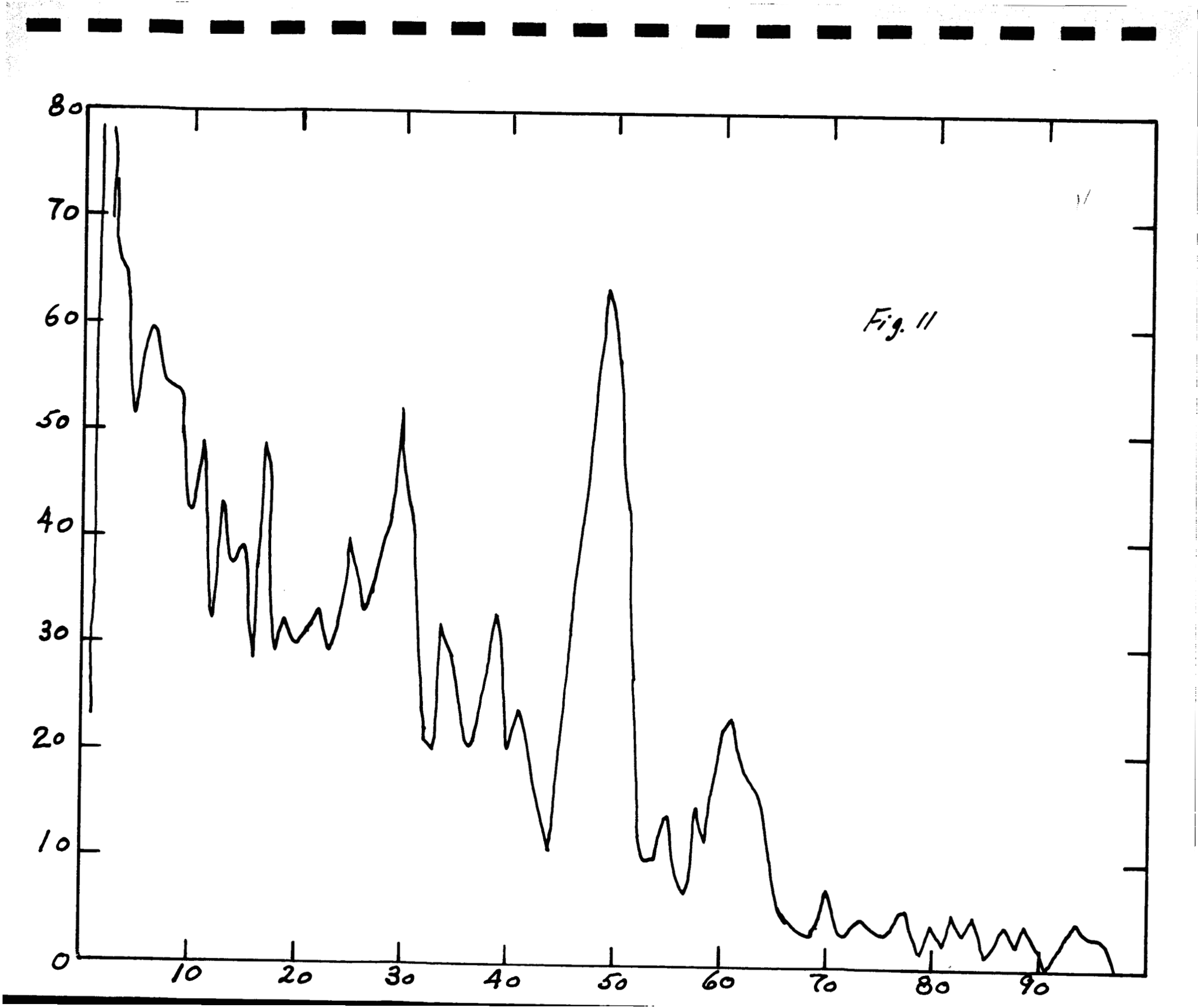

Fig. 11

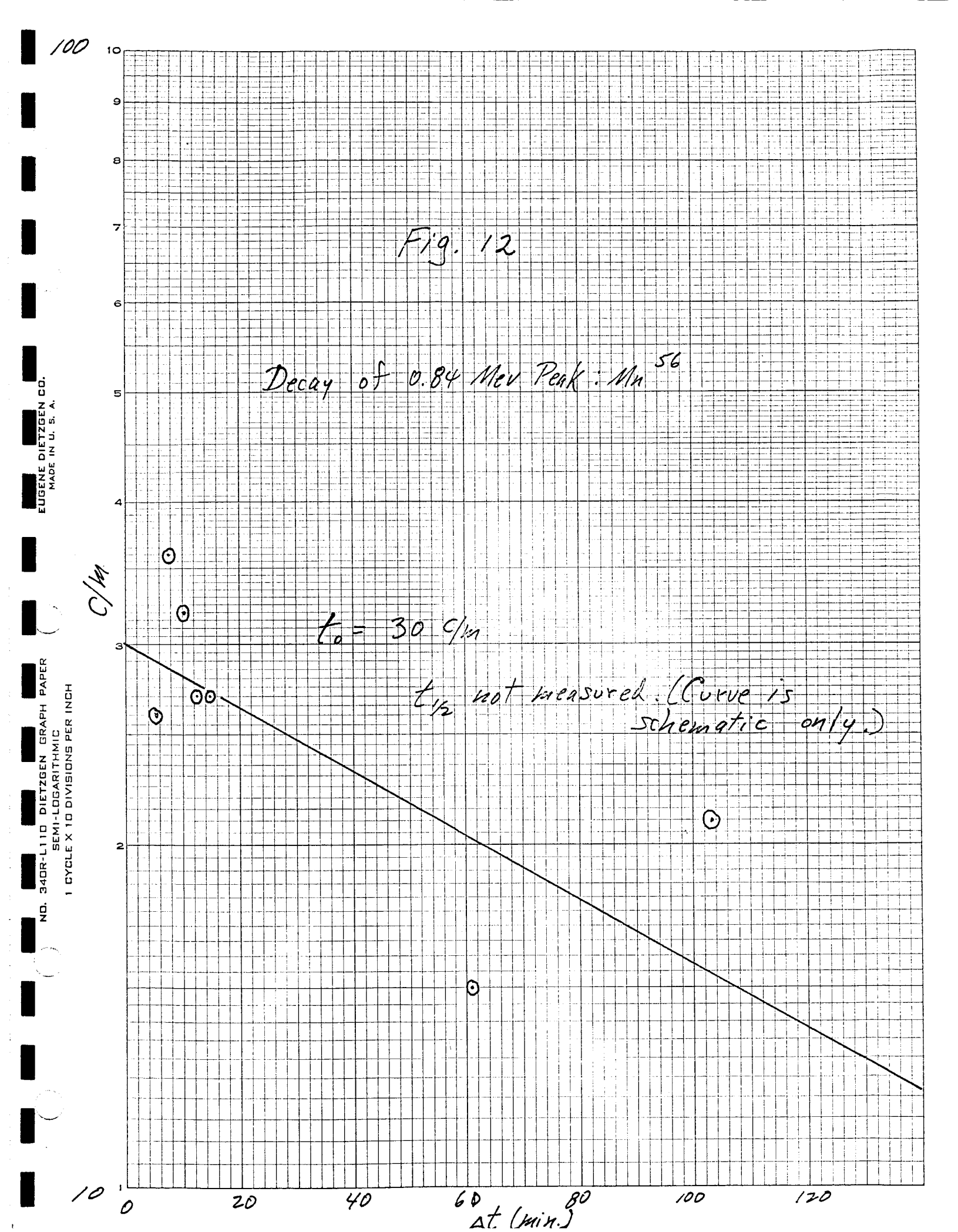
100
10
9
8
7
6
5
4
3
2
1
C/m
Fig. 12
Decay of 0.84 Mev Peak : Mn^{56}
t_o = 30 c/m
$t_{1/2}$ not measured. (Curve is schematic only.)
0
20
40
60
80
100
120
Δt (min.)
EUGENE DIETZGEN CO.
MADE IN U. S. A.
NO. 340R-L11D DIETZGEN GRAPH PAPER
SEMI-LOGARITHMIC
1 CYCLE X 10 DIVISIONS PER INCH

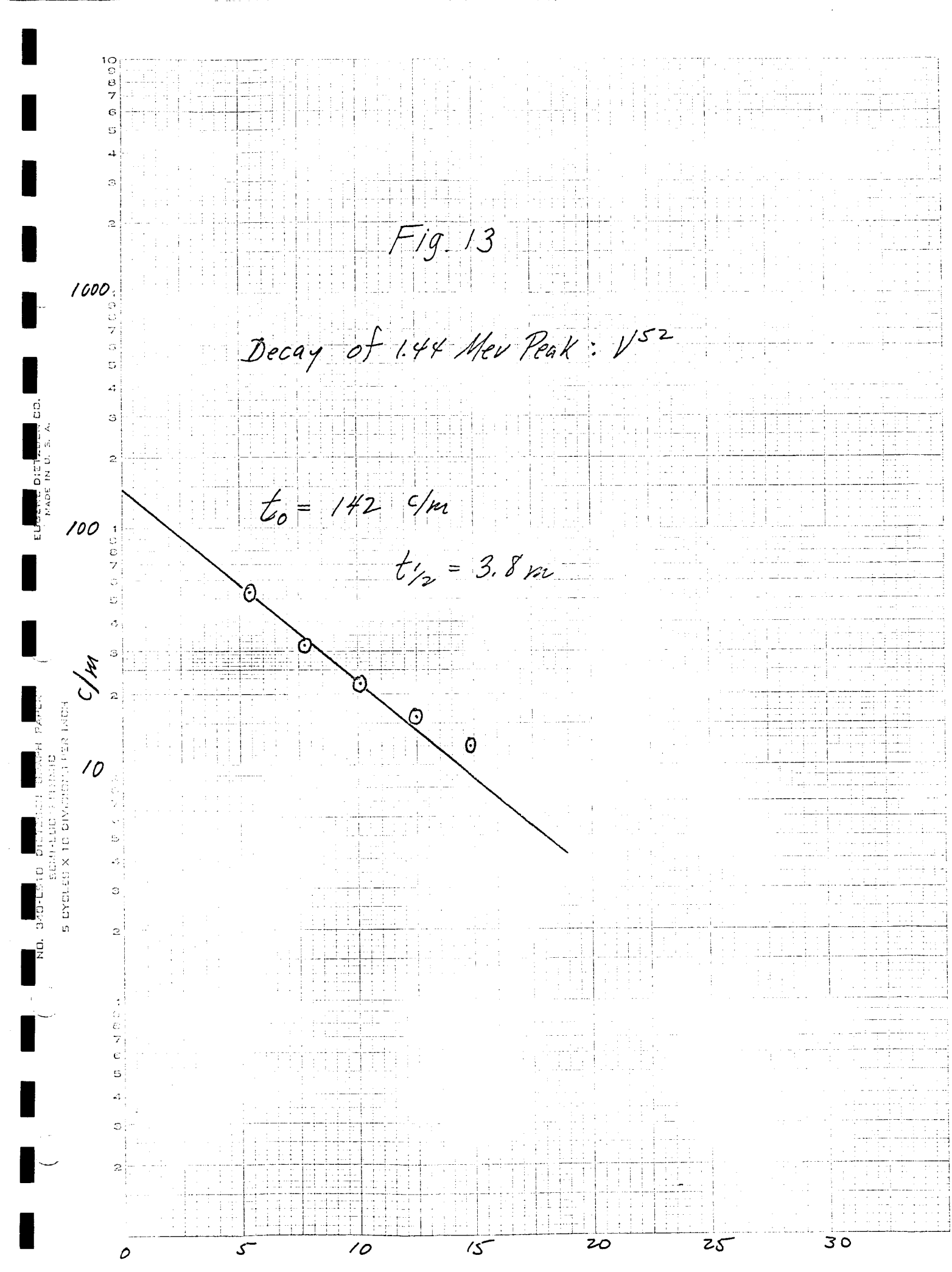
Fig. 13
Decay of 1.44 Mev Peak : V^{52}
t_0 = 142 c/m
$t_{1/2}$ = 3.8 m
c/m
1000
100
10
0
5
10
15
20
25
30

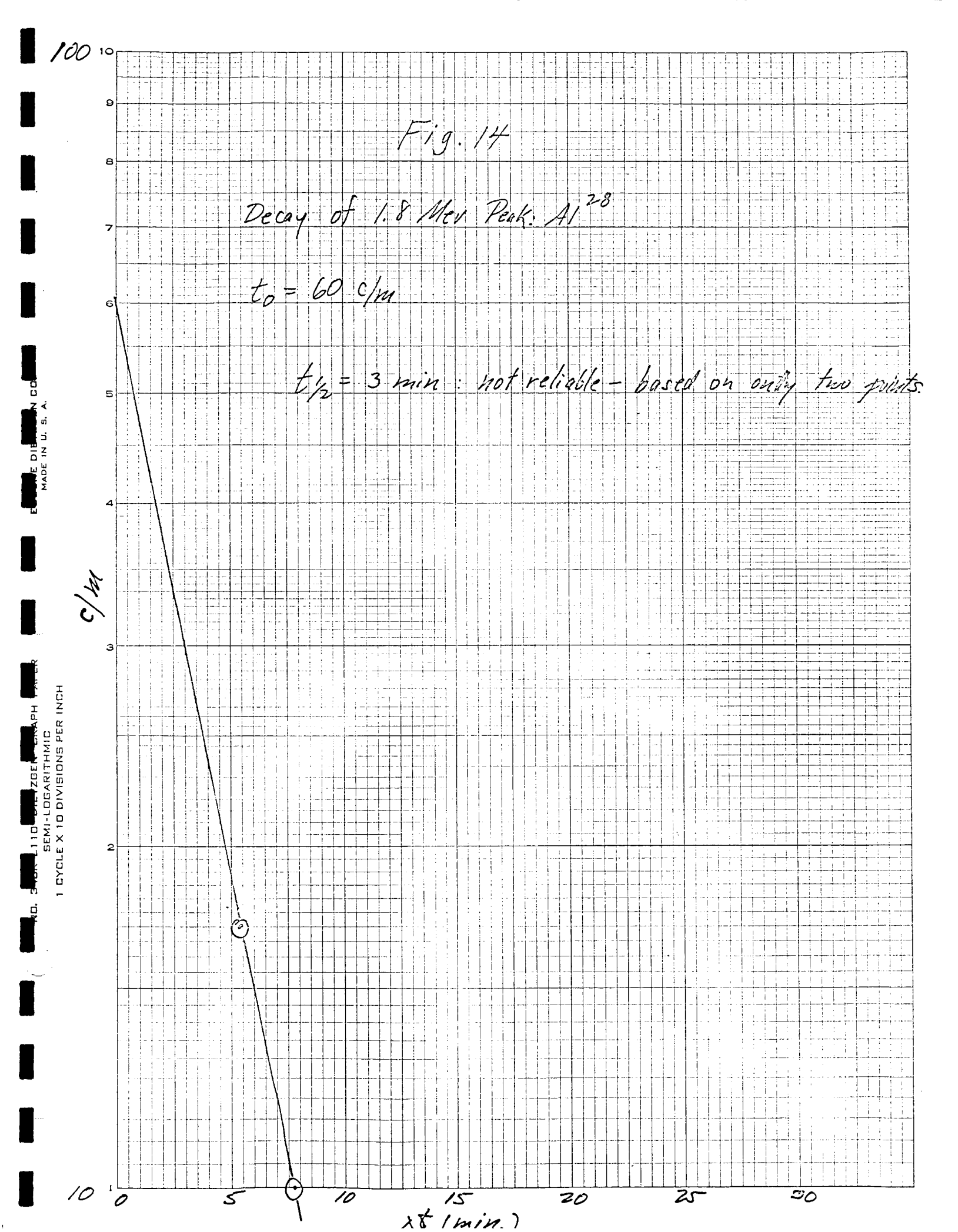
100
10
9
8
7
6
5
4
3
2
1
10
c/m
0
5
10
15
20
25
30
Δt (min.)
Fig. 14
Decay of 1.8 Mev Peak: Al^{28}
t_o = 60 c/m
$t_{1/2}$ = 3 min : not reliable – based on only two points.
MADE IN U. S. A.
SEMI-LOGARITHMIC
1 CYCLE X 10 DIVISIONS PER INCH

Fig. 15 Natural spherule NS 4. Shiny, black, rod-shaped magnetic particle 100x500 μ from Lamont core V 16-30. 30 sec irradiation, one-minute count. $_{A}t$=5m40s peaks at 0.84 Mev channel 29 (Mn^{56}); 1.8 Mev channel 61 (Al^{28}, Mn^{56}).

Fig. 16 NS 4 decay curve, Mn^{56}

Fig. 17 NS 4 decay curve, Al^{28}(?)

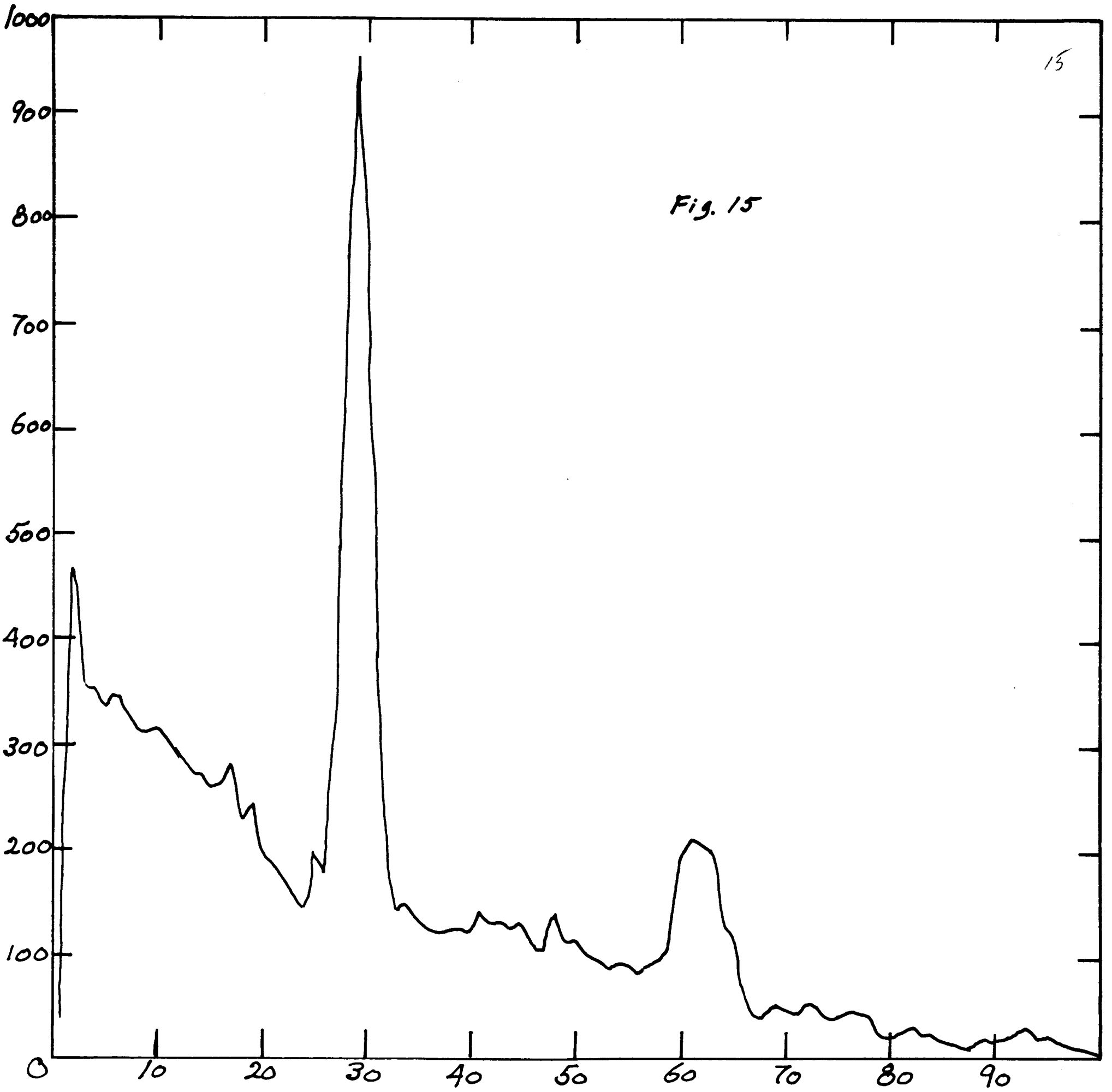
1000
900
800
700
600
500
400
300
200
100
0
10
20
30
40
50
60
70
80
90

Fig. 15

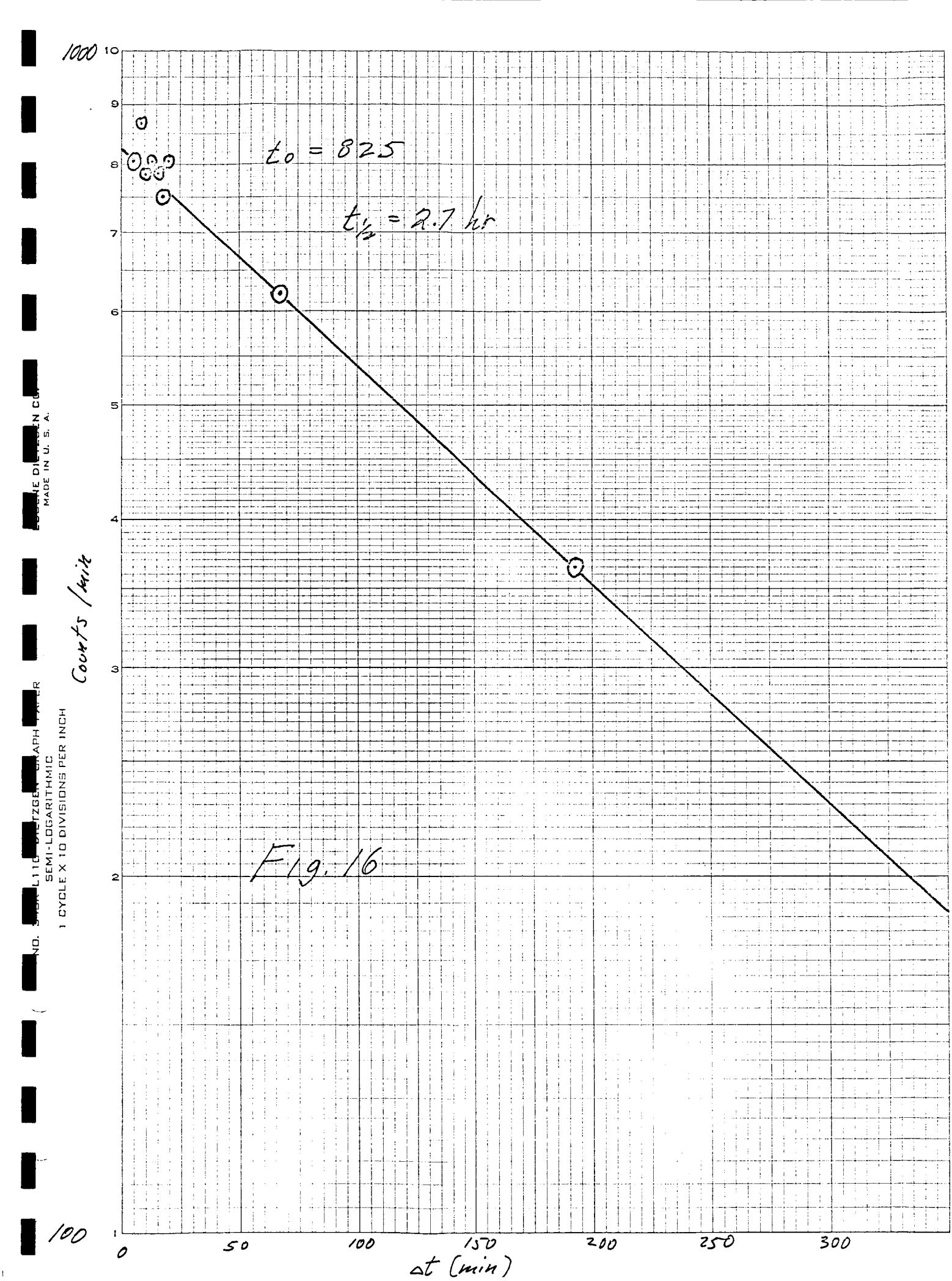
1000
100
$t_0 = 825$
$t_{1/2} = 2.7$ hr
Counts / min
Δt (min)
0
50
100
150
200
250
300
1
2
3
4
5
6
7
8
9
10
Fig. 16
SEMI-LOGARITHMIC
1 CYCLE X 10 DIVISIONS PER INCH
MADE IN U. S. A.

Fig. 17

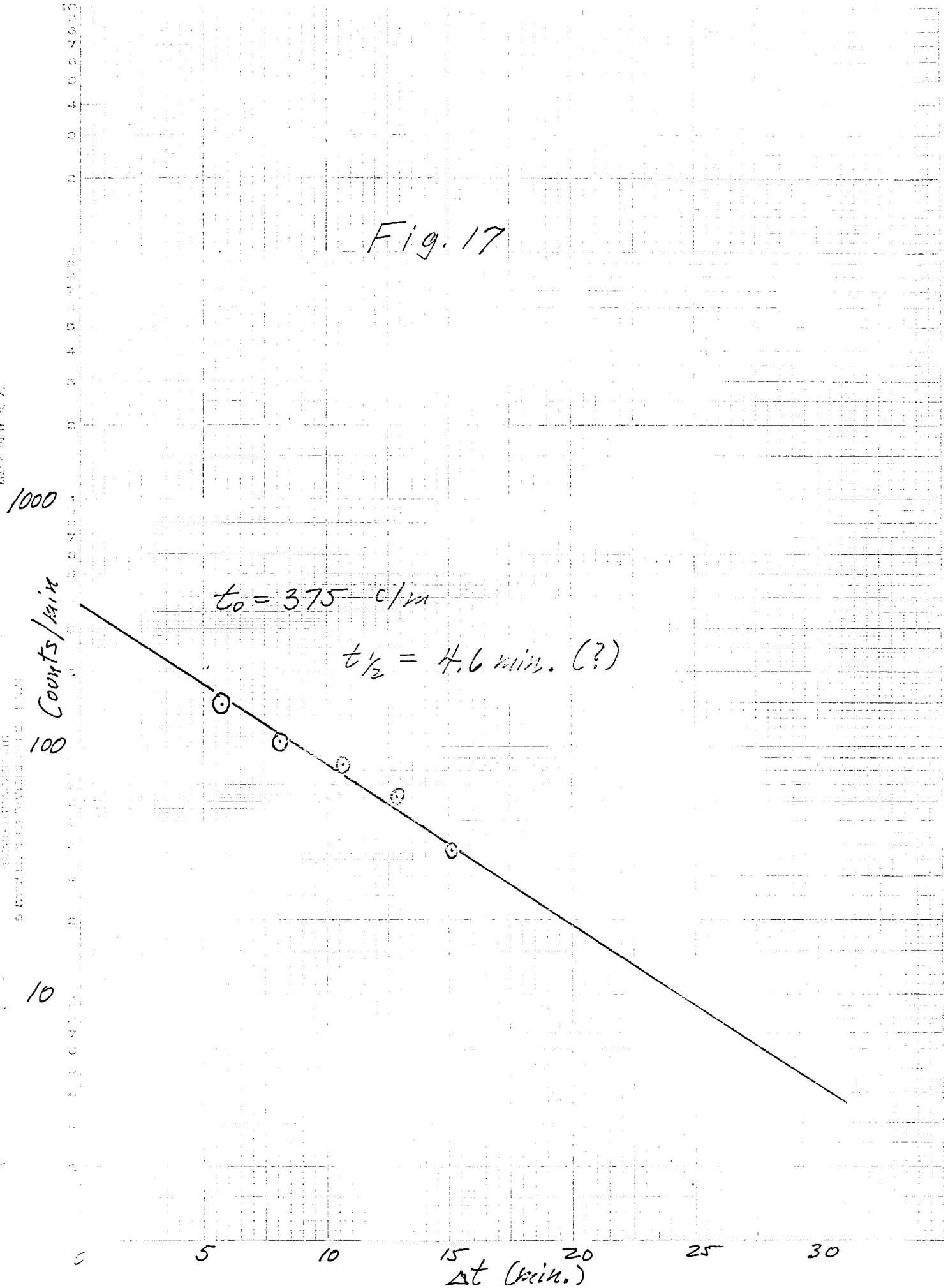

Fig. 18 Natural spherule NS 5. Shiny, black, magnetic spherule, 200μ diam. with tail 160μ long. 10 sec irradiation, one-minute count. Δt=8m25s. Peaks at 0.84 Mev channel 29 (Mn^{56}); 1.8 Mev channel 60 (Al^{28}, Mn^{56}).

Fig. 19 NS 5 decay curve, Mn^{56}

Fig. 20 NS 5 decay curve, prob. Mn^{56}

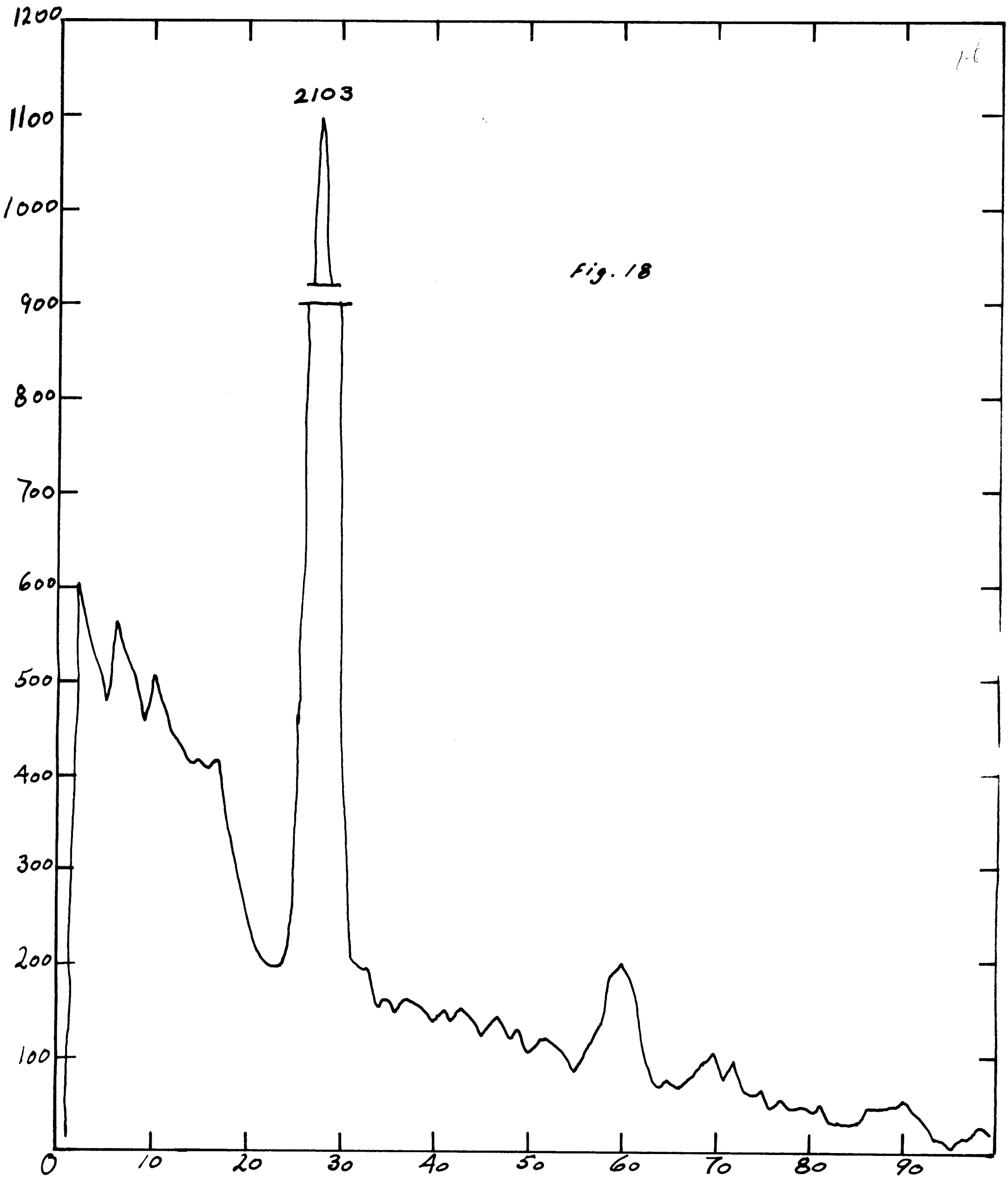
2103
1200
1100
1000
900
800
700
600
500
400
300
200
100
0
10
20
30
40
50
60
70
80
90

Fig. 18

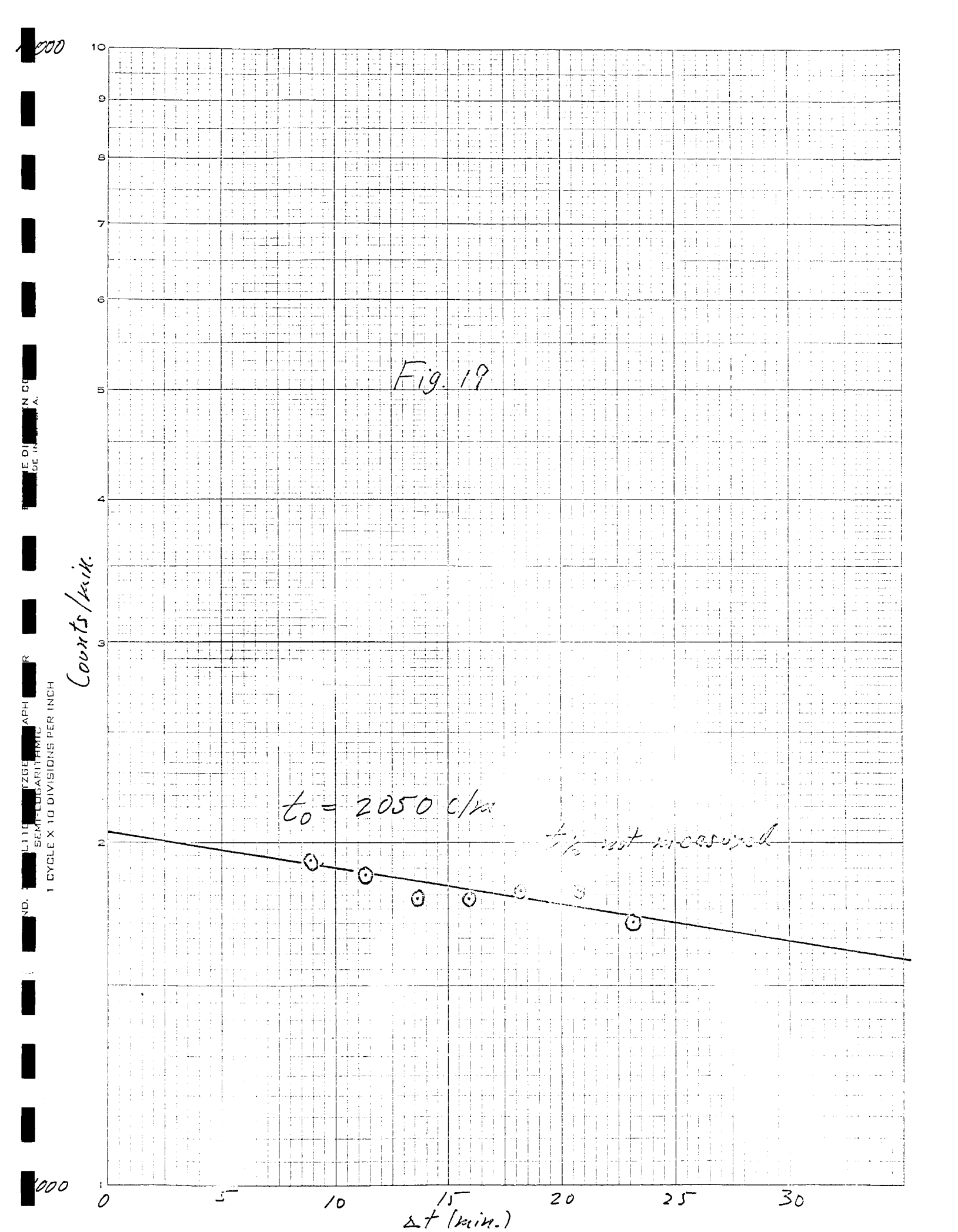
Fig. 19
Counts/min.
t_0 = 2050 c/m
$t_{1/2}$ not measured
Δt (min.)
0
5
10
15
20
25
30
1
2
3
4
5
6
7
8
9
10
1 CYCLE X 10 DIVISIONS PER INCH

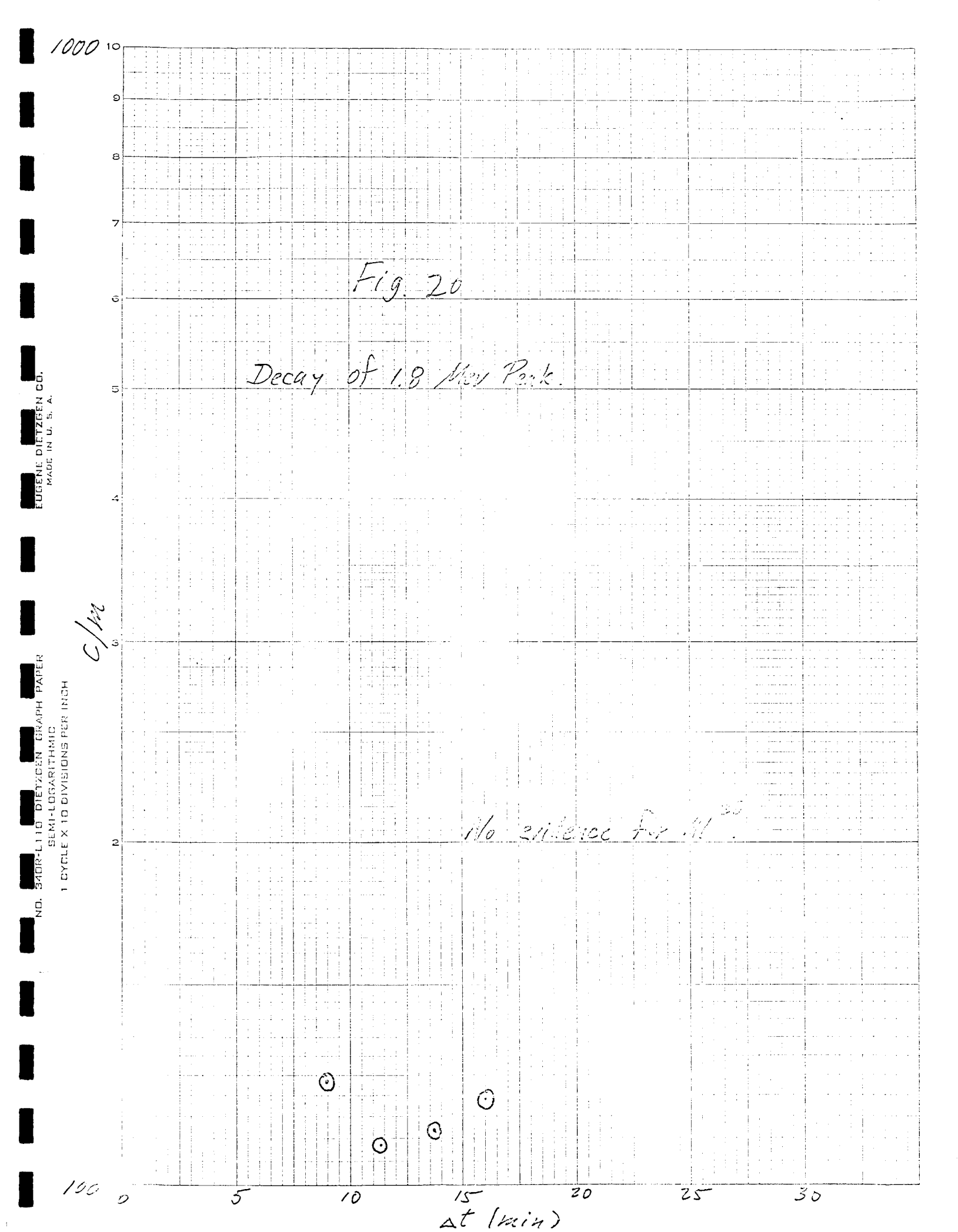
1000
10
9
8
7
6
5
4
3
2
100
C/m
Fig. 20
Decay of 1.8 Mev Peak.
No evidence for N20.
0
5
10
15
20
25
30
Δt (min)
EUGENE DIETZGEN CO.
MADE IN U. S. A.
NO. 340R-L110 DIETZGEN GRAPH PAPER
SEMI-LOGARITHMIC
1 CYCLE X 10 DIVISIONS PER INCH

Fig. 21 Natural spherule NS 6. Shiny, black, magnetic spherule 650μ diam. from Lamont core V 16-79. 10 sec irradiation, one-minute count. Δt=6m31s. Peaks at 0.84 Mev channel 28 (Mn^{56}); 1.8 Mev channel 60 (Mn^{56}); 2.1 Mev channel 69 (Mn^{56}); 2.6 Mev channel 89 (Mn^{56}).

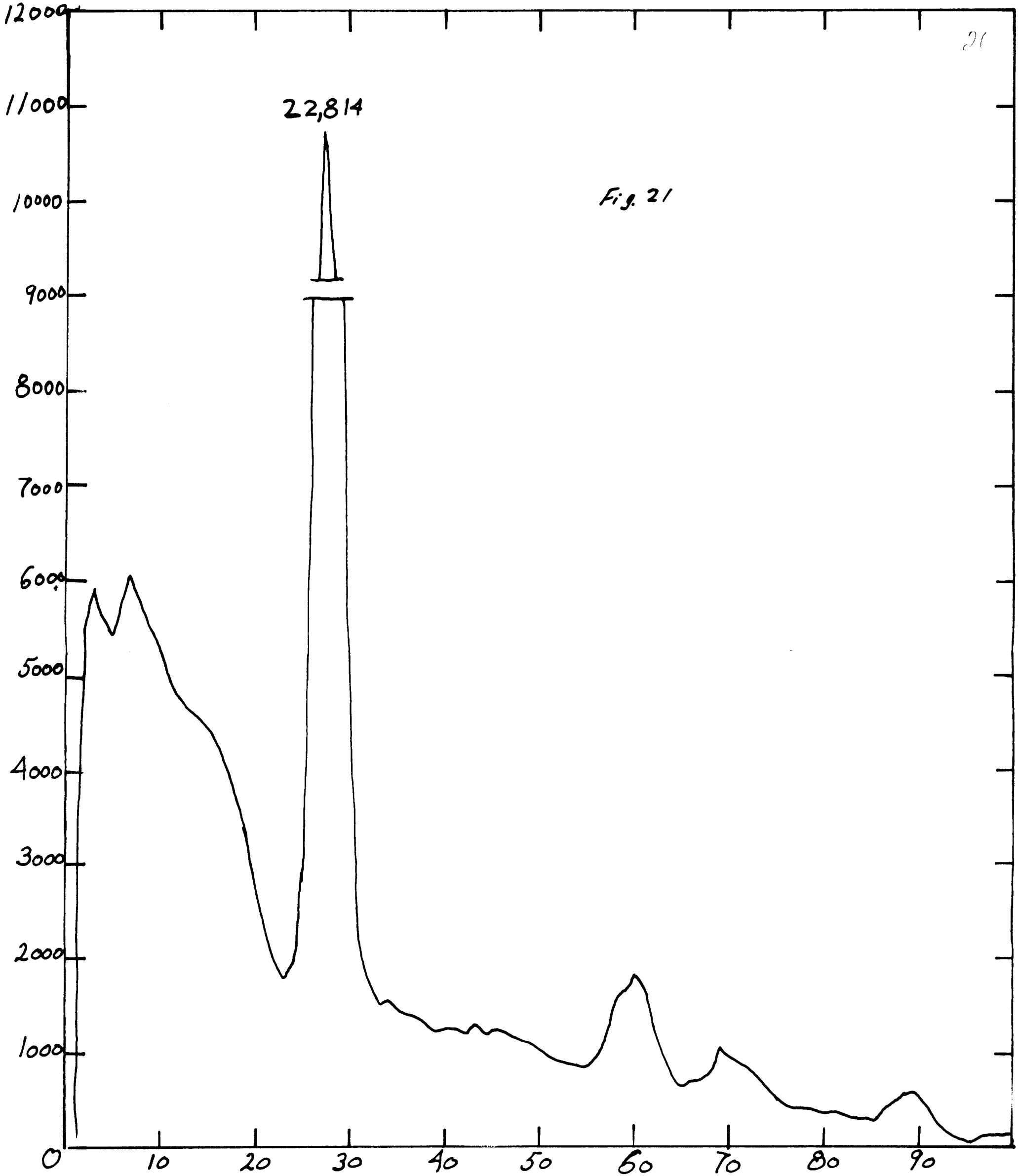
12000
11000
10000
9000
8000
7000
6000
5000
4000
3000
2000
1000
0
22,814
10
20
30
40
50
60
70
80
90

Fig. 21

Fig. 22 Natural spherule NS 7. Shiny, black, magnetic, hollow, half-spherule 240μ diam., from Lamont core V 16-79. 30 sec irradiation, one-minute count. Δt=4m43s. Identifiable peaks at 0.84 channel 29 (Mn^{56}); 1.8 Mev channel 62 (Al^{28}, Mn^{56}).

Fig. 23 NS 7 decay curve, Mn^{56}

Fig. 24 NS 7 decay curve, not identified.

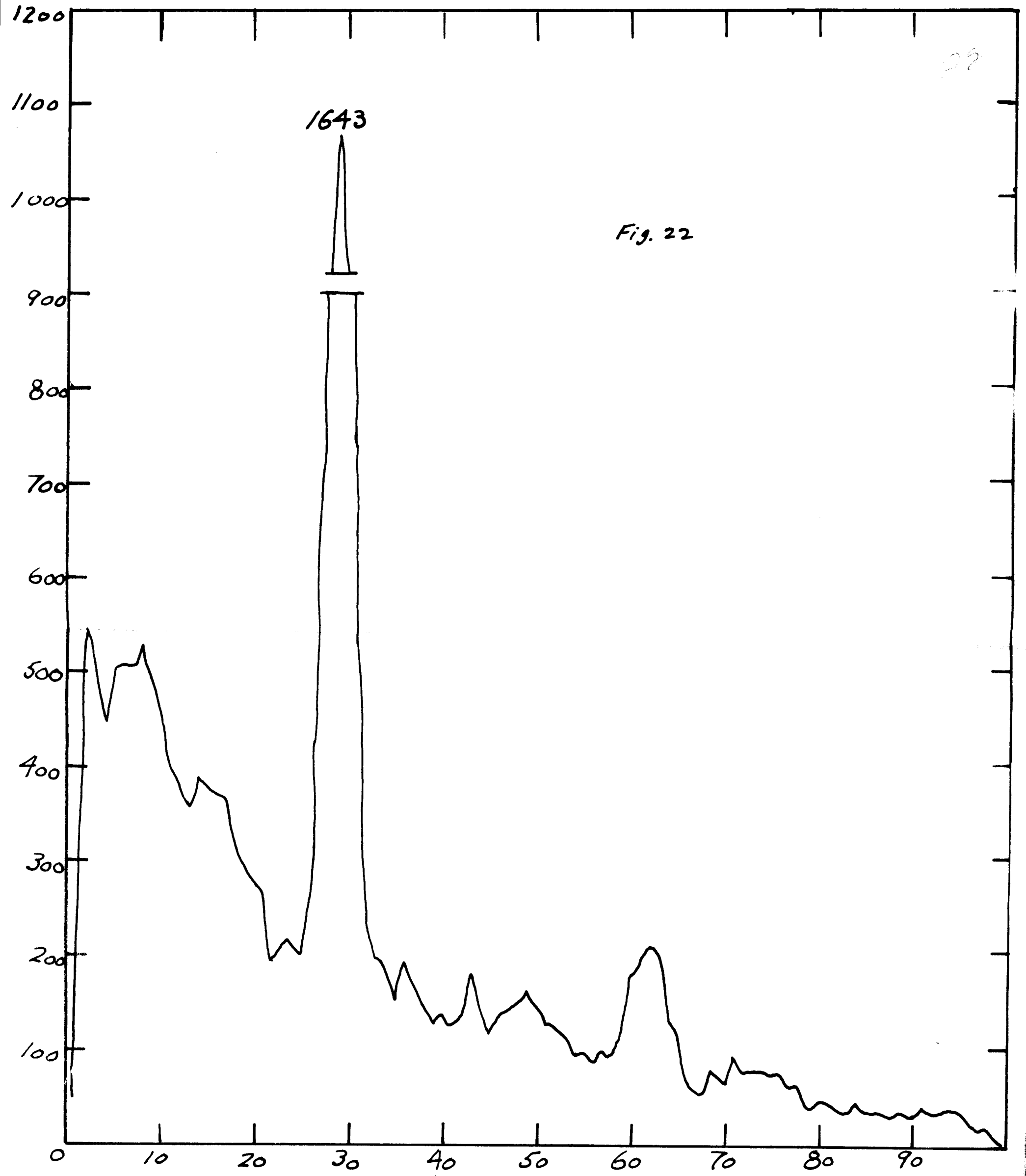
1200
1100
1000
900
800
700
600
500
400
300
200
100
0
10
20
30
40
50
60
70
80
90
1643

Fig. 22

Fig. 23

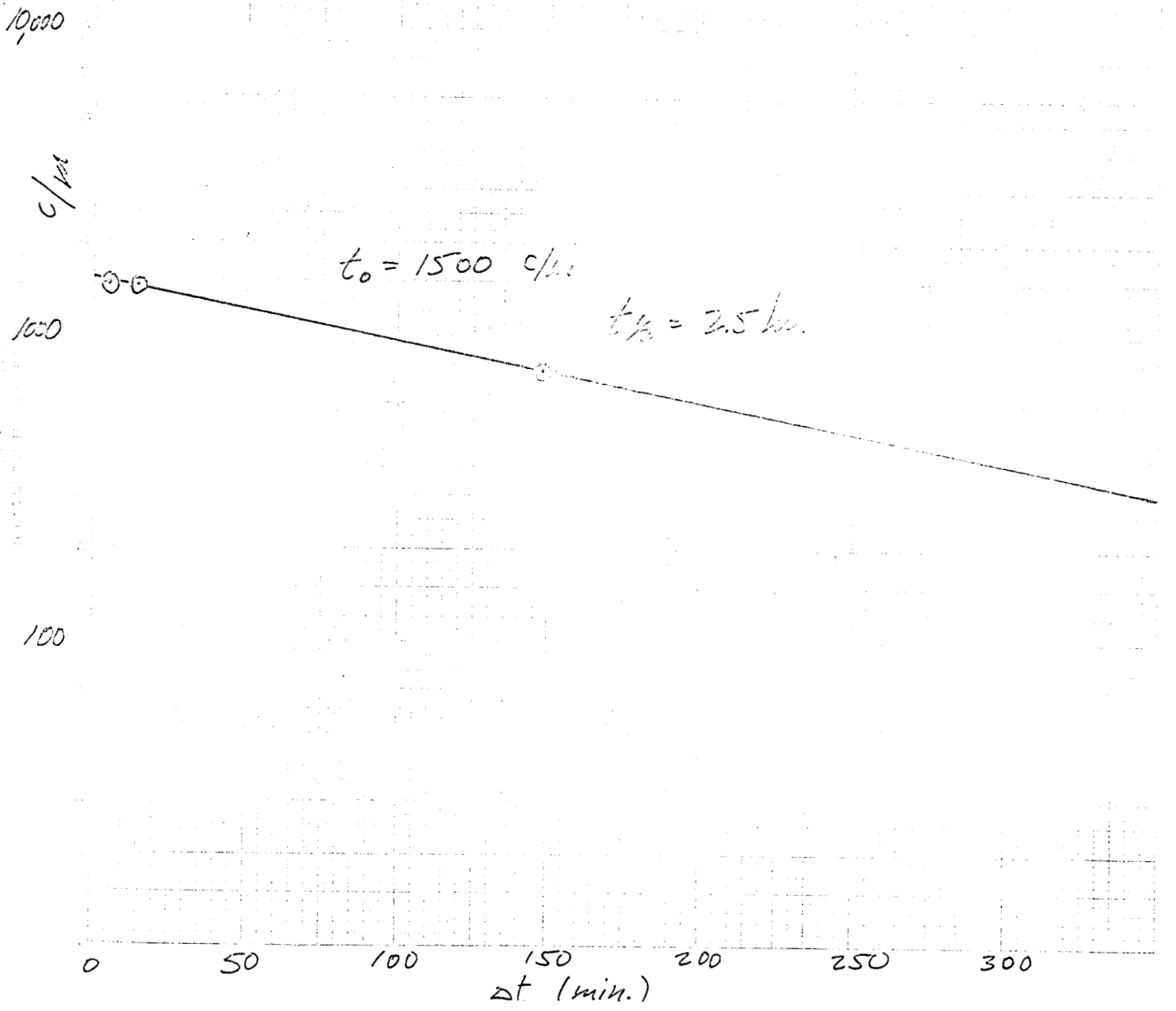
10,000
c/μl
1000
100
t_o = 1500 c/μl
$t_{1/2}$ = 2.5 hr.
0
50
100
150
200
250
300
Δt (min.)

Fig. 24

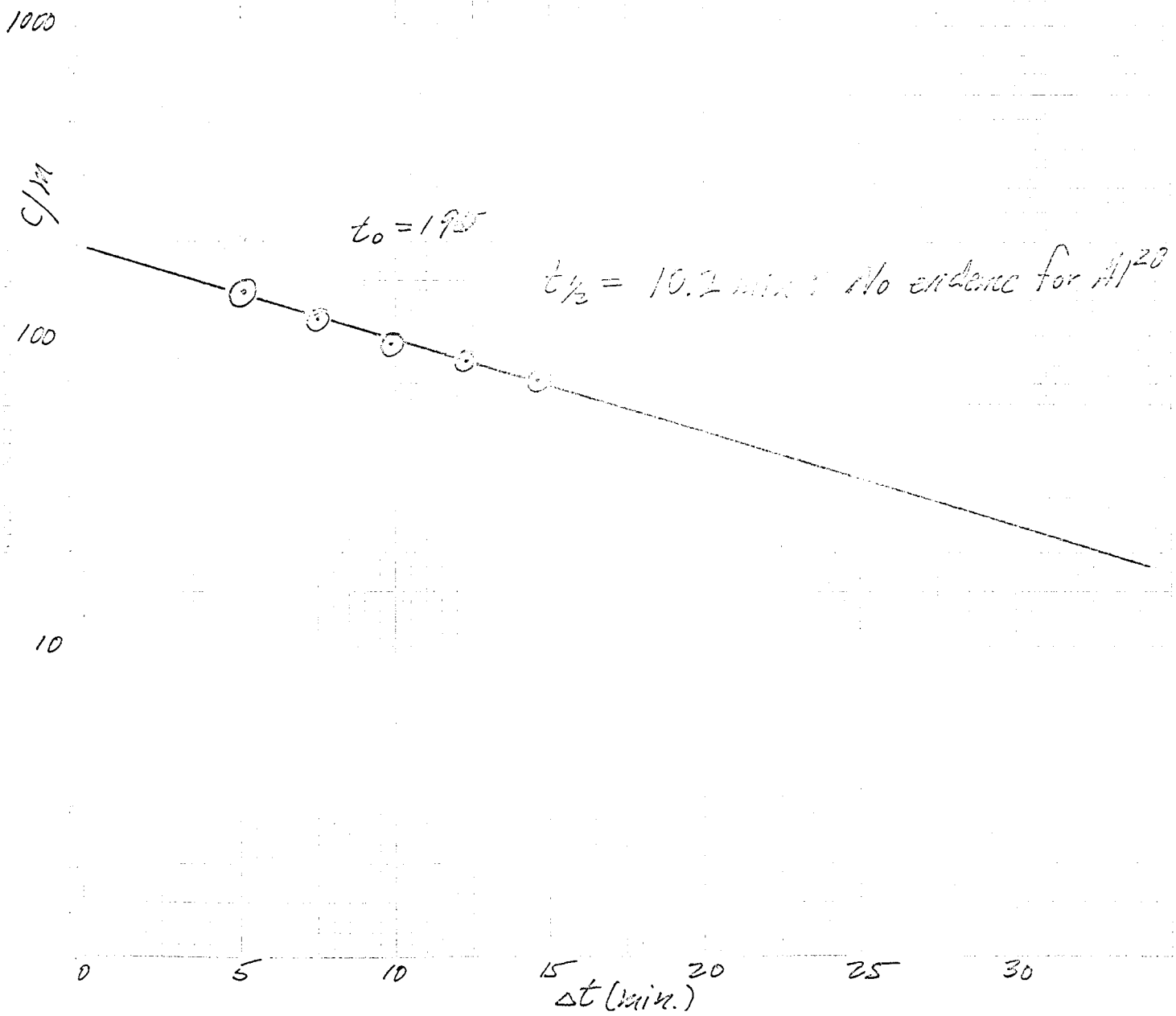
1000
C/m
100
10
$t_0 = 19^{5}$
$t_{1/2}$ = 10.2 min ; No evidence for ^{41}
0
5
10
15
20
25
30
Δt (min.)

Fig. 25 Natural spherule NS 8. Black, shiny, magnetic half-spherule 450μdiam. from Lamont core V 16-79. 30 sec irradiation, three-minute count. Δt=4m40s. Identifiable peaks are 0.84 Mev channel 29 (Mn^{56}); 1.8 Mev channel 62 (Al^{28}, Mn^{56}); 2.1 Mev channel 72 (Mn^{56}); 2.65 Mev channel 93 (Mn^{56}).

Fig. 26 NS 8 decay curve, Mn^{56}

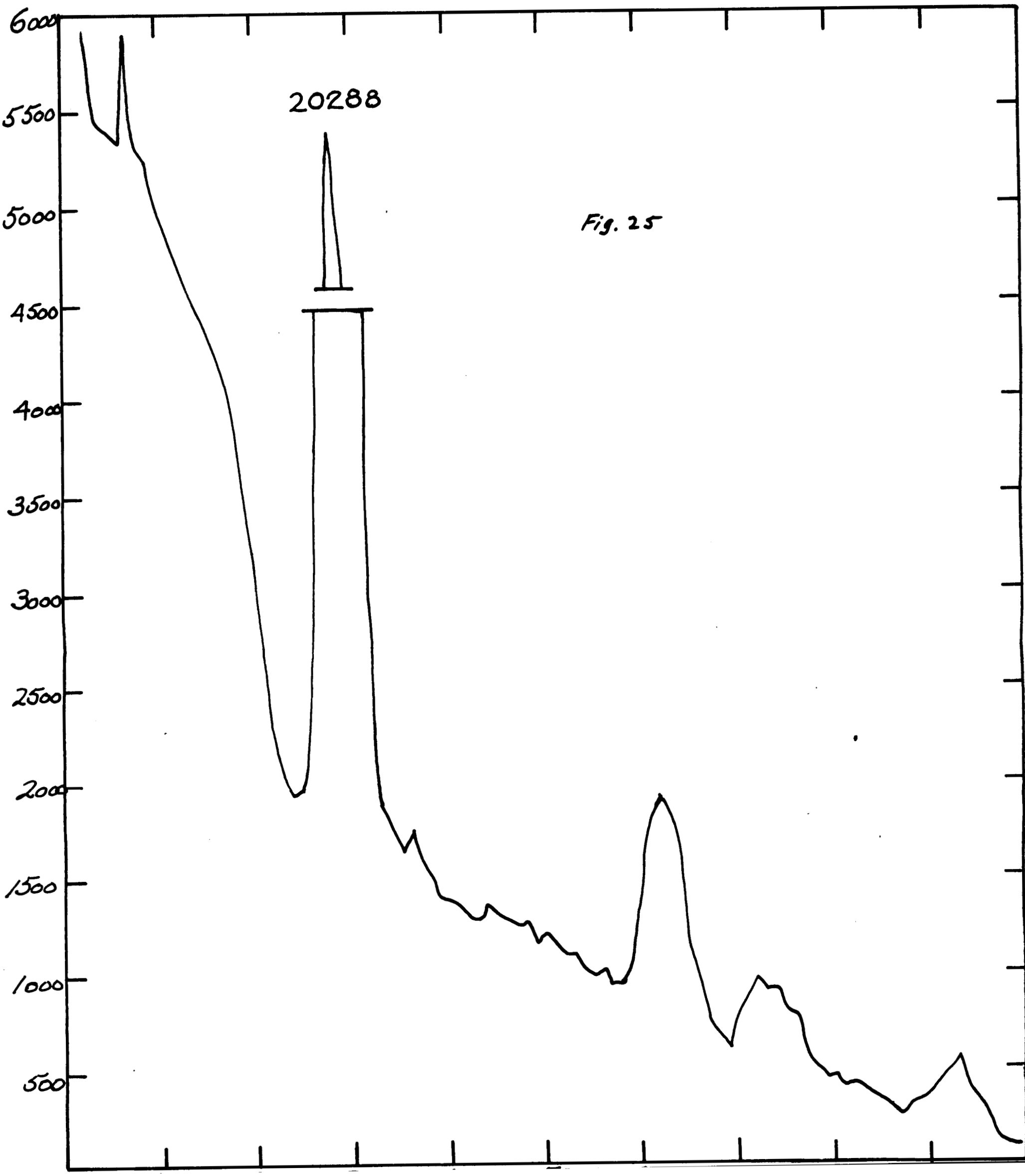
6000
5500
5000
4500
4000
3500
3000
2500
2000
1500
1000
500
20288

Fig. 25

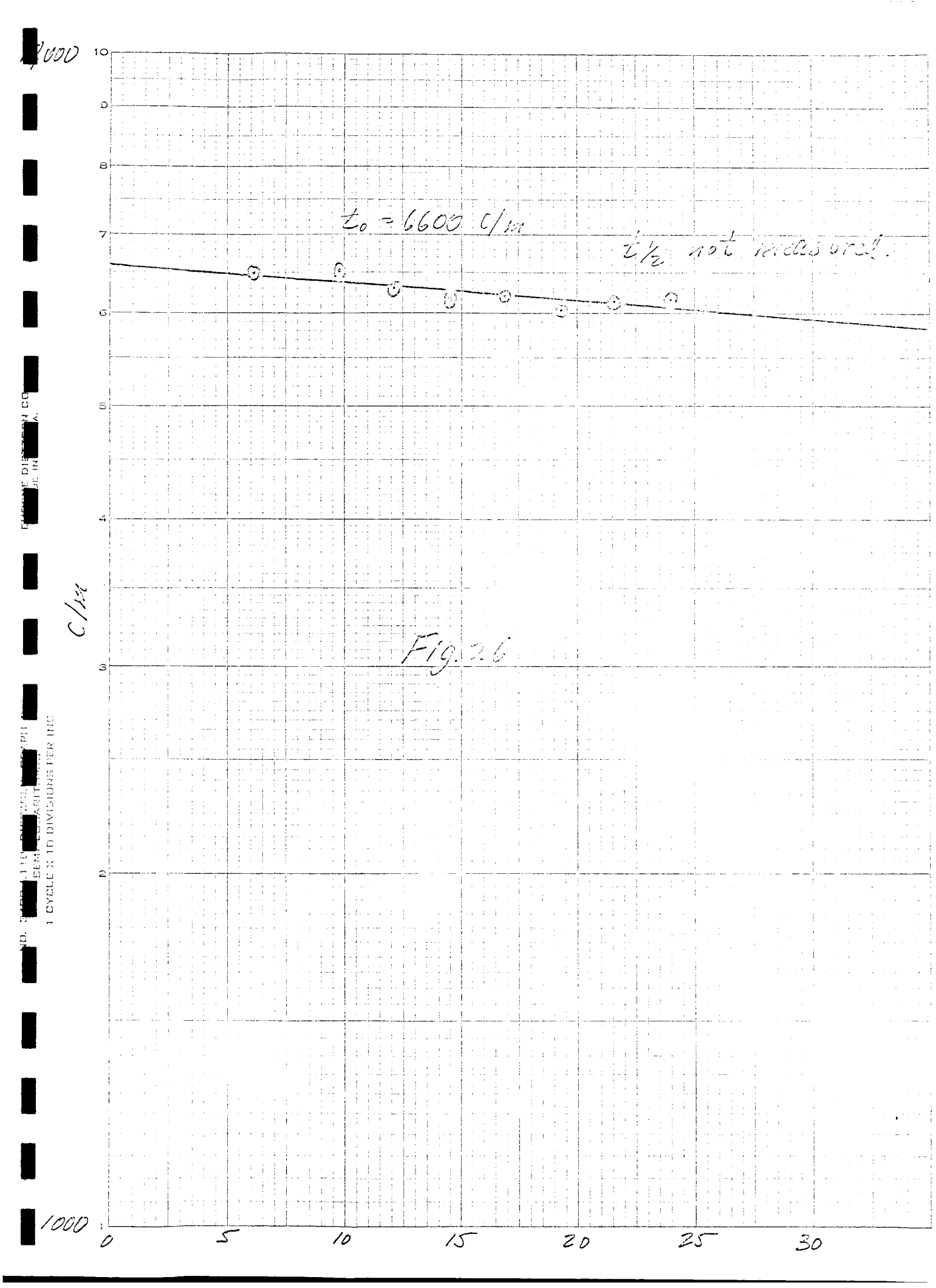
t_0 = 6600 c/m
$t_{1/2}$ not measured.
c/m
10
9
8
7
6
5
4
3
2
1000
0
5
10
15
20
25
30

Fig. 26

Fig. 27 Natural spherule NS 9. Green, Transparent, non-magnetic spherule containing dark inclusions and charged with bubbles. 300μin diam. from Lamont core A 153-156. 30 sec irradiation, one-minute count. $_{\Delta}t$=6m45s. Identifiable peak at 1.8 Mev channel 60 (Al^{28}).

Fig. 28 Same, $_{\Delta}t$=9m7s

Fig. 29 Same, with identifiable peaks at 0.84 Mev channel 28 (Mn^{56}); 1.37 Mev channel 47 (Na^{24}); 1.8 Mev channel 59 (Al^{28}). $_{\Delta}t$=11m29s.

Figs. 30 and 31 Same, $_{\Delta}t$=13m51s and 16m13s

Figs. 32,33 and 34 Same, but 2.4 minute Al^{28} peak has disappeared. Fifteen-hour Na^{24} gradually becomes more prominent than 2.6-hour Mn^{56} $_{\Delta}t$=105m283m, and 417m. 5-minute, 10-minute, and 10-minute counts, respectively.

Fig. 35 NS 9 decay curve, Mn^{56}

Fig. 36 NS 9 decay curve, Al^{28}

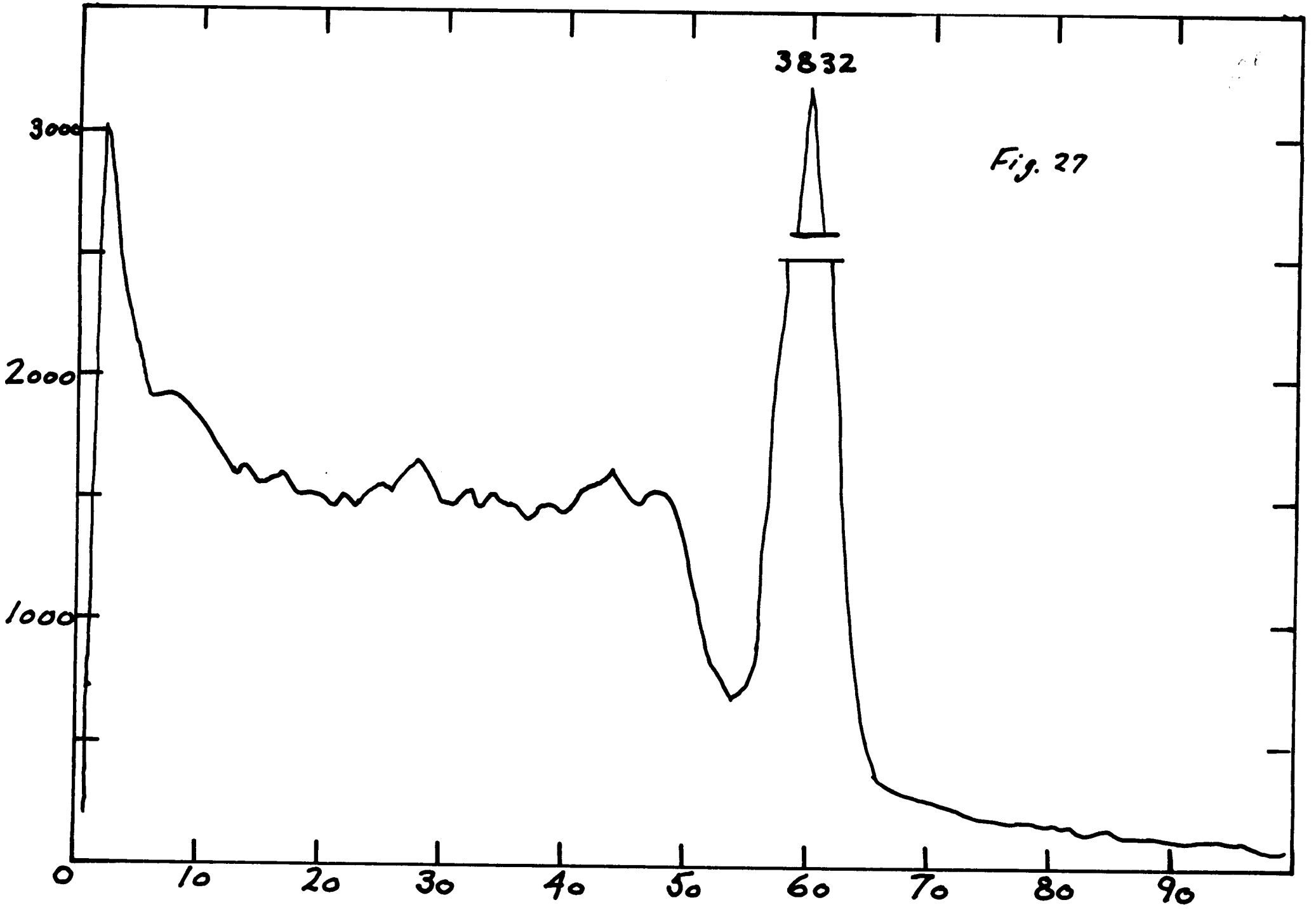

Fig. 27

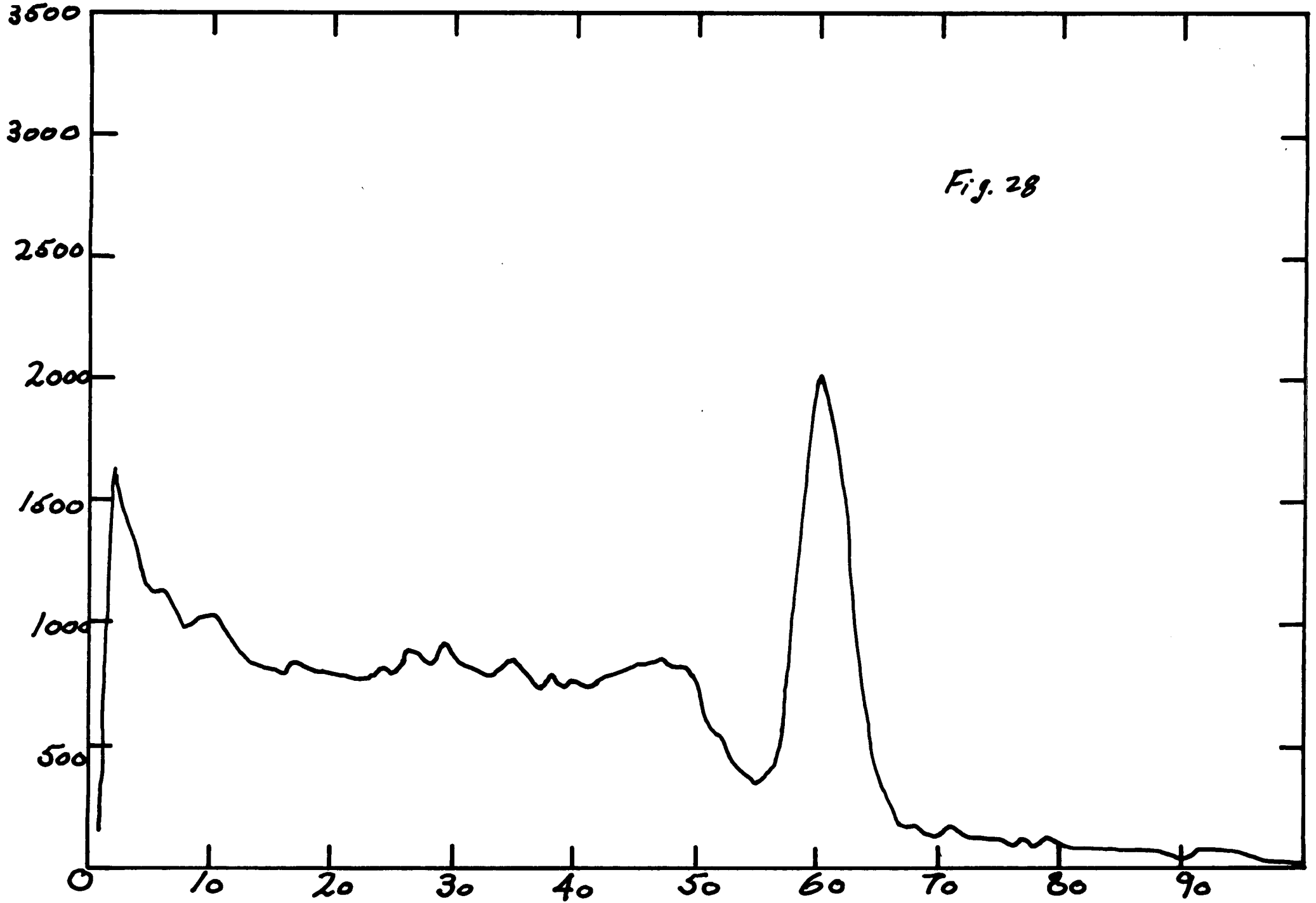

Fig. 28

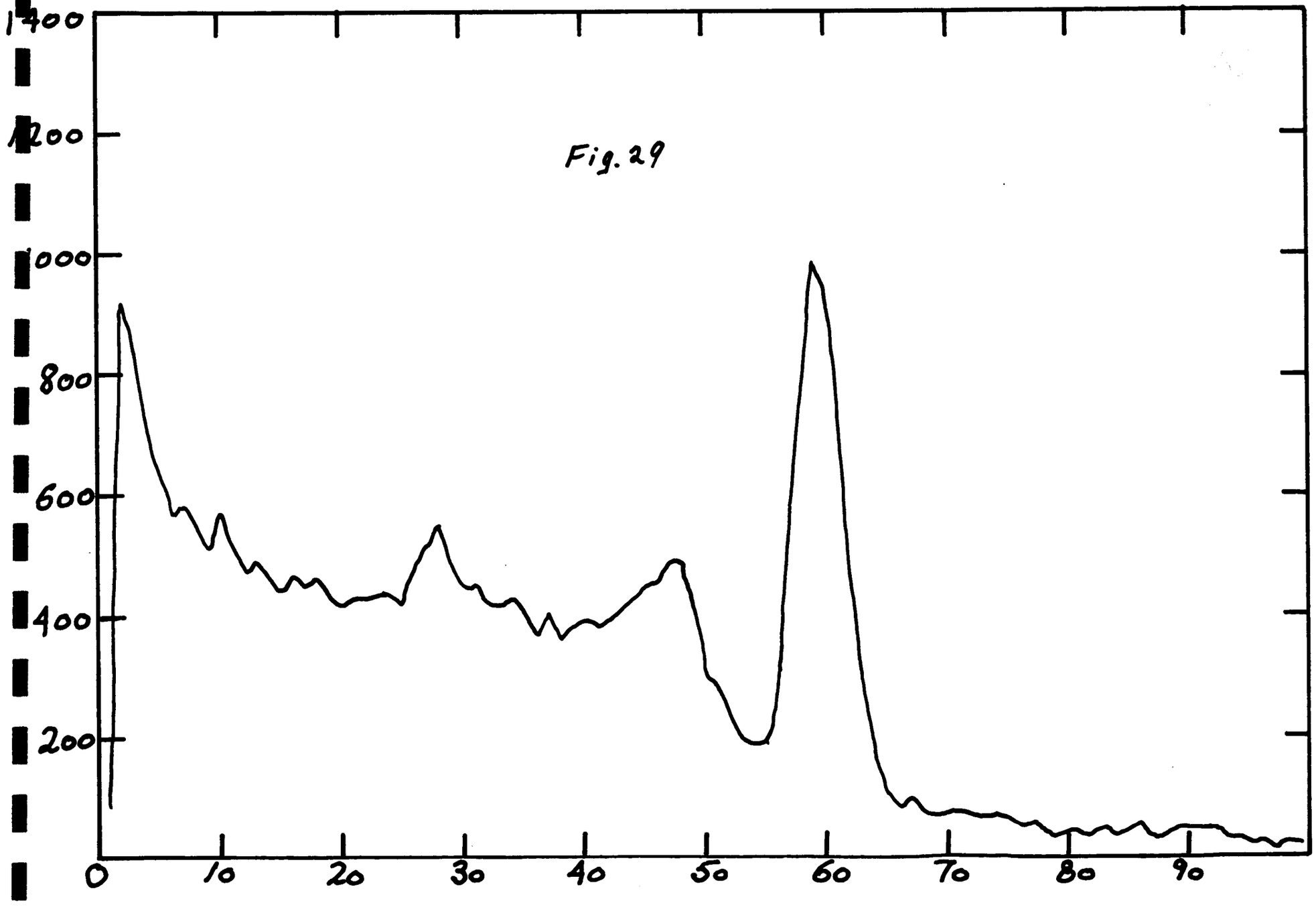

Fig. 29

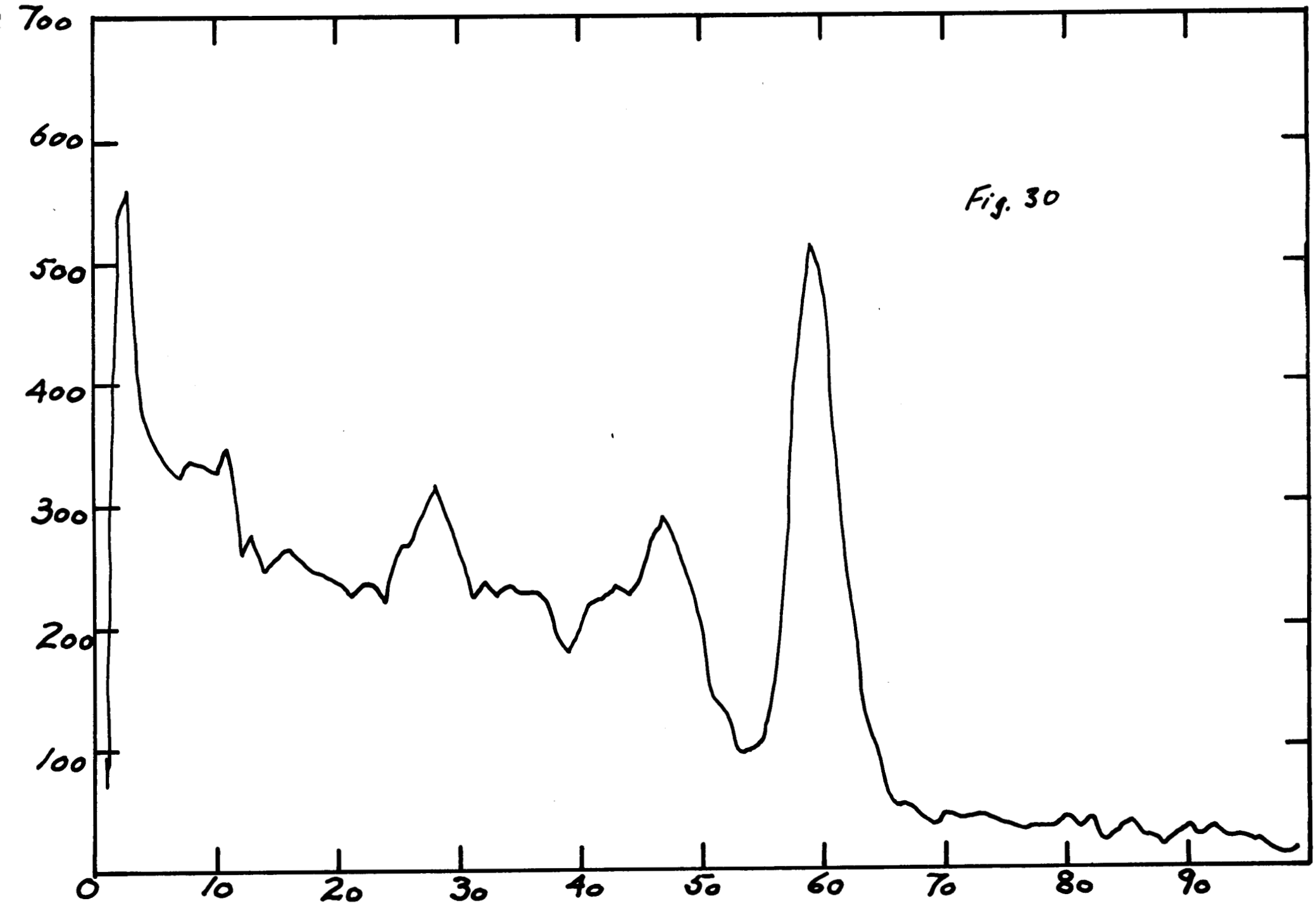

Fig. 30

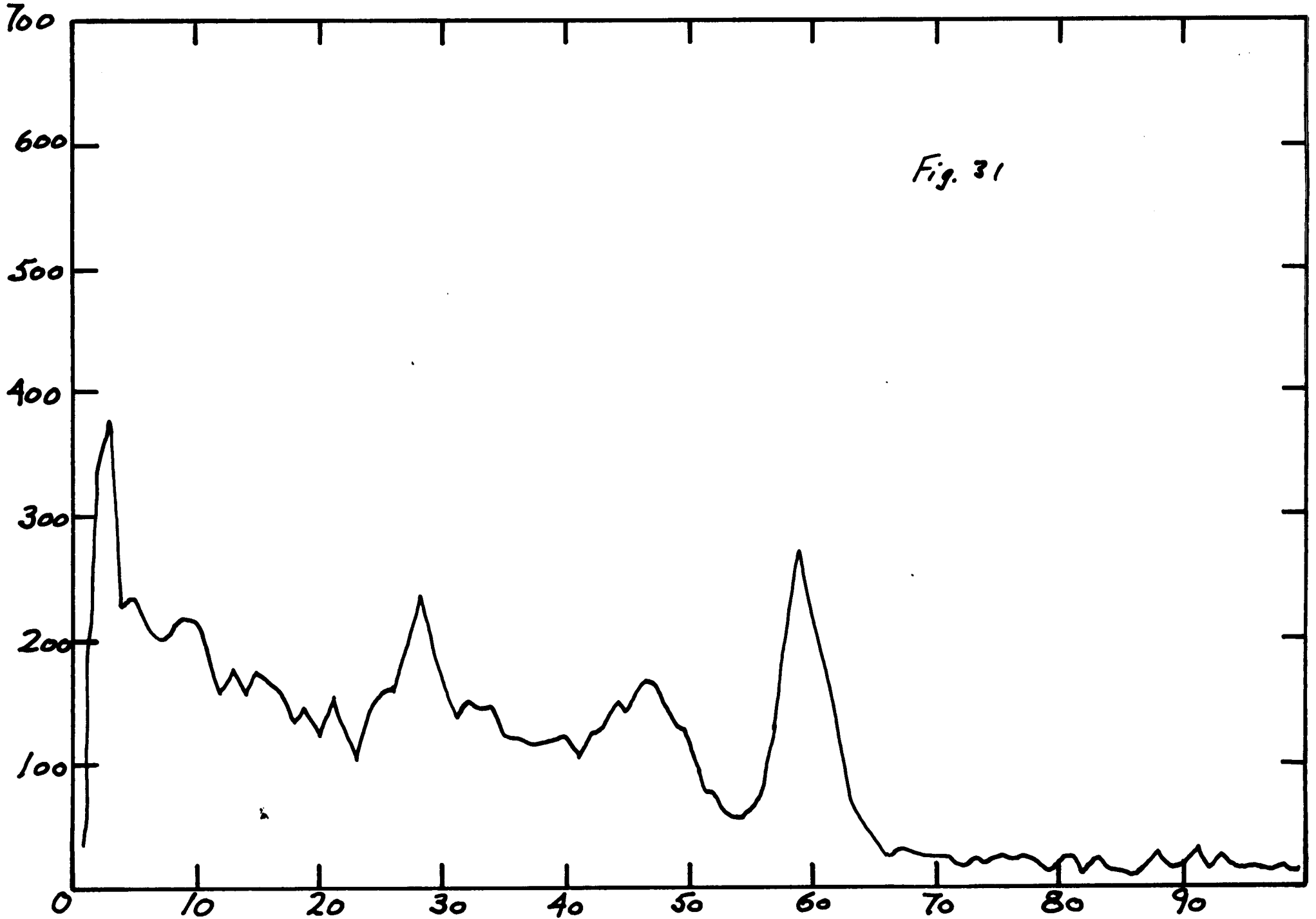

Fig. 31

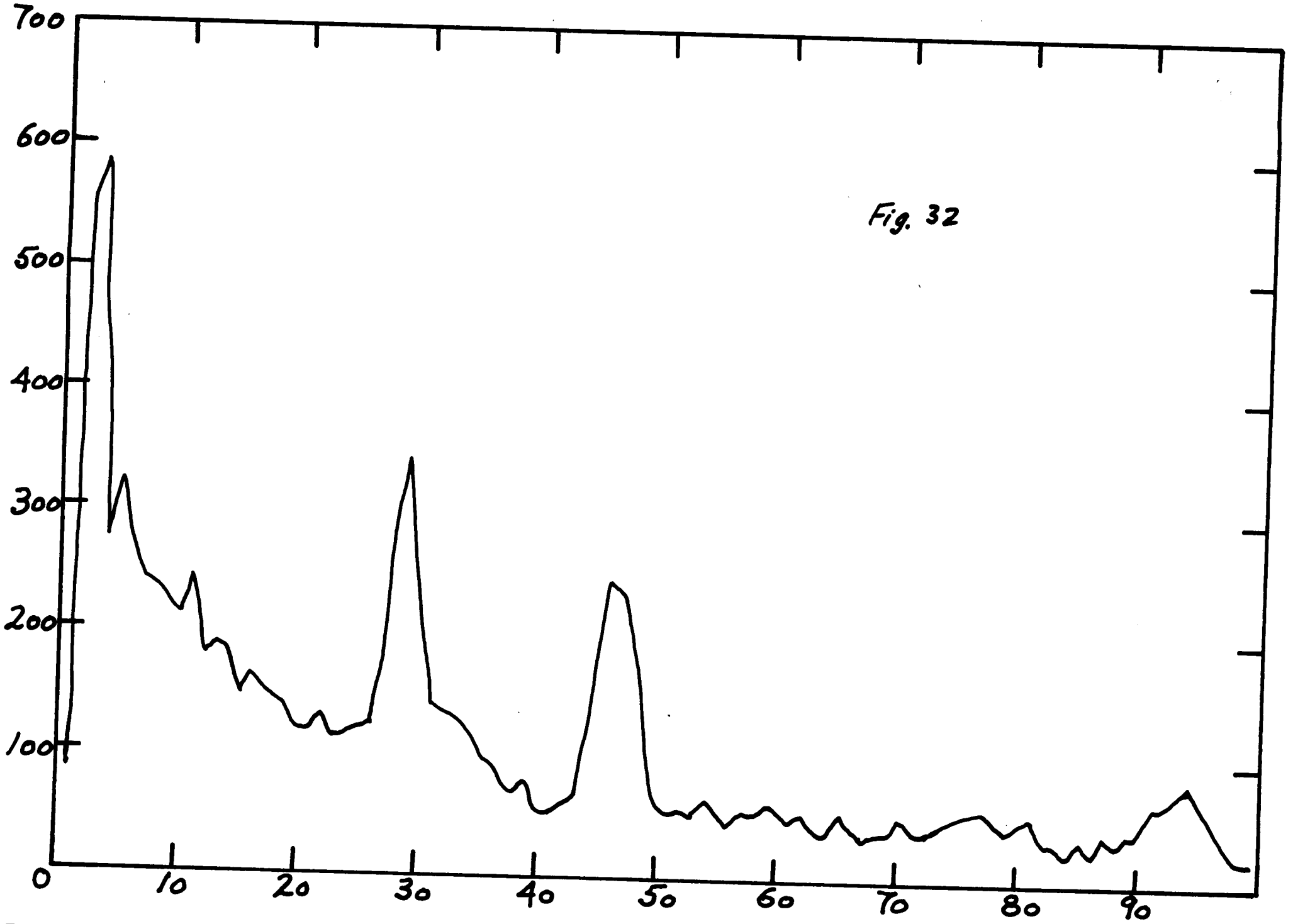

Fig. 32

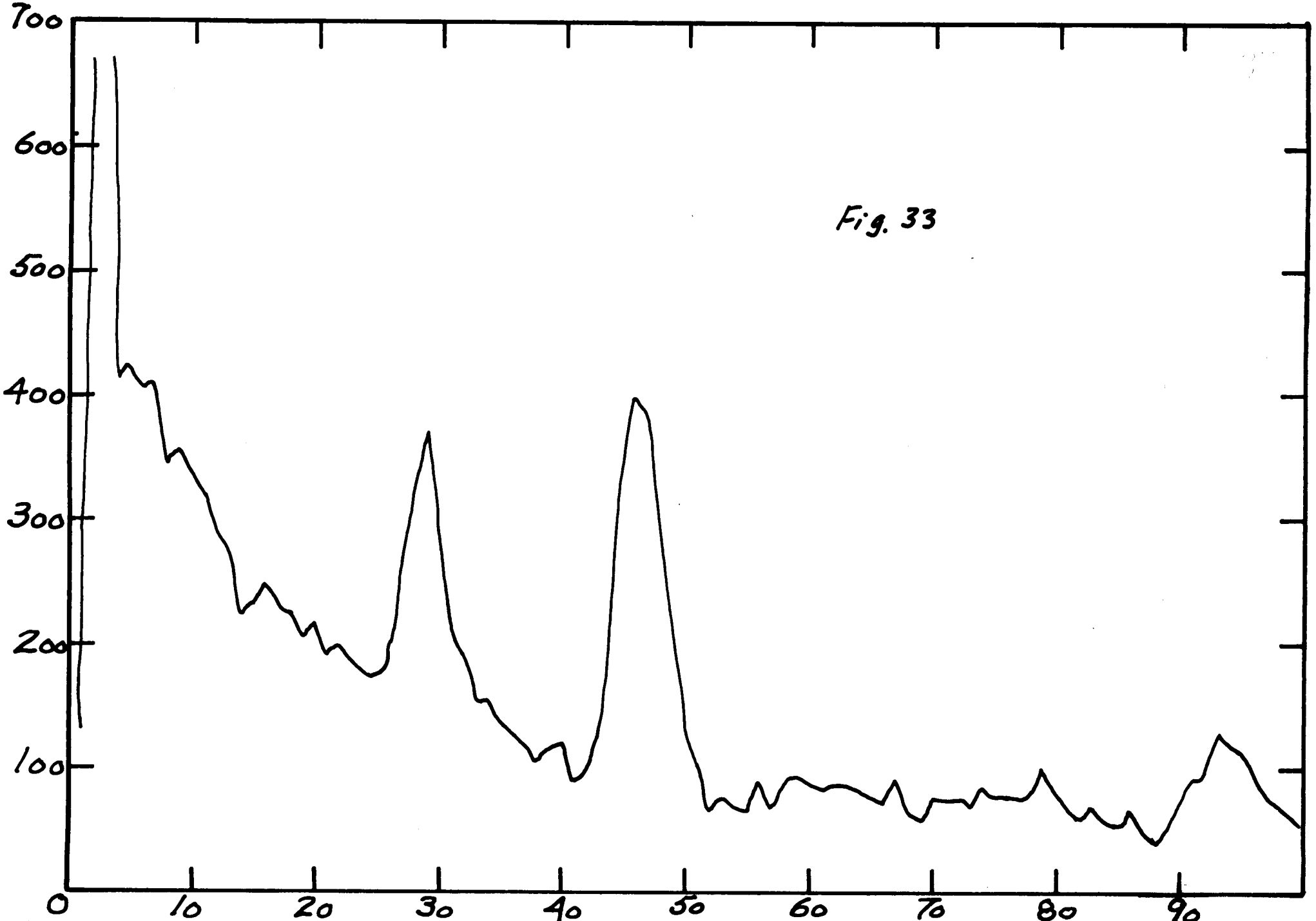

Fig. 33

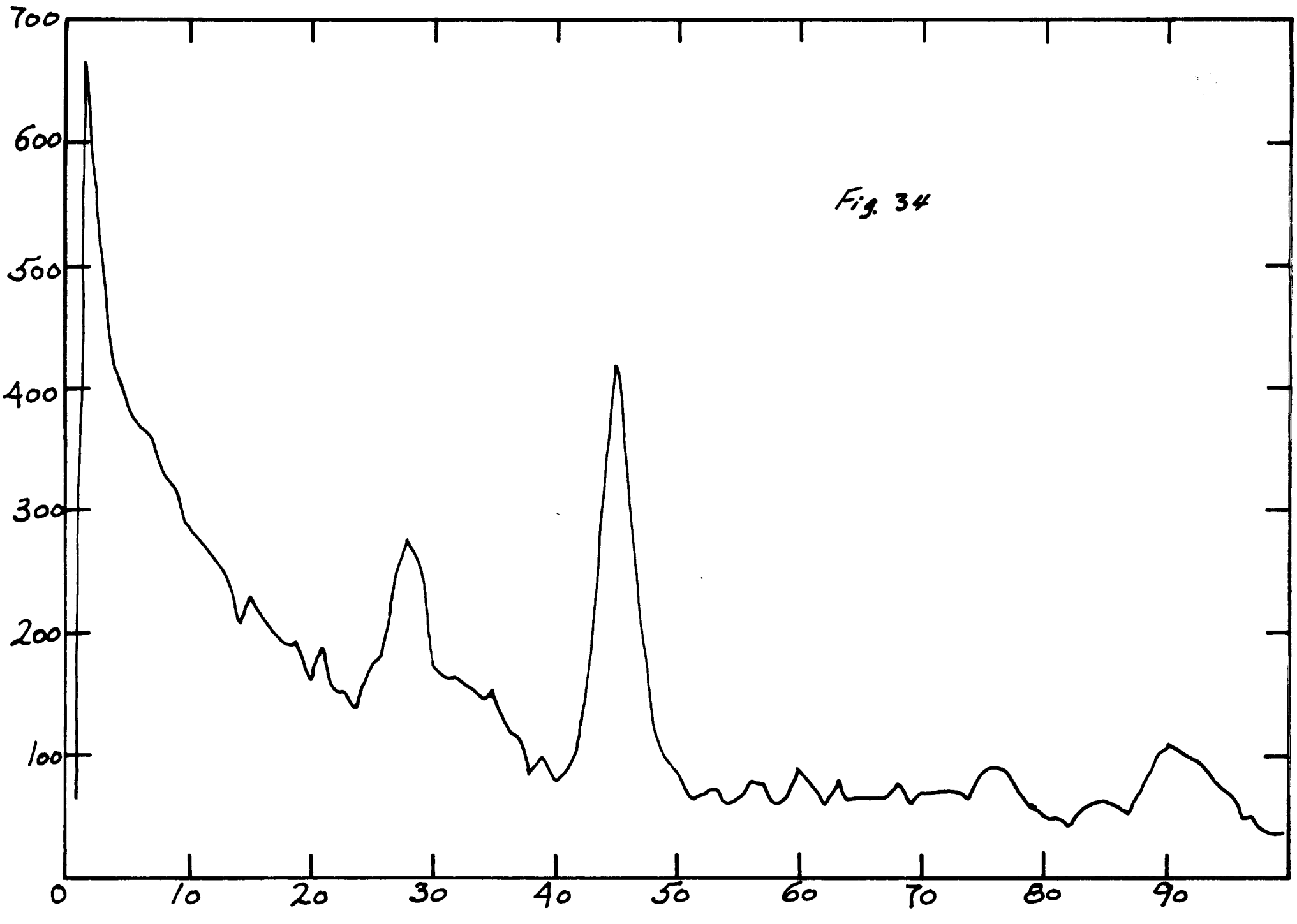

Fig. 34

Fig. 35

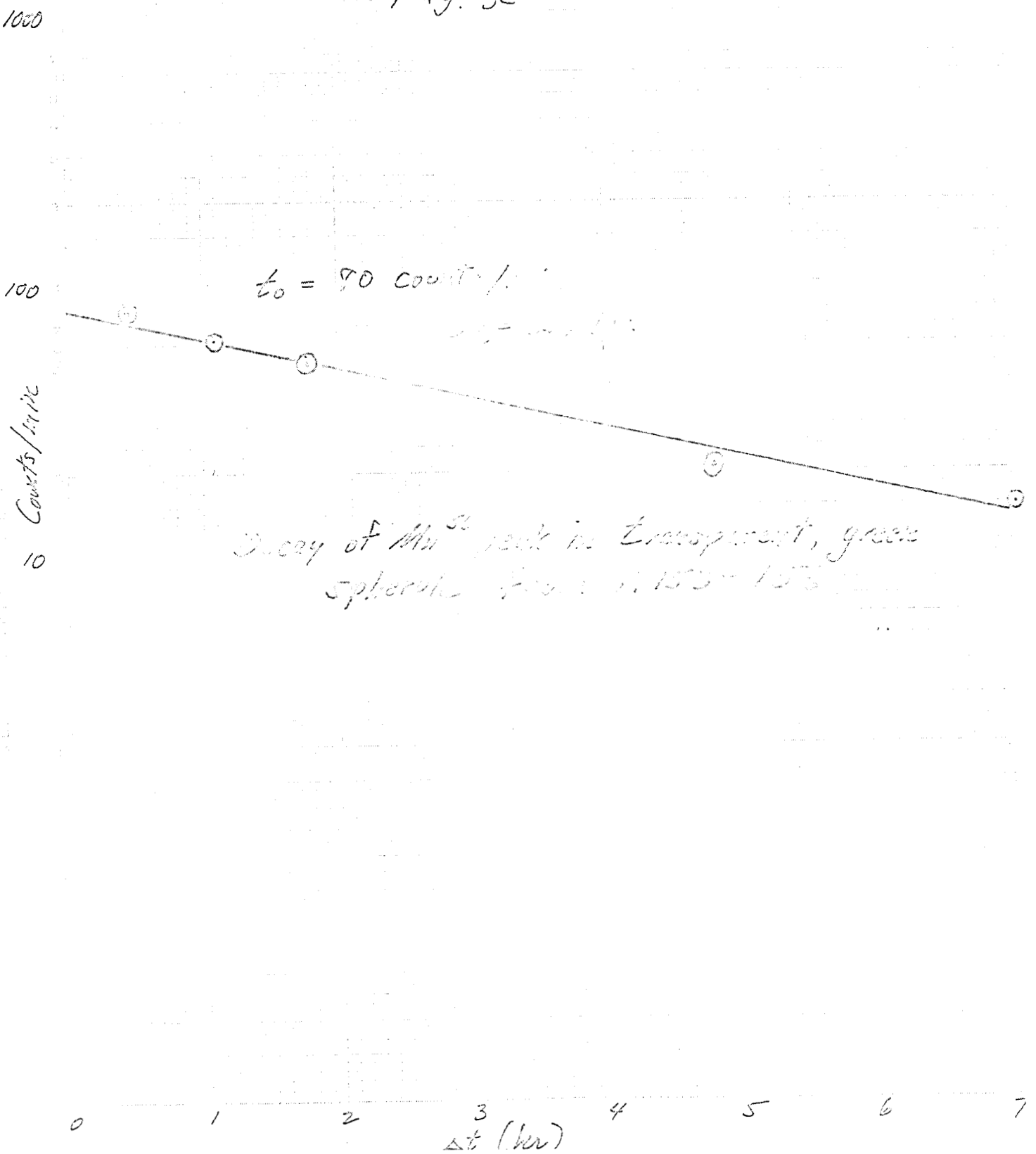

Decay of Mn^{52} peak in Evaporant, grass

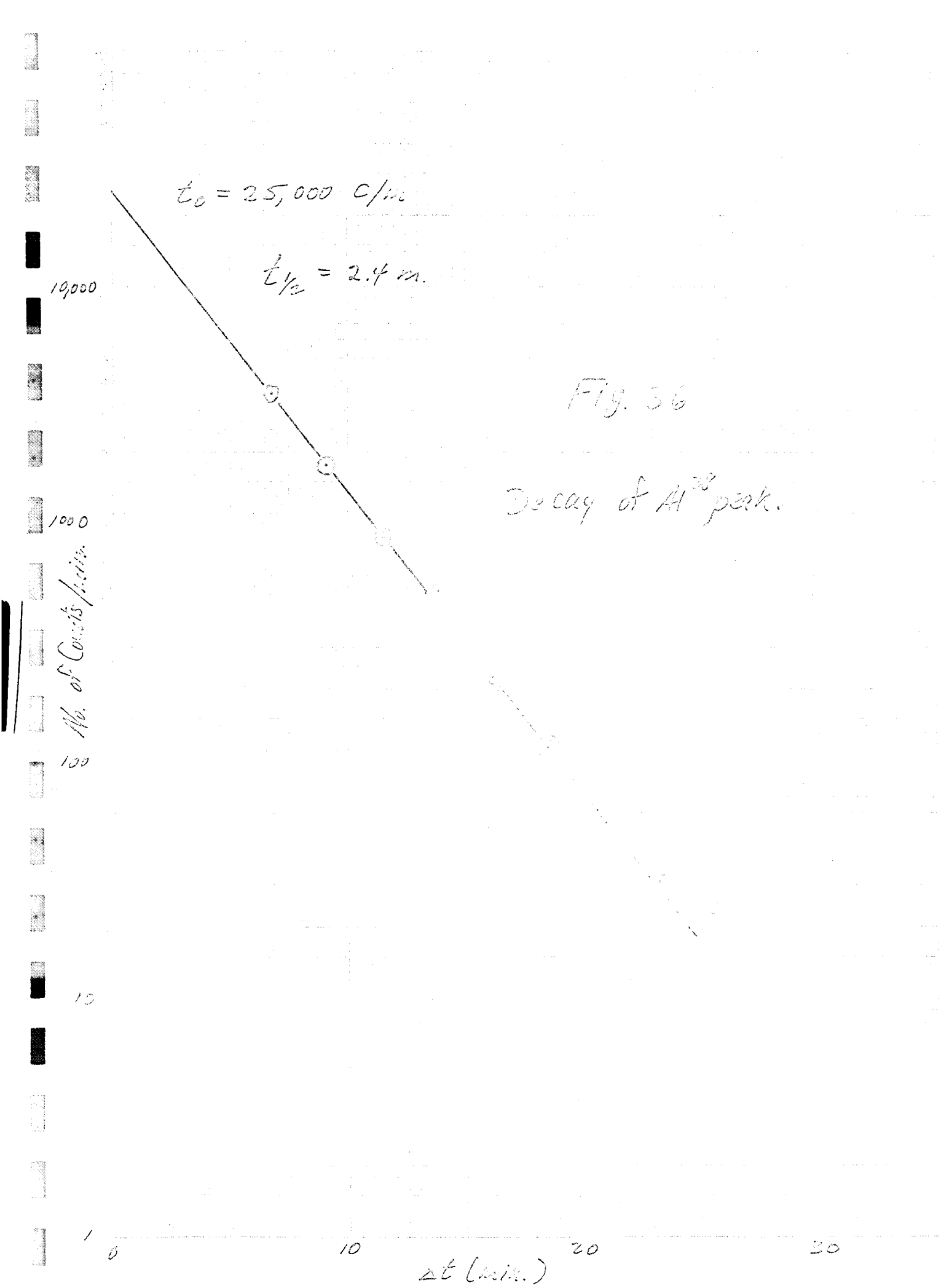

Fig. 36

Decay of Al^{28} peak.

Fig. 37 Artificial spherule WB 1. Brassy magnetic welding bead 440 μ diam. 30 sec irradiation, one-minute count. Δt=5mlls. Identifiable peaks at 0.84 Mev channel 29 (Mn^{56}); 1.4 Mev channel 49 (?) and 1.8 Mev channel 61 (?).

Fig. 38 WB 1 decay curve, Mn^{56}

Fig. 39 WB 1 decay curve, unidentified nuclide

Fig. 40 WB 1 decay curve, unidentified nuclide

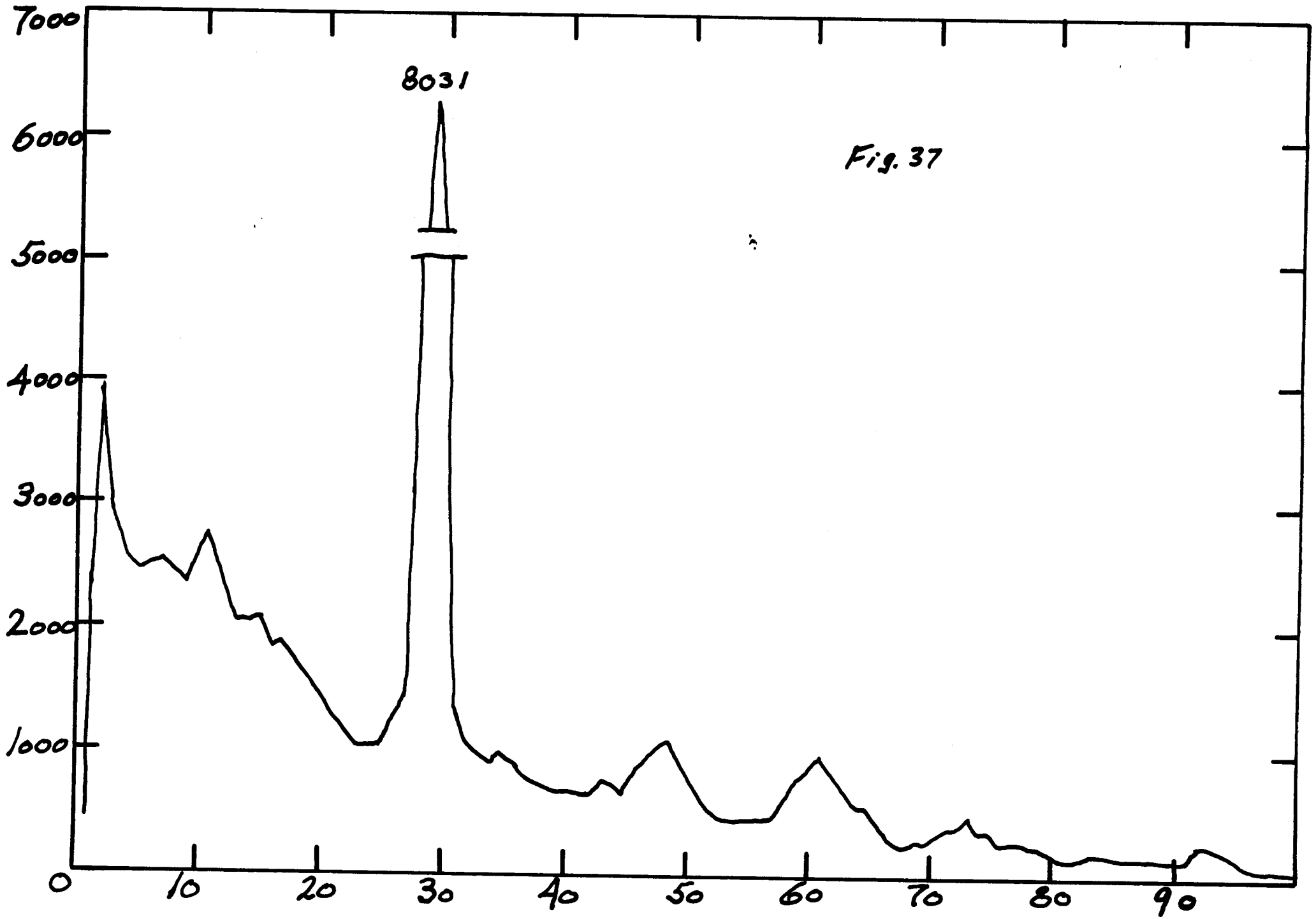
7000
6000
5000
4000
3000
2000
1000
0
8031
10
20
30
40
50
60
70
80
90

Fig. 37

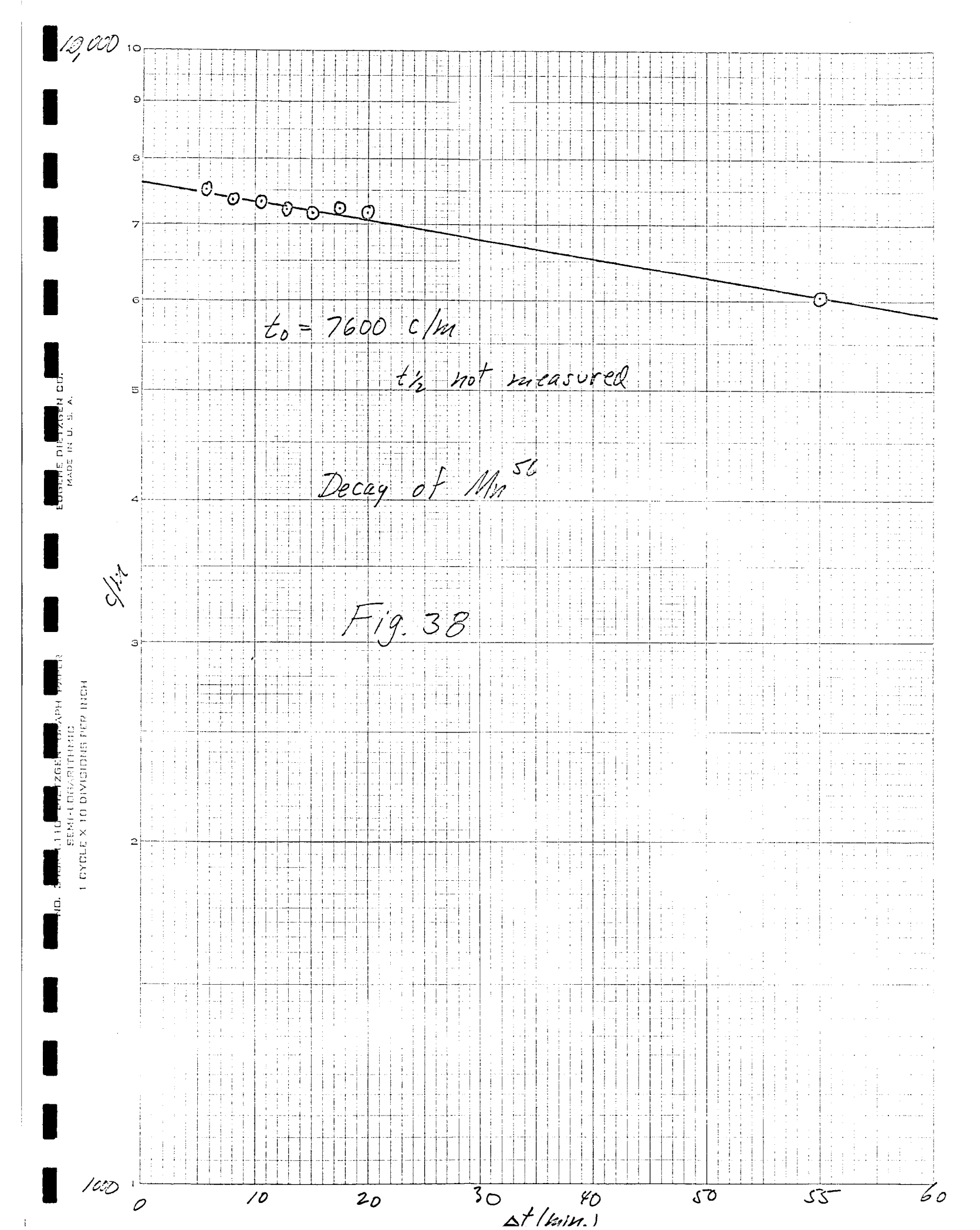
12,000
10
9
8
7
6
5
4
3
2
1000
0
10
20
30
40
50
55
60
c/m
Δt (min.)
t_0 = 7600 c/m
$t_{1/2}$ not measured
Decay of Mn^{56}
Fig. 38
EUGENE DIETZGEN CO.
MADE IN U. S. A.
SEMI-LOGARITHMIC
1 CYCLE X 10 DIVISIONS PER INCH

Fig. 39

Decay curve of peak at Channel 19.

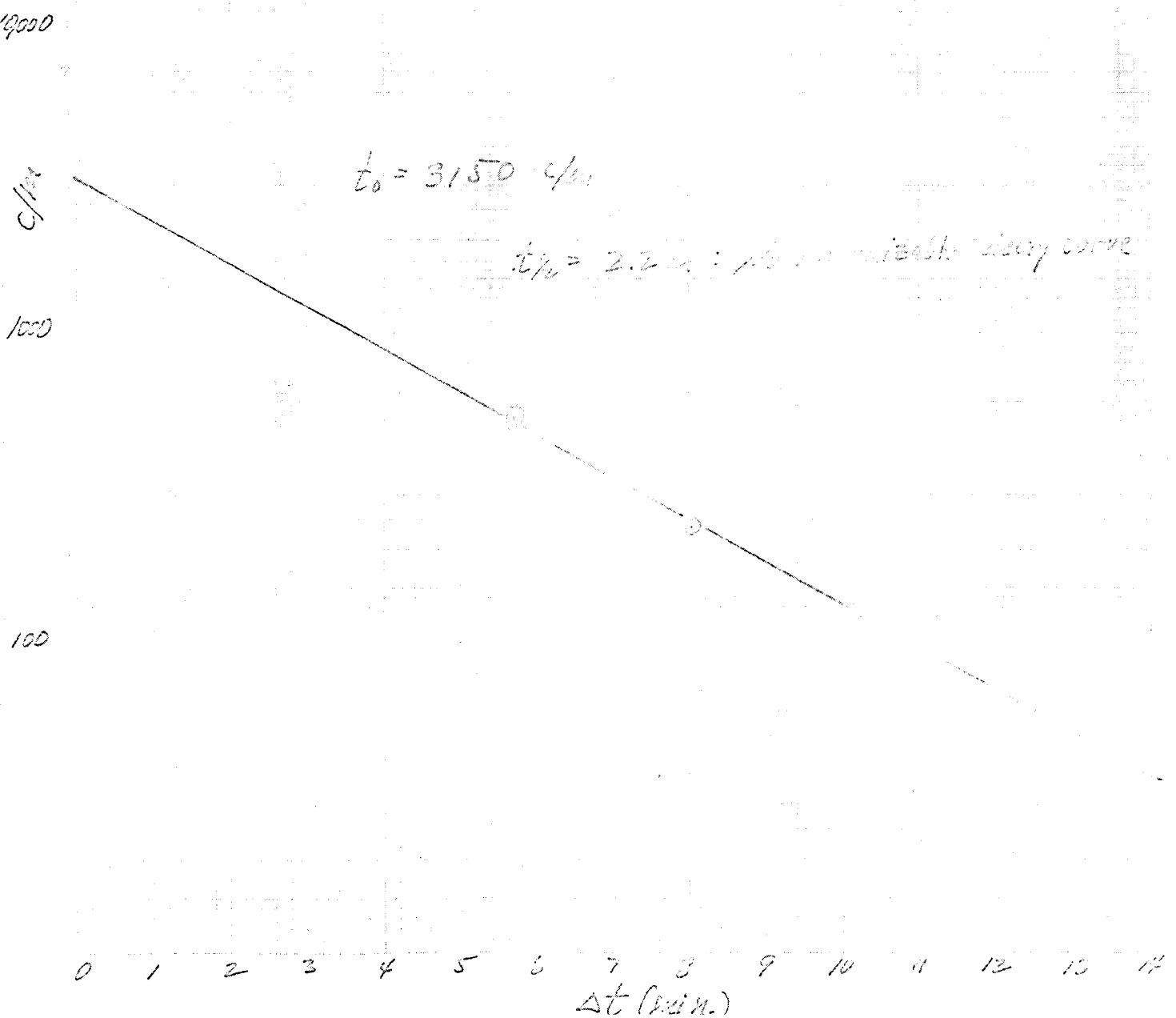

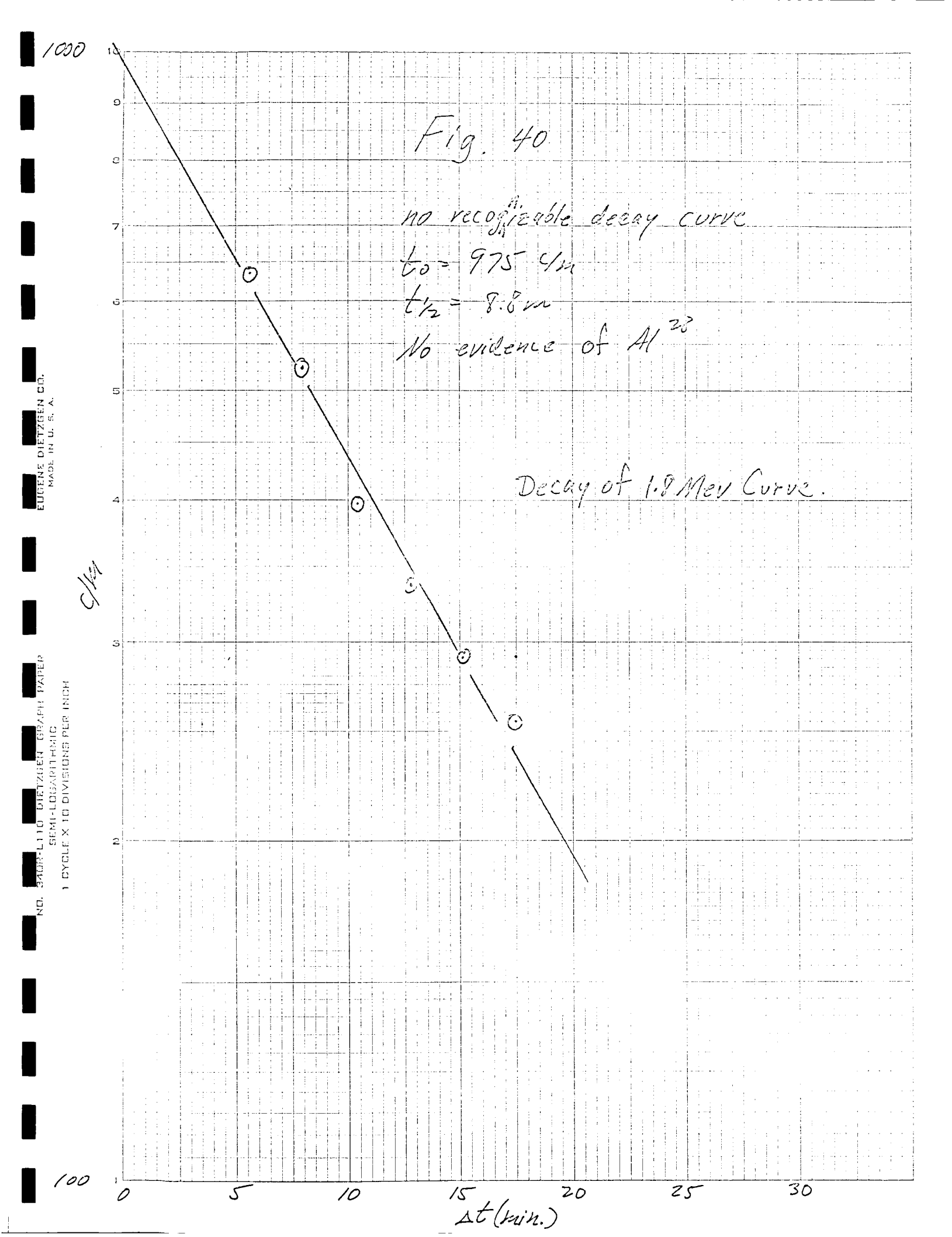
1000
100
c/m
Δt (min.)
0
5
10
15
20
25
30
Fig. 40
no recognizable decay curve
t_0 = 975 c/m
$t_{1/2}$ = 8.8 m
No evidence of A^{23}
Decay of 1.9 Mev Curve.
EUGENE DIETZGEN CO.
MADE IN U. S. A.
NO. 340R-L110 DIETZGEN GRAPH PAPER
SEMI-LOGARITHMIC
1 CYCLE X 10 DIVISIONS PER INCH

Fig. 41 Artificial spherule WB 2. Very shiny, magnetic welding bead 300 μ diameter. 10 sec irradiation, one-minute count. Δt approximately 9 minutes. Identifiable peak at 0.84 Mev channel 29 (Mn^{56}). Unidentified peaks at 0.37 Mev channel 11 and 1.8 Mev channel 62.

Fig. 42 WB 2 decay curve, Mn^{56}

Fig. 43 WB 2 decay curve, 0.37 Mev

Fig. 44 WB 2 decay curve, 1.8 Mev

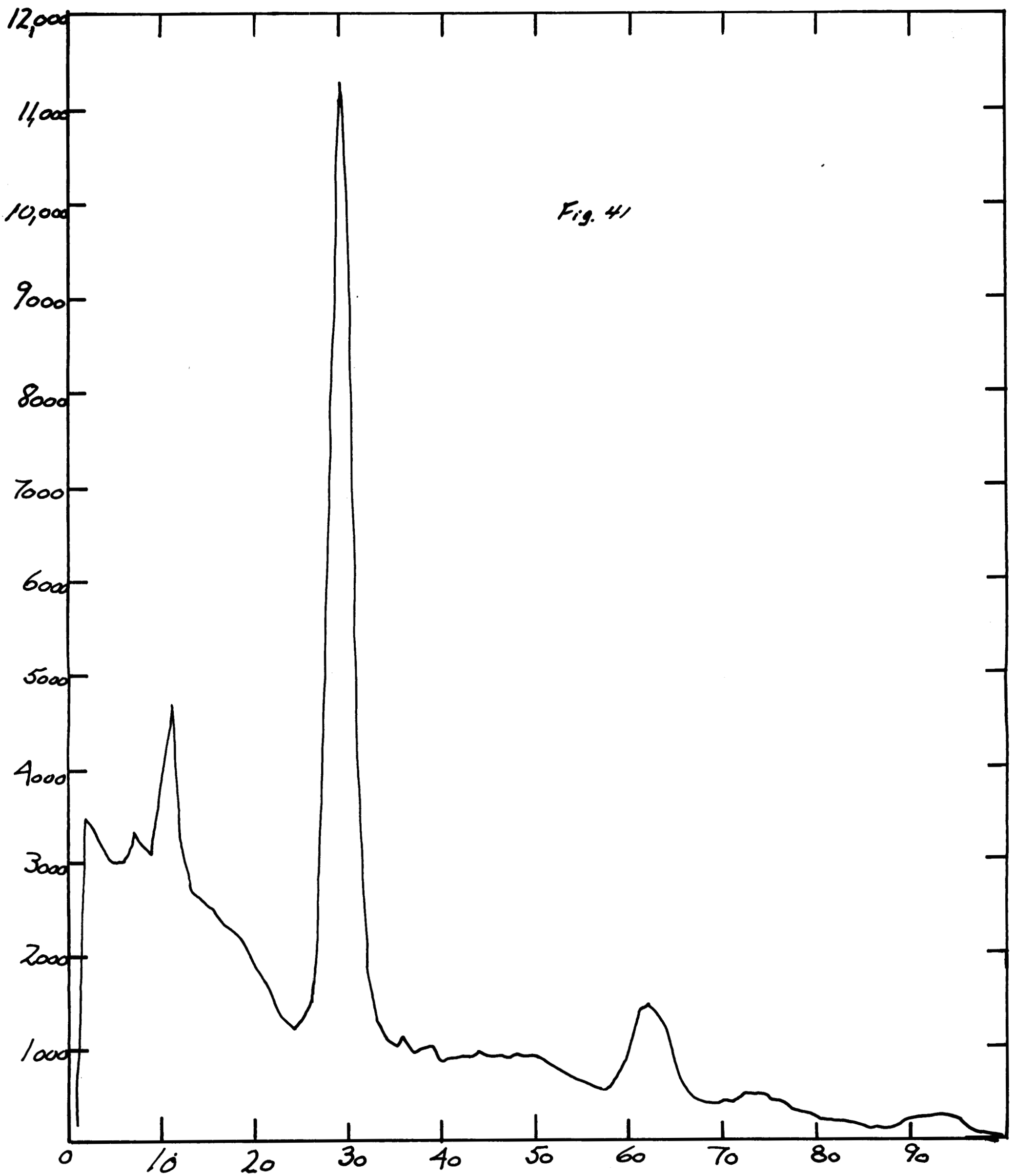
12,000
11,000
10,000
9000
8000
7000
6000
5000
4000
3000
2000
1000
0
10
20
30
40
50
60
70
80
90

Fig. 41

Fig. 42

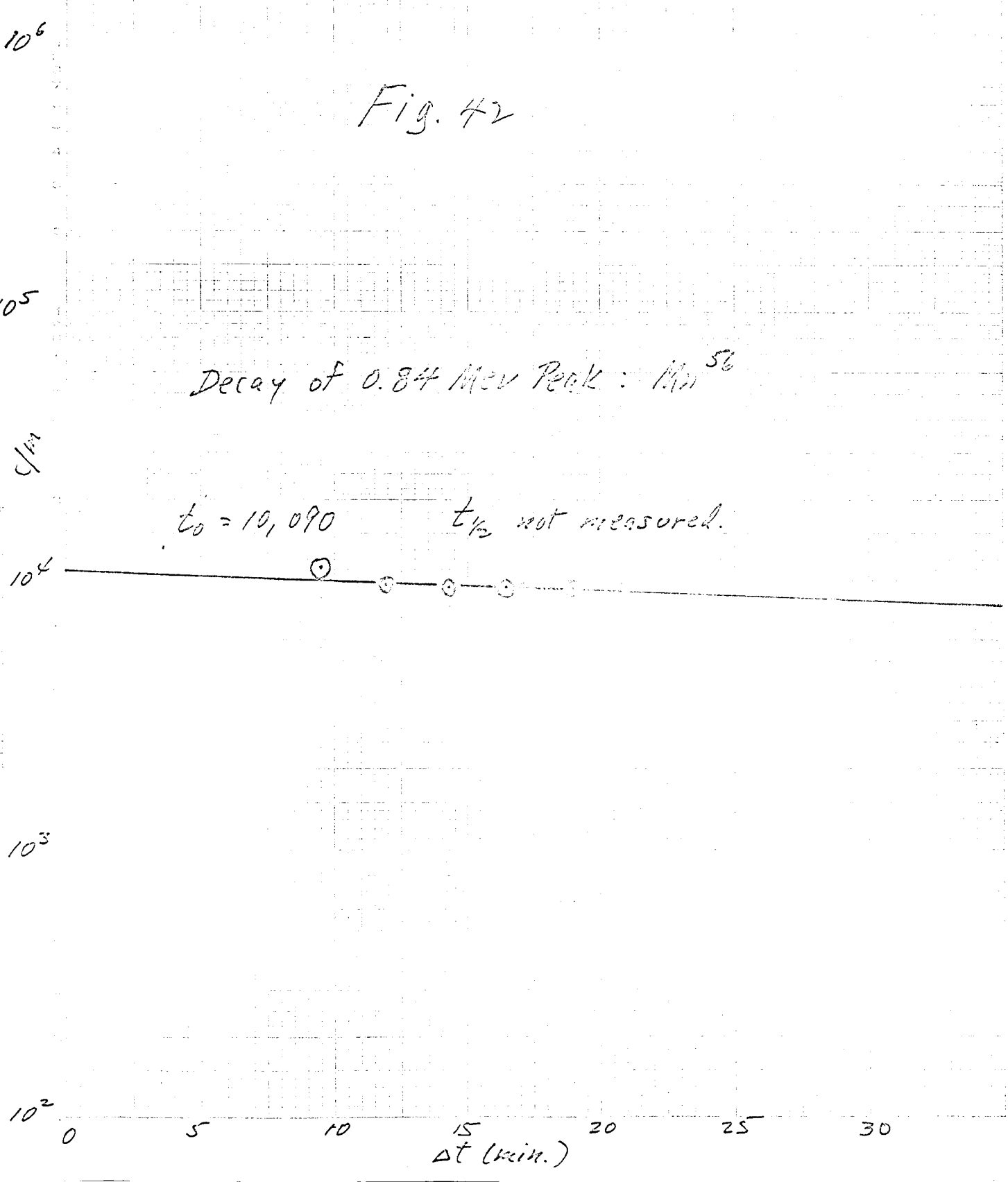
Decay of 0.84 Mev Peak : Mn^{56}
t_0 = 10,090
$t_{1/2}$ not measured.
10^6
10^5
10^4
10^3
10^2
C/m
0
5
10
15
20
25
30
Δt (min.)

Fig. 43

Decay of 0.37 Mev Peak

t_0 = 7100 c/m

$t_{1/2}$ = 5.25 min

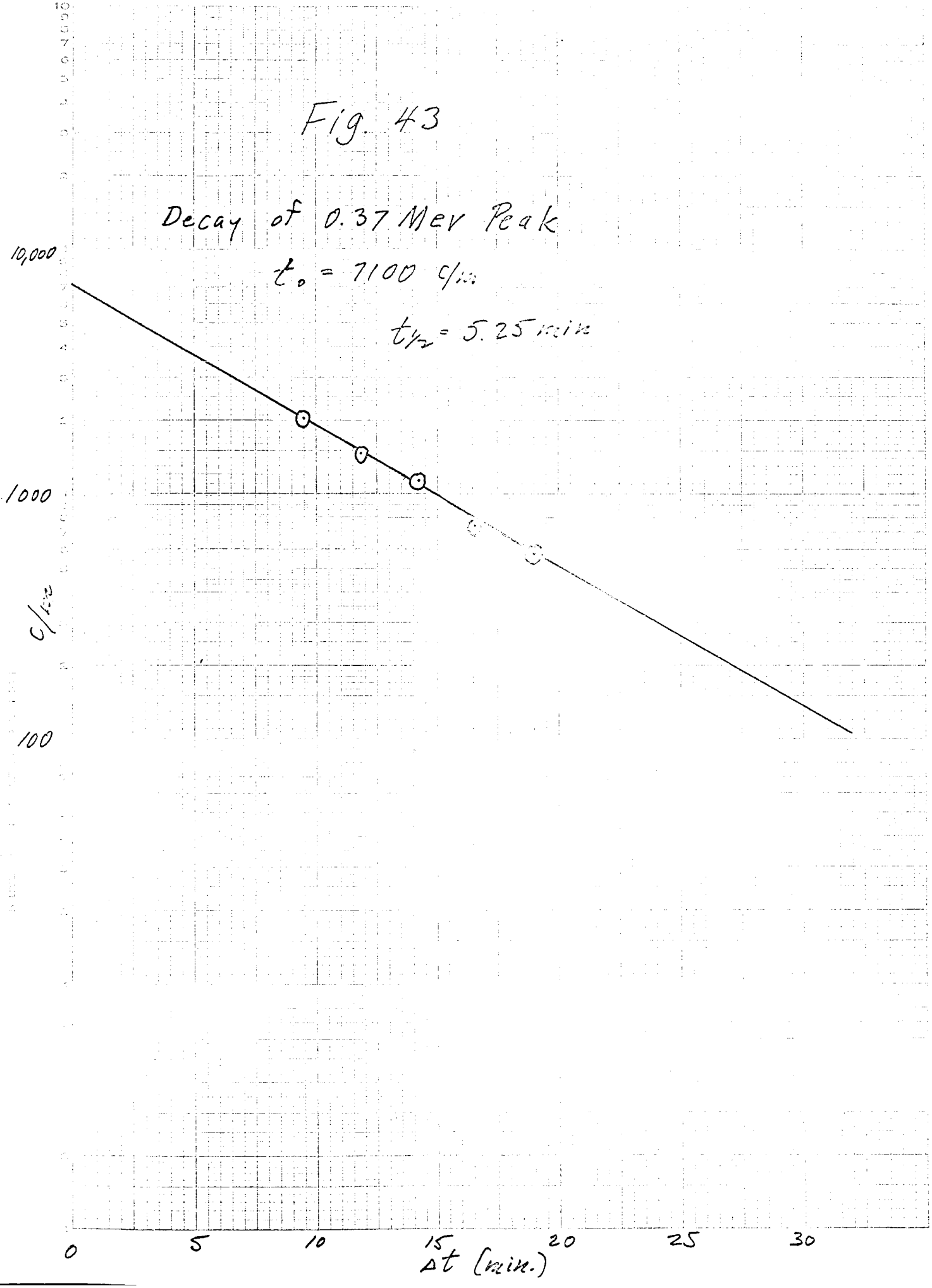

Fig. 44

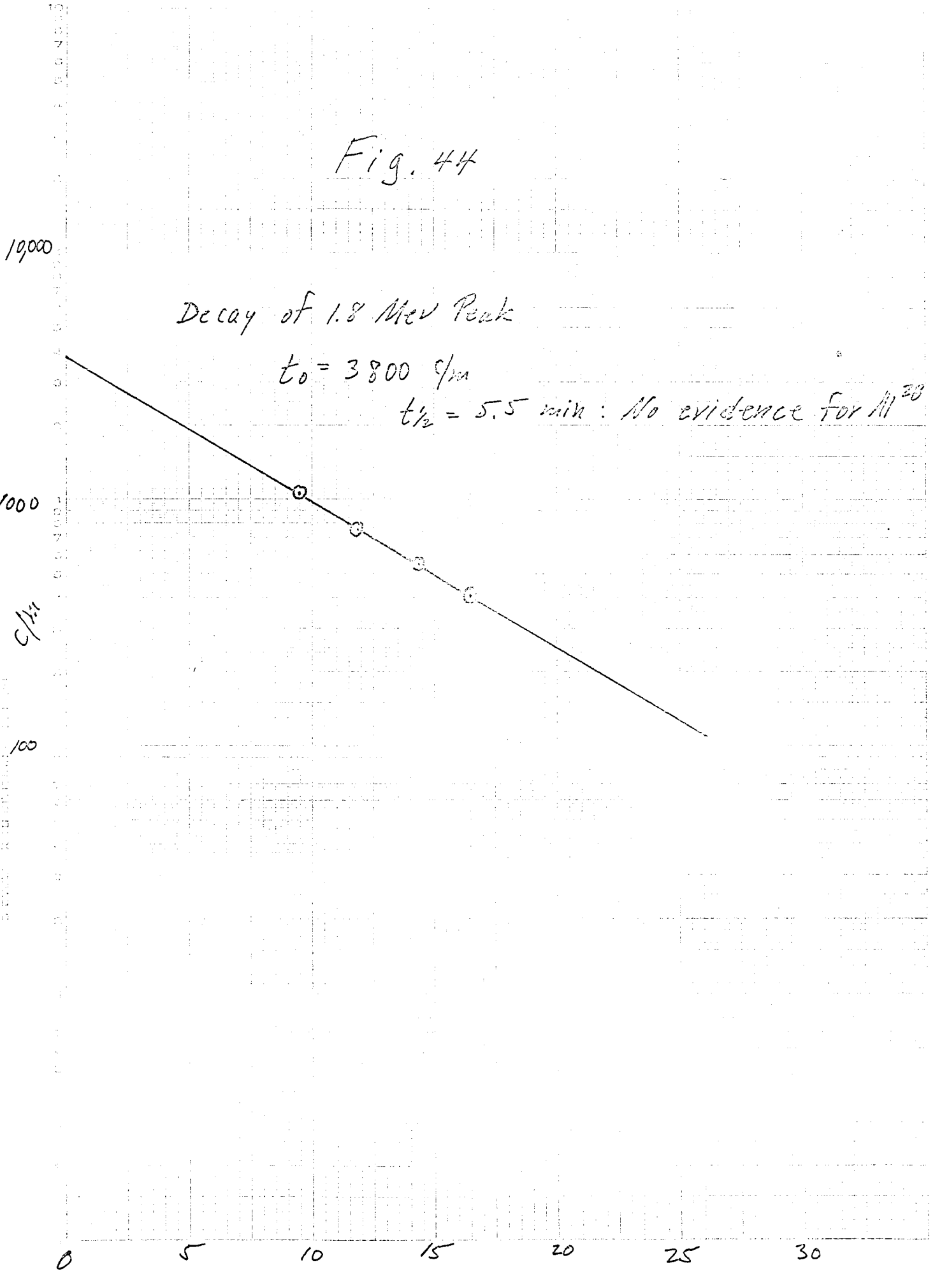

Decay of 1.8 Mev Peak

t_0 = 3800 c/m

$t_{1/2}$ = 5.5 min : No evidence for Al^{28}

Fig. 45 Artificial spherule WB 3. Shiny, magnetic welding bead 600μ diam., 30 sec irradiation, one-minute count. Δt=4m18s. Identifiable peaks at 0.84 Mev channel 29 (Mn^{56}); 1.43 Mev channel 50 (V^{52}). Unidentified peak at 1.8 Mev channel 62.

Fig. 46 WB 3 decay curve, Mn^{56}

Fig. 47 WB 3 decay curve, V^{52}

Fig. 48 WB 3 decay curve, 1.8 Mev.

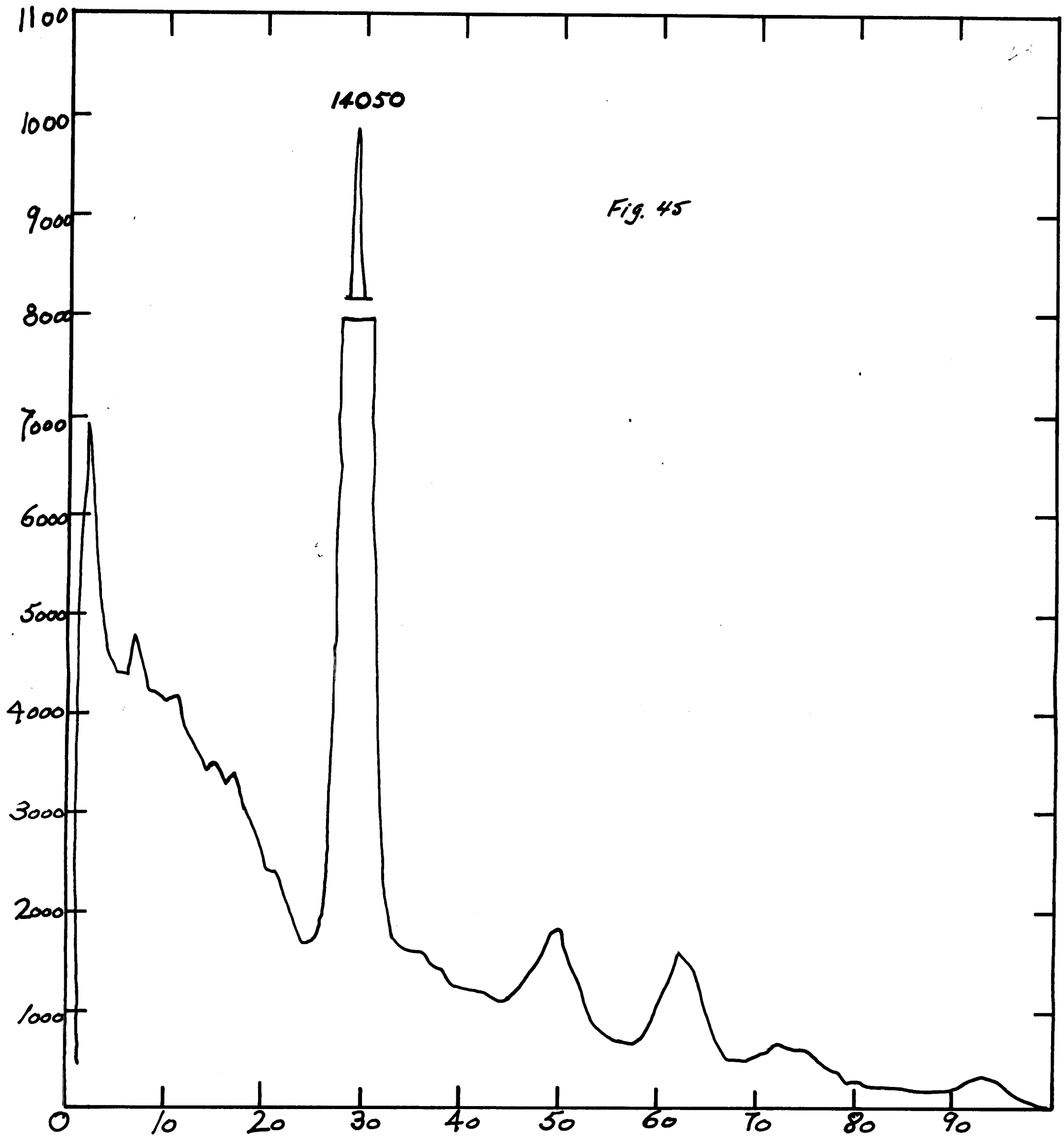
1100
1000
9000
8000
7000
6000
5000
4000
3000
2000
1000
14050
0
10
20
30
40
50
60
70
80
90

Fig. 45

Fig. 46.

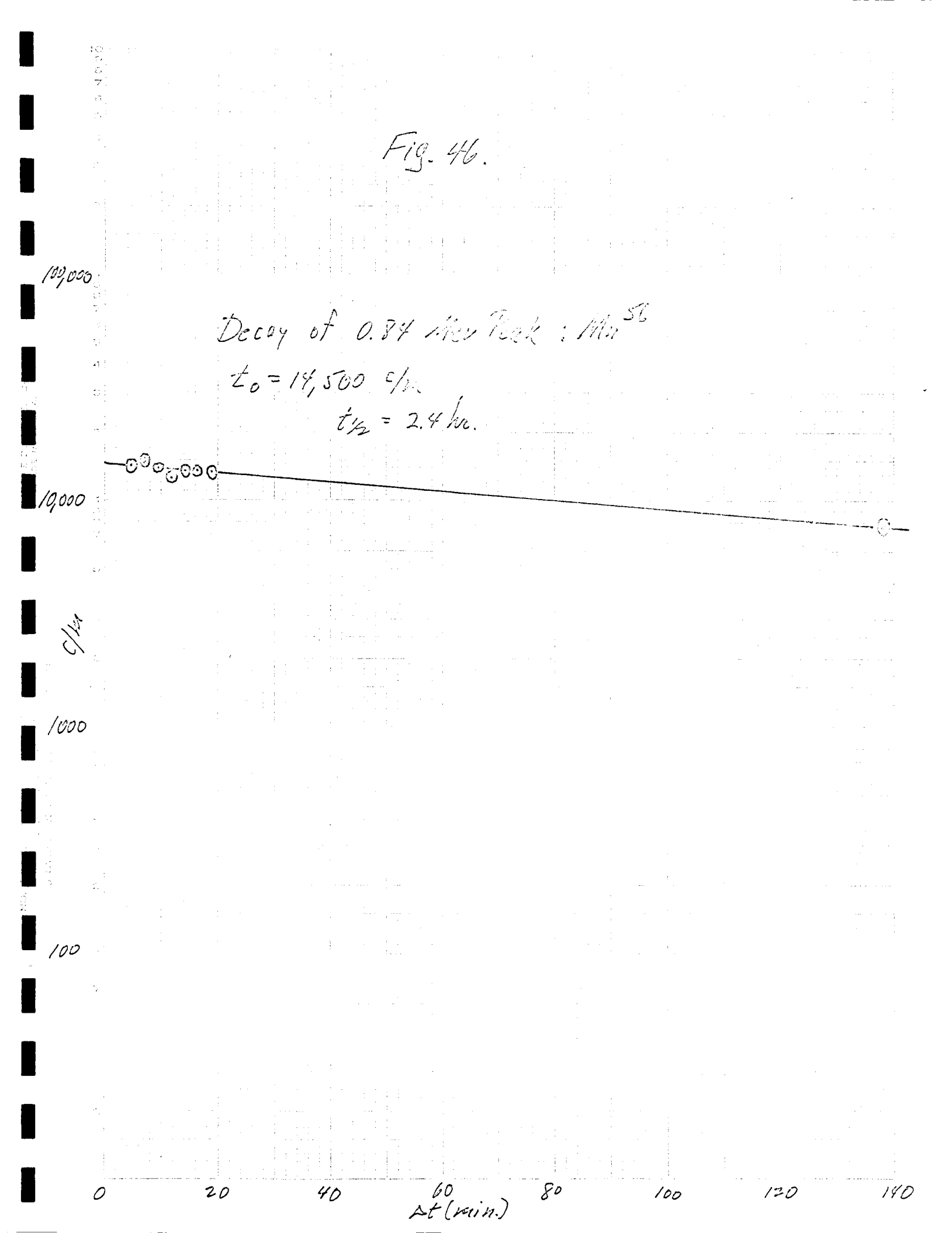
Decay of 0.87 MeV Peak : Mn^{54}
$t_0 = 14,500$ c/m.
$t_{1/2} = 2.4$ hr.
100,000
10,000
1000
100
c/m
0
20
40
60
80
100
120
140
Δt (min.)

Fig. 47

Decay of 1.4 Mev Peak : V^{52}

$t_0 = 2800$ c/m

$t_{1/2} = 4'$ m

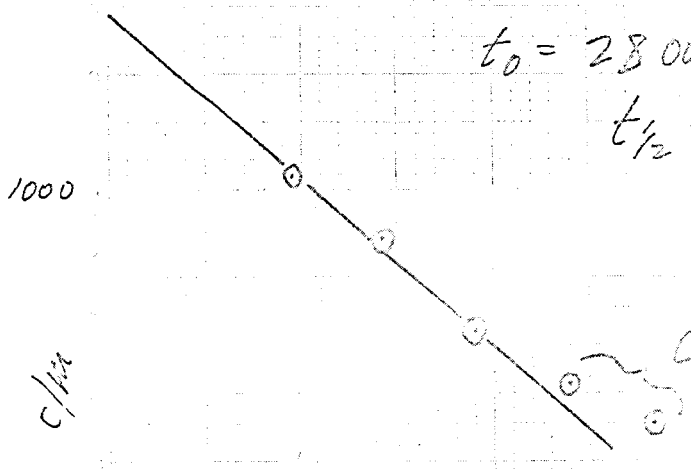

Curve merges here with longer-lived background.

Fig. 48

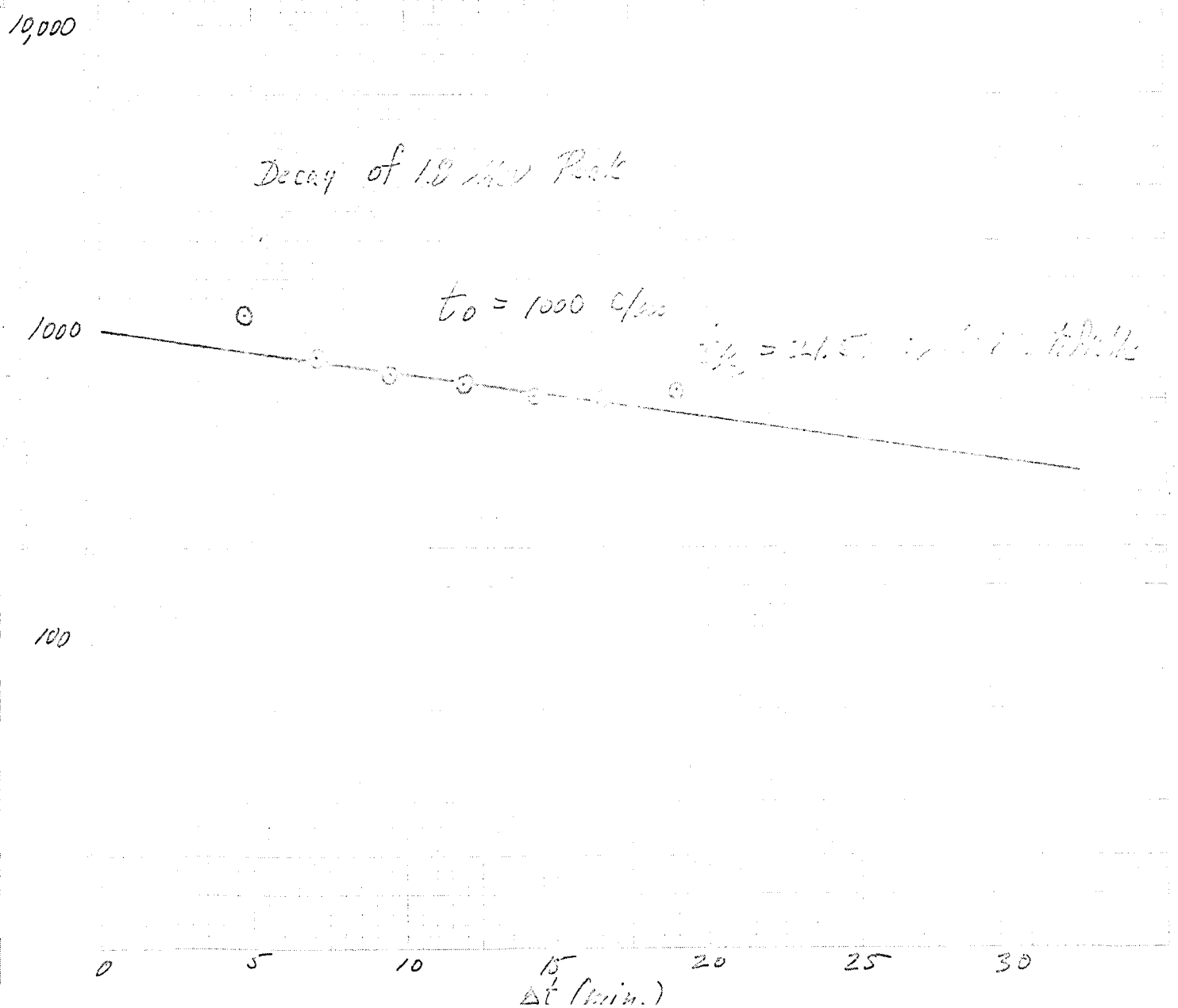
10,000
Decay of 1.8 MeV Peak
t_0 = 1000 c/m
1000
100
0
5
10
15
20
25
30
Δt (min.)

Fig. 49 Artificial spherule WB 4. Shiny, magnetic welding bead 220μ diam., 30-sec irradiation, one-minute count. Δt=9m14s. Only three spectra were taken, so decay curves not calculated. Identifiable peak is 0.84 Mev channel 30 (Mn^{56}).

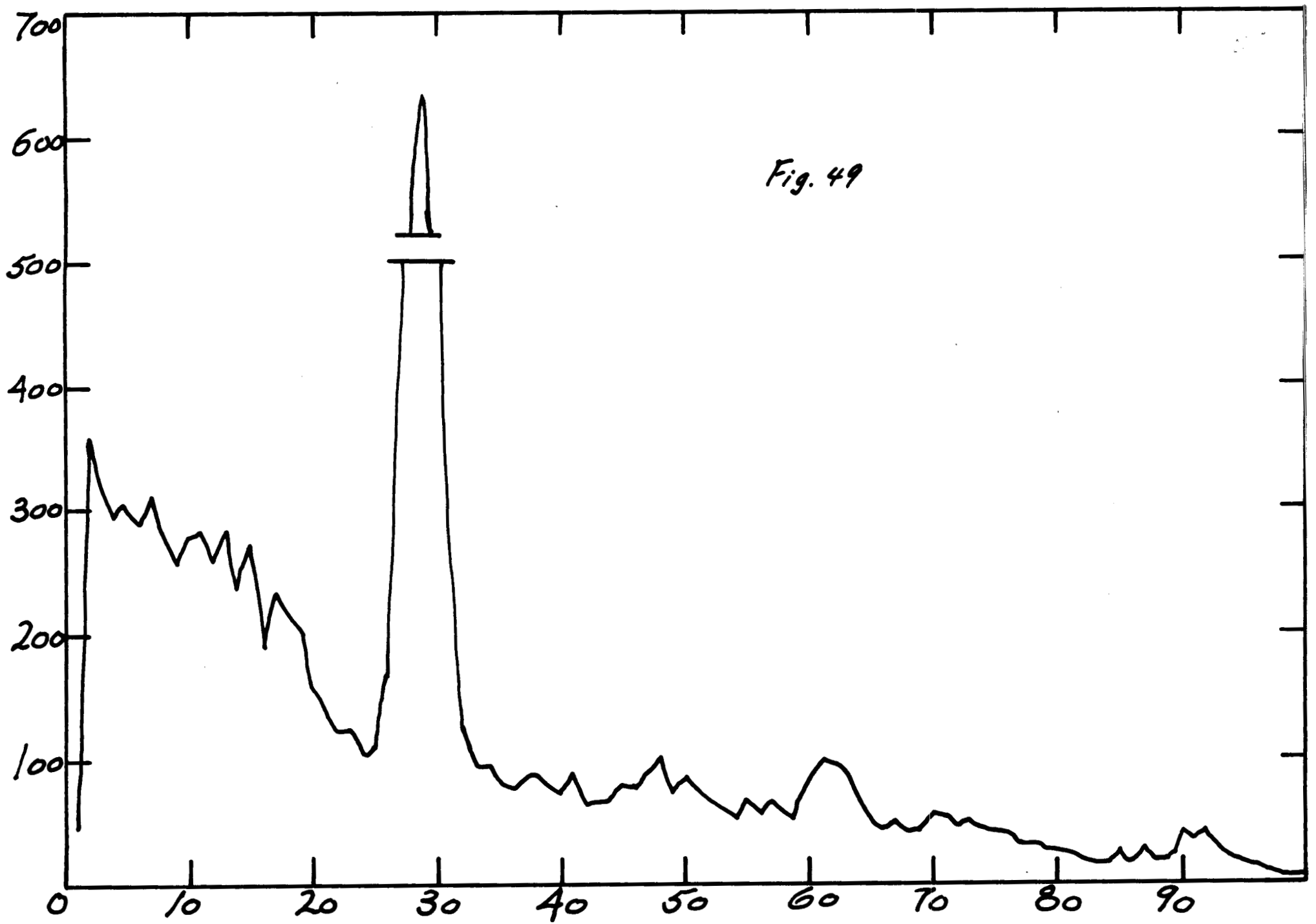

Fig. 49

Fig. 50 Spherule of unknown origin PN 1 collected in plankton net at ocean surface. Black, magnetic, 250μ diam. 30 sec irradiation, one-minute count. Δt=5m33s. Identifiable peaks at 0.84 Mev channel 29 (Mn^{56}); 1.4 Mev channel 49 (V^{52}).

Fig. 51 PN 1 decay curve, Mn^{56}

Fig. 52 PN 1 decay curve, V^{52}

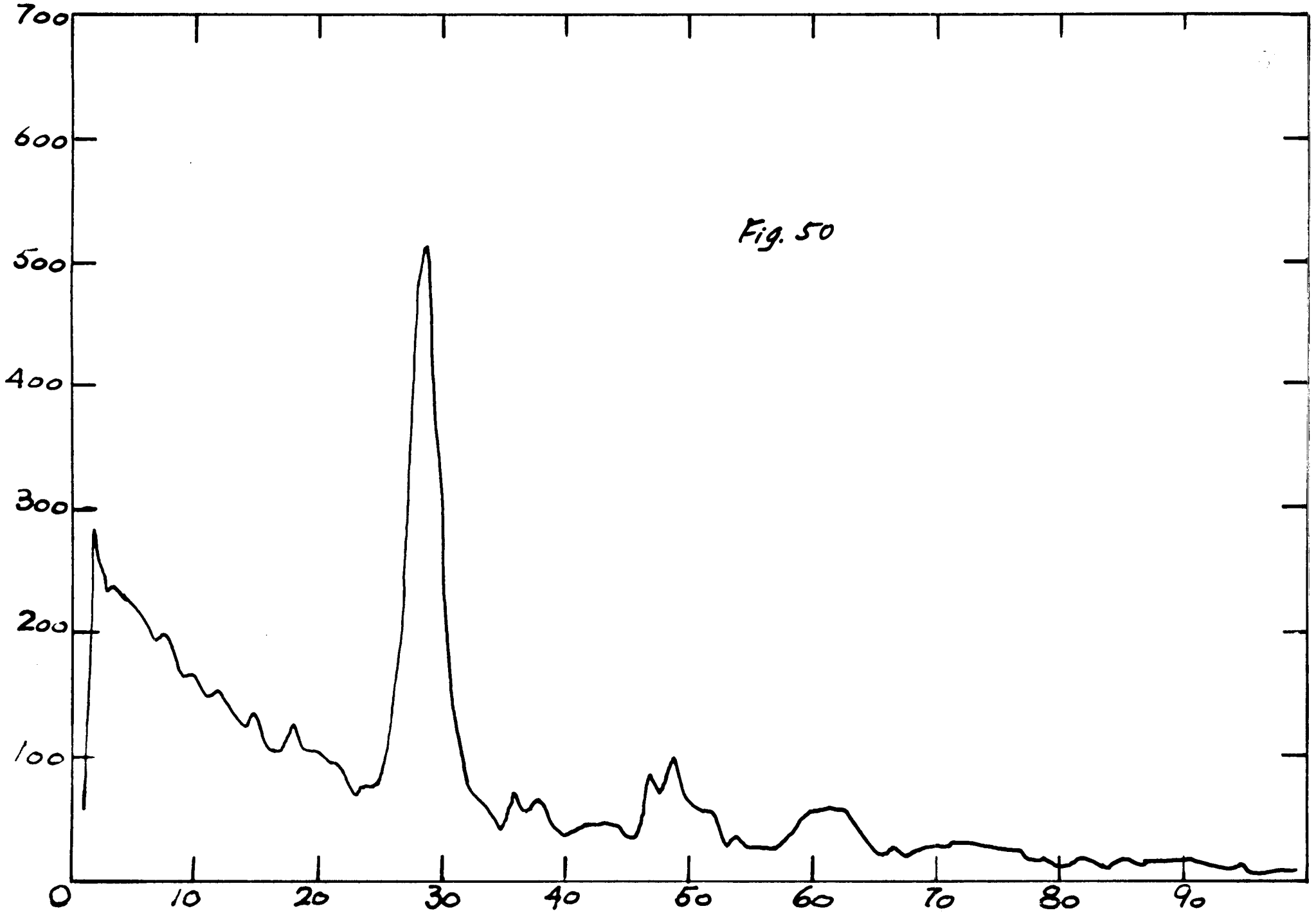

Fig. 50

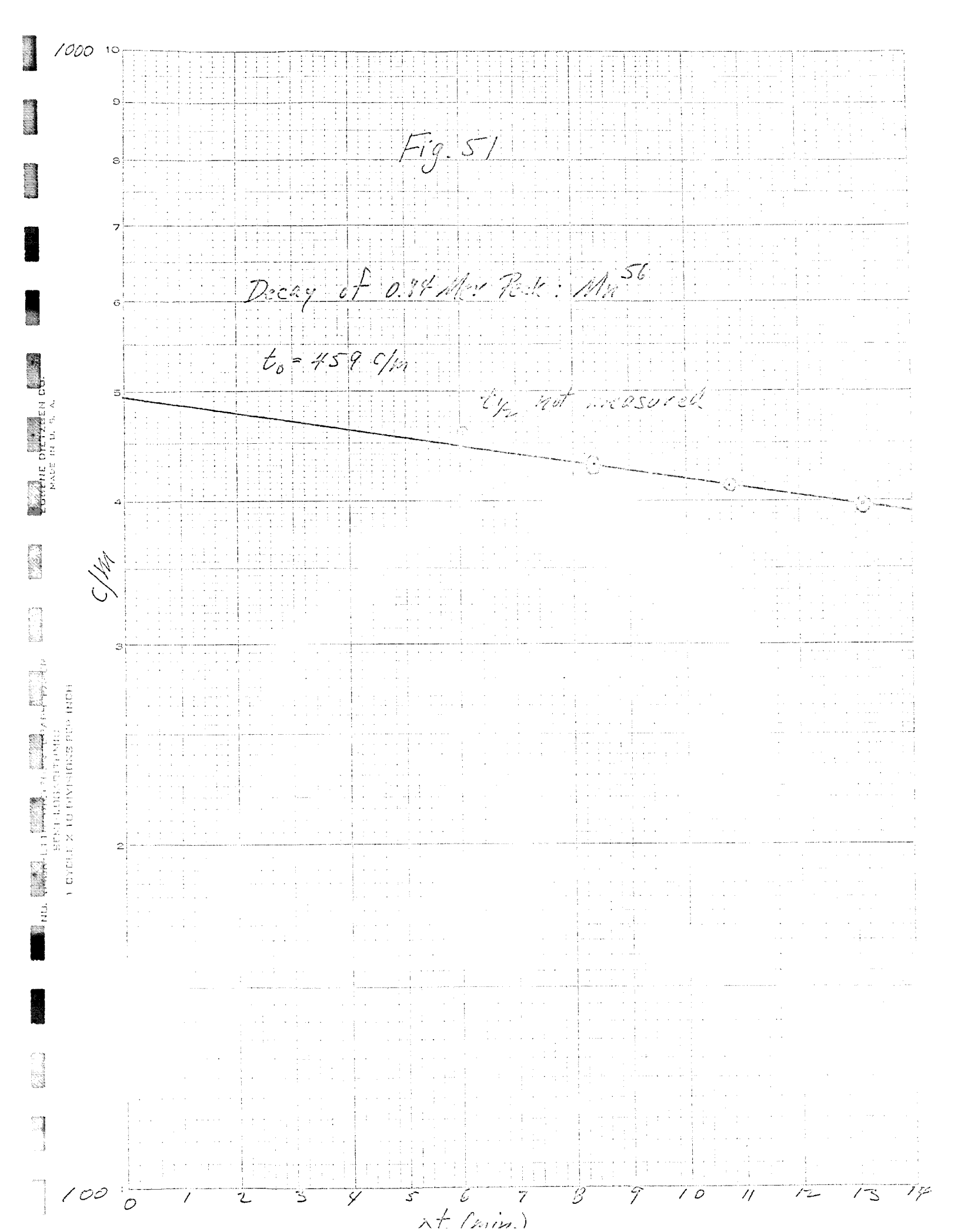
Fig. 51
Decay of 0.84 Mev Peak : Mn^{56}
t_0 = 459 c/m
$t_{1/2}$ not measured
c/m
1000
100
10
9
8
7
6
5
4
3
2
0 1 2 3 4 5 6 7 8 9 10 11 12 13 14
Δt (min.)

Fig. 52

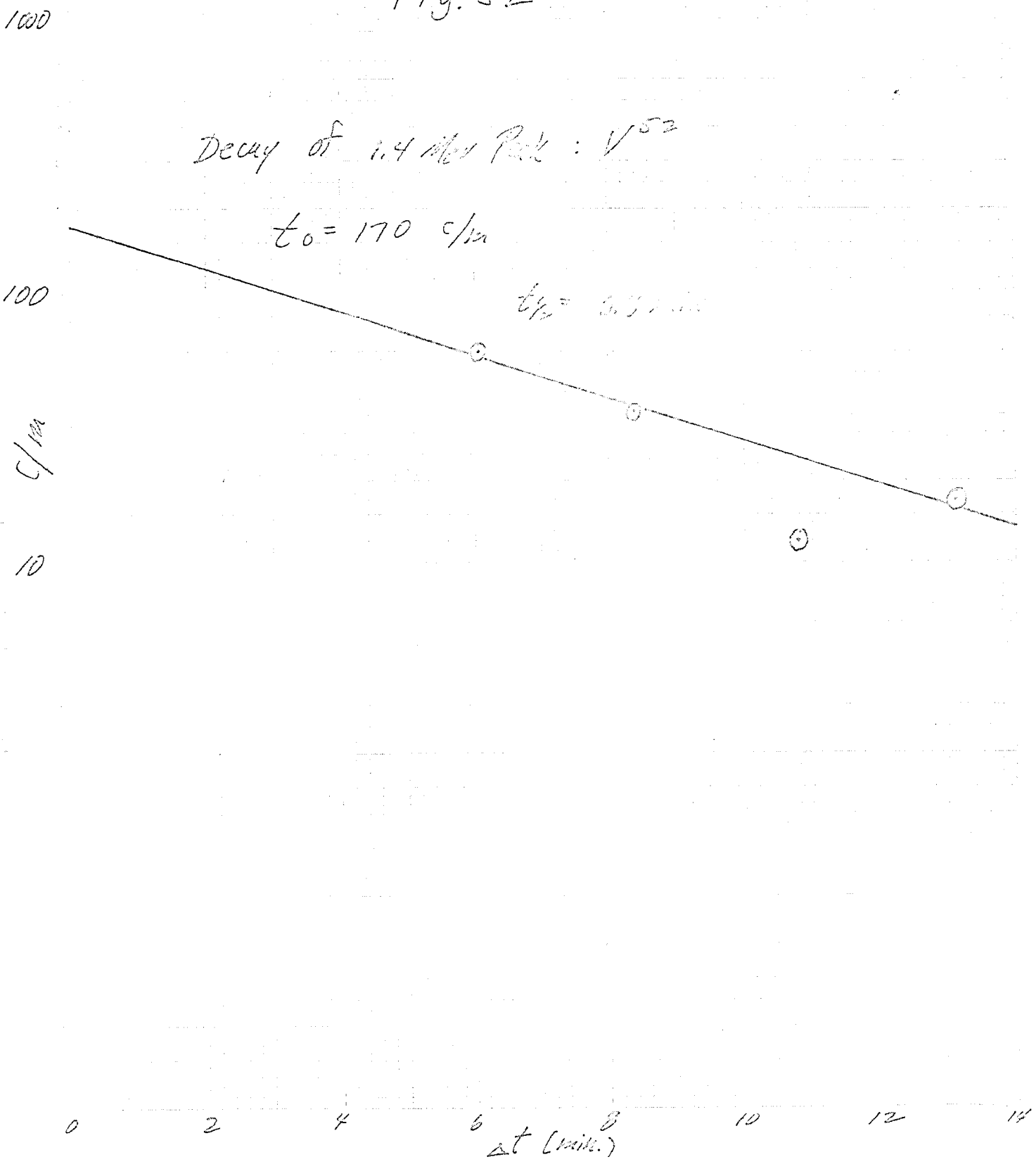
1000
100
10
c/m
Decay of 1.4 Mev Pk : V^52
t_0 = 170 c/m
$t_{1/2}$ = 3.7 m
0
2
4
6
8
10
12
14
Δt (min.)

Fig. 53 Spherule of unknown origin PN 2 collected in plankton net at ocean surface. Black, magnetic, 300μdiam. 10 sec irradiation, one-minute count. Δt=4m23s. Identifiable peaks at 0.84 Mev channel 29 (Mn^{56}); 1.8 Mev channel 61 (Al^{28}). Unidentified peak at 0.37 Mev channel 10.

Fig. 54 PN 2 decay curve, Mn^{56}

Fig. 55 PN 2 decay curve, Al^{28}

Fig. 56 Pn 2 decay curve, 0.37 Mev peak

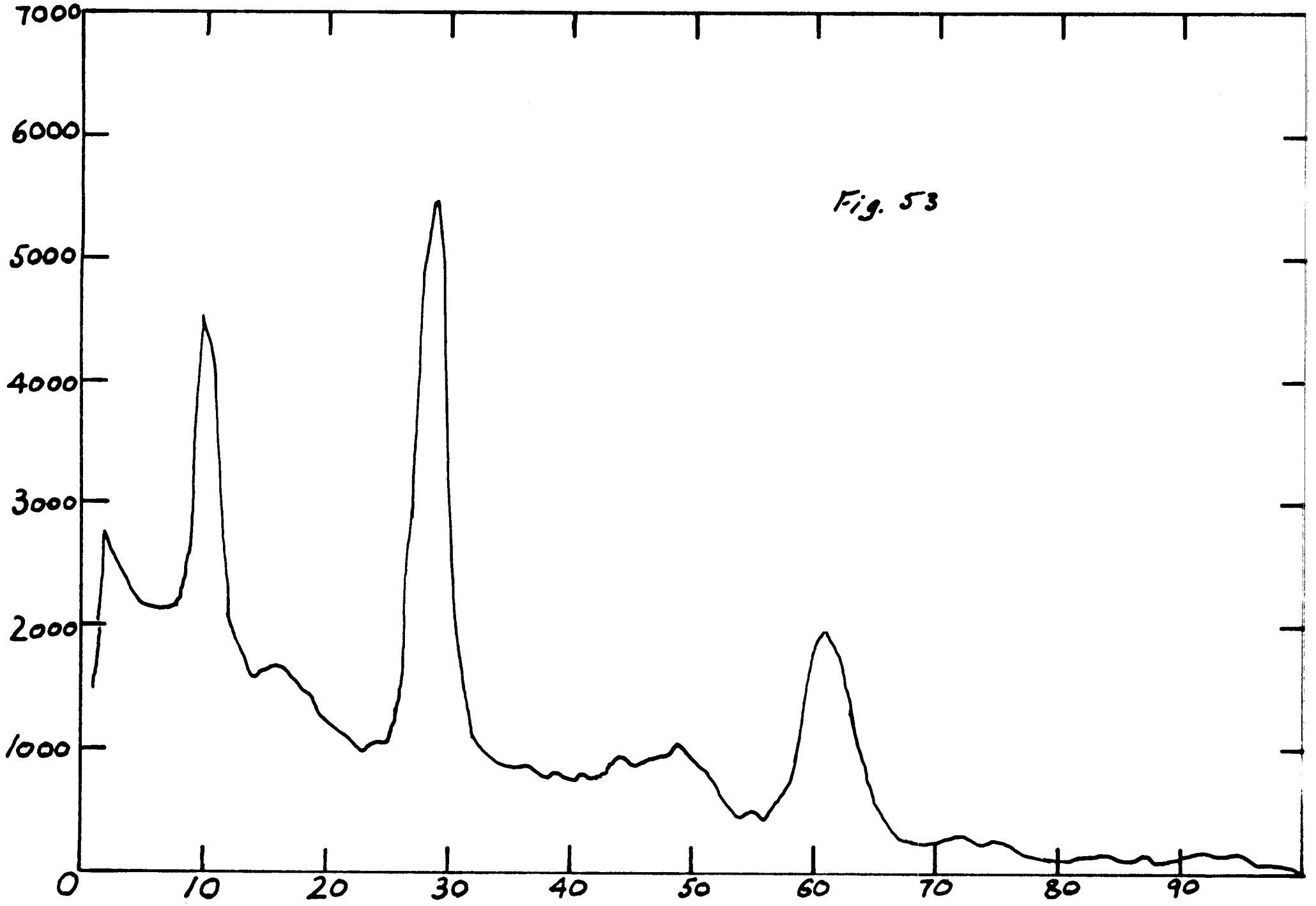

Fig. 53

1900

Fig. 54

Decay of 0.84 Mev Peak : Mn^{56}

$t_0 = 4750$ c/hr.

$t_{1/2} = 2.5$ hr.

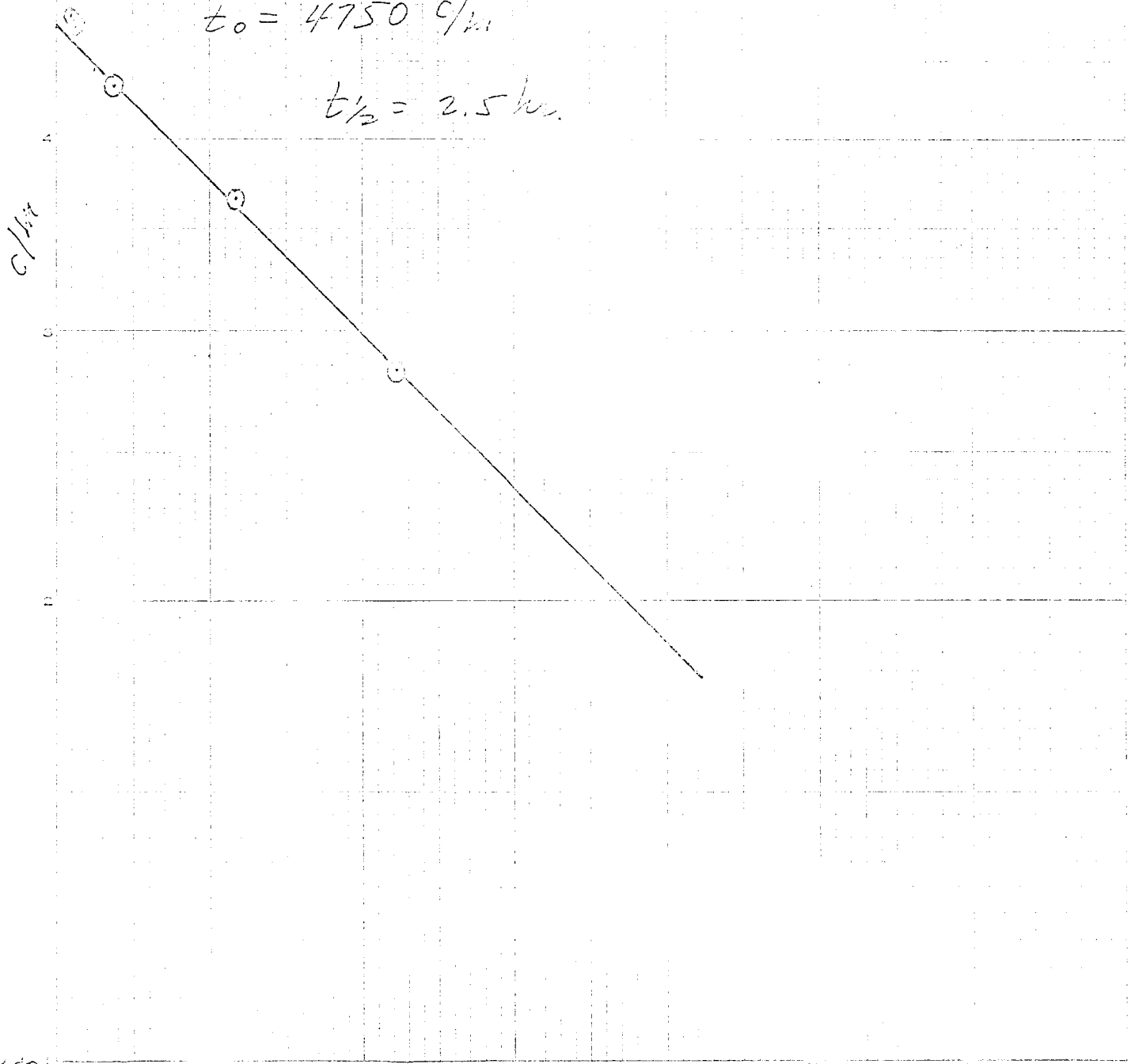

Fig. 55

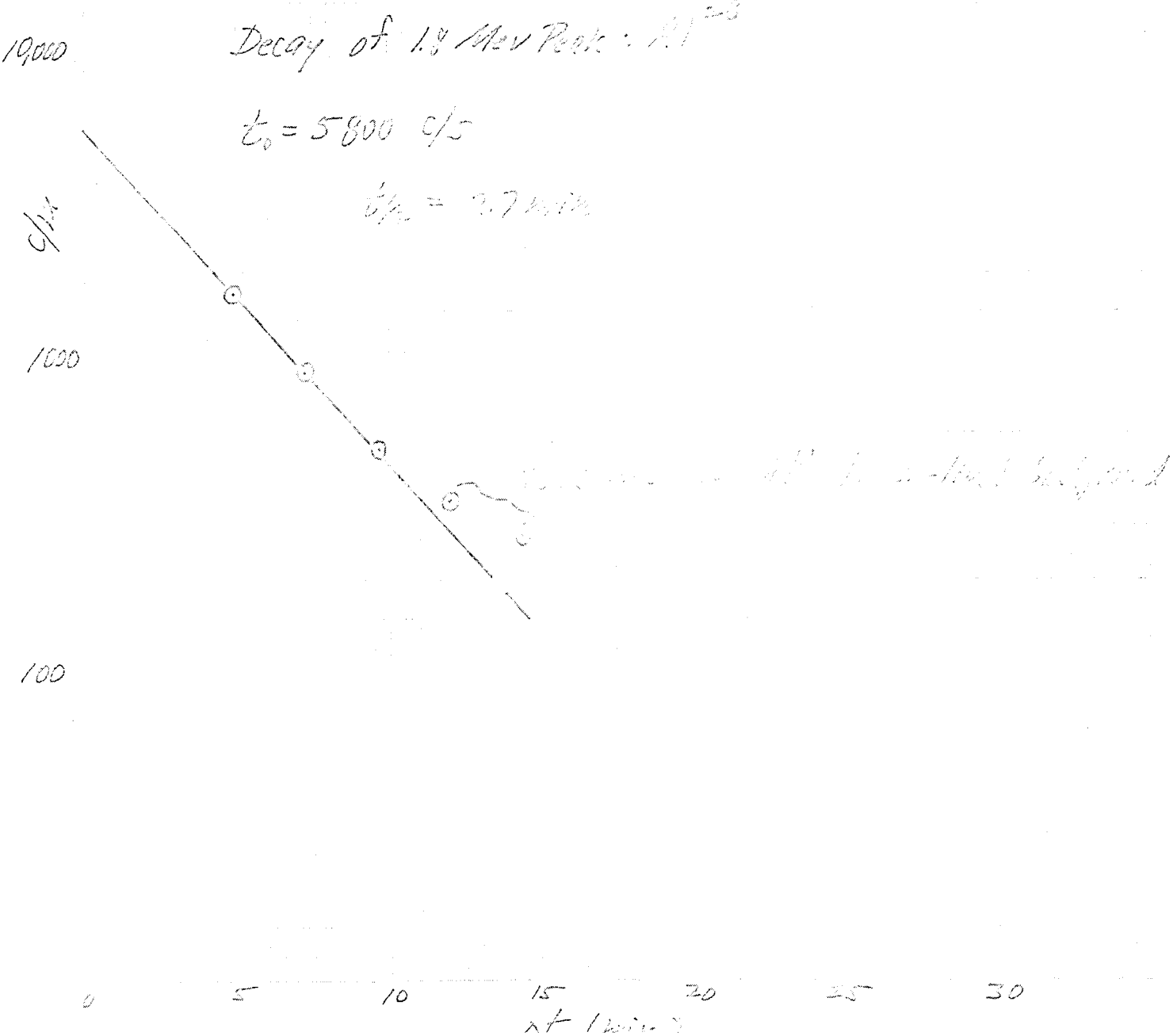
Decay of 1.8 Mev Peak
t_0 = 5800 c/s
$t_{1/2}$ = 2.7 min
c/μc
10000
1000
100
0
5
10
15
20
25
30
Δt (min.)

Fig. 56.

Decay of 0.37 Mev Peak: Not identified.

$C_0' = 47{,}000$ c/m

$t_{1/2} = 5.1$ min.

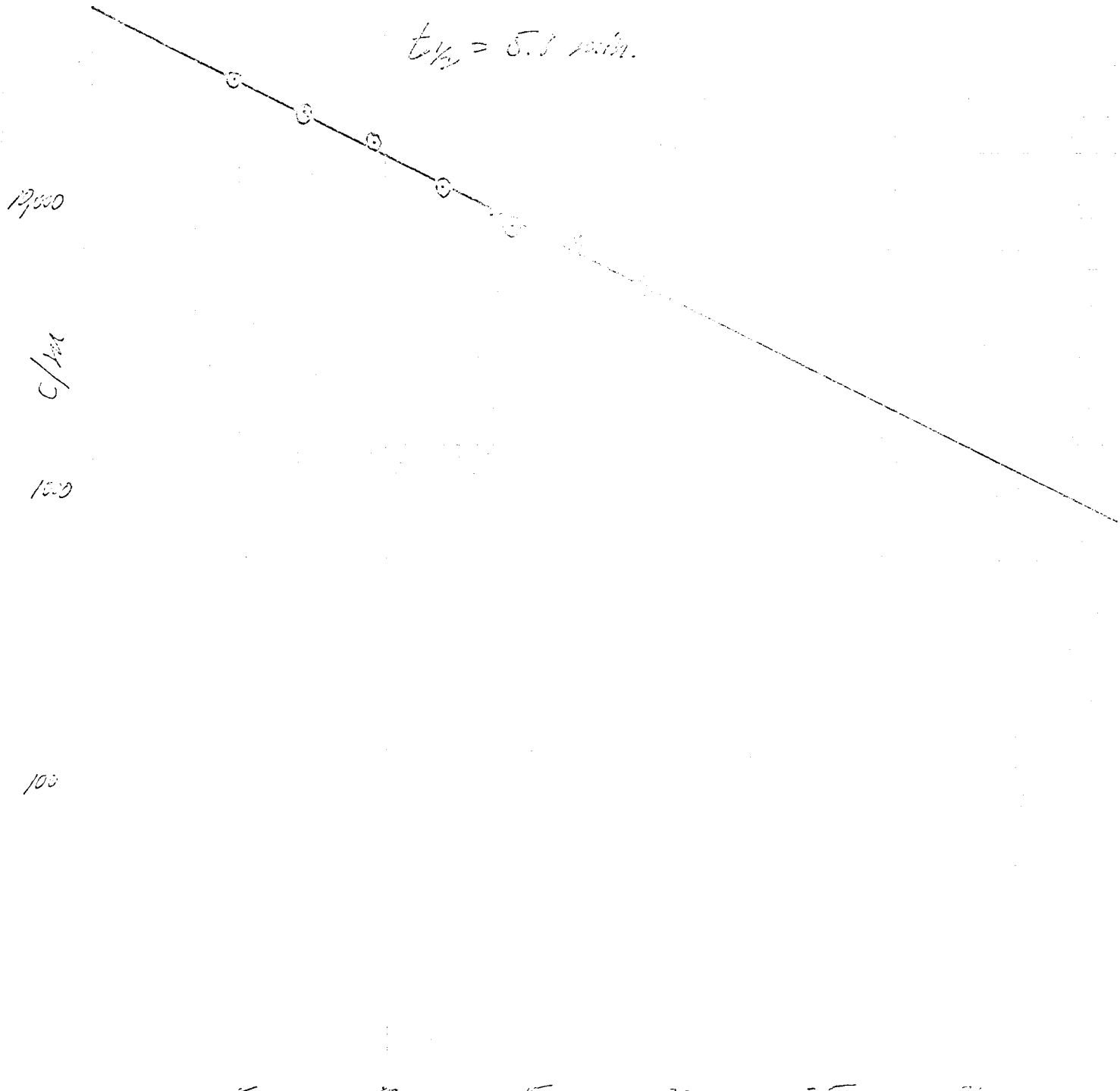

Fig. 57 Spherule of unknown origin PN 3 collected in plankton net at ocean surface. Black, magnetic, 400μ diam. 30 sec irradiation, one-minute count. Δt=4m49s. Identifiable peaks are at 0.84 Mev channel 29 (Mn^{56}) and 1.8 Mev channel 61 (Al^{28}). The peak at 0.37 Mev channel 11 is unidentified.

Fig. 58 PN 3 decay curve, Mn^{56}

Fig. 59 PN 3 decay curve, Al^{28}

Fig. 60 PN 3 decay curve, 0.37 Mev peak

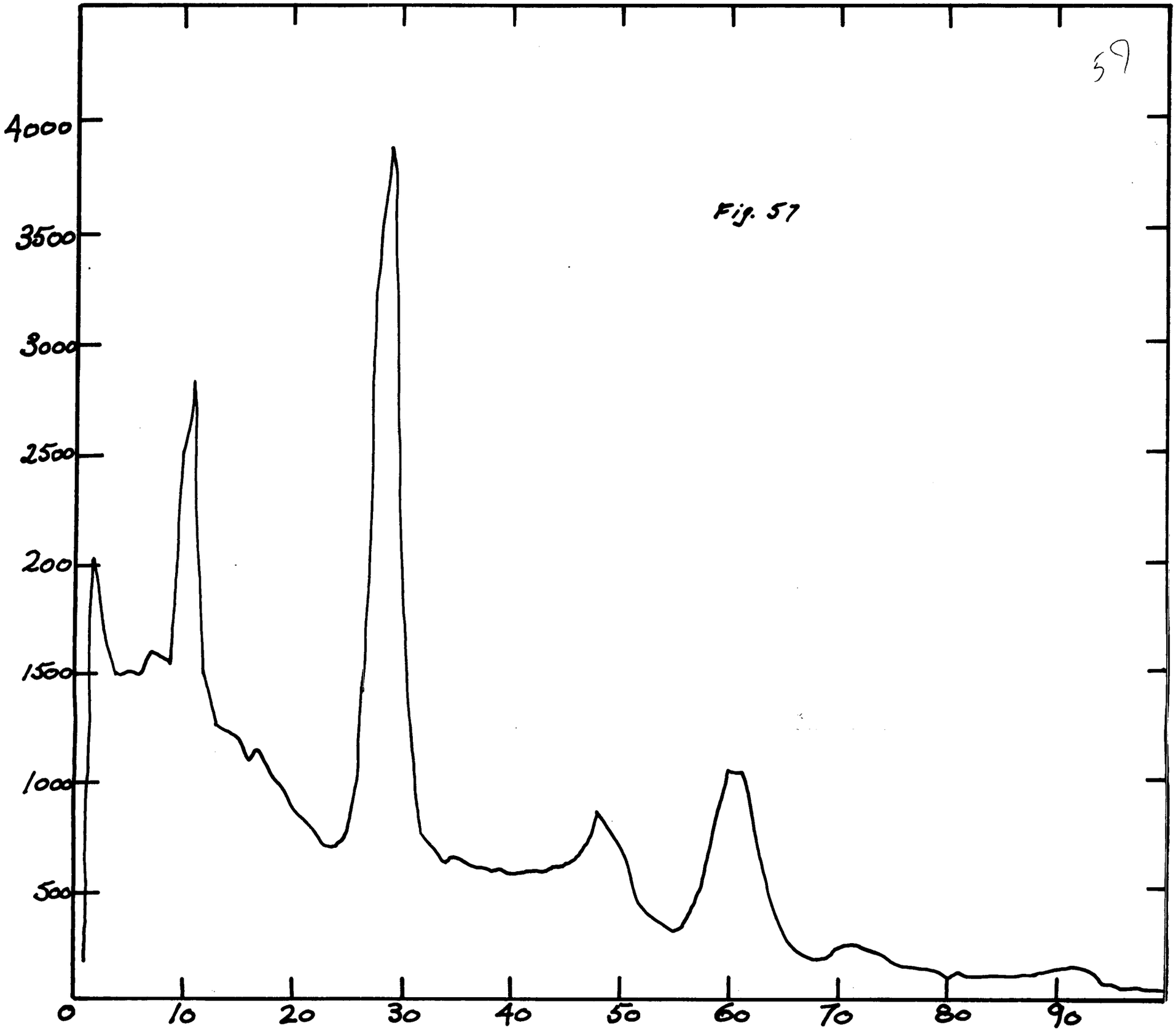

Fig. 57

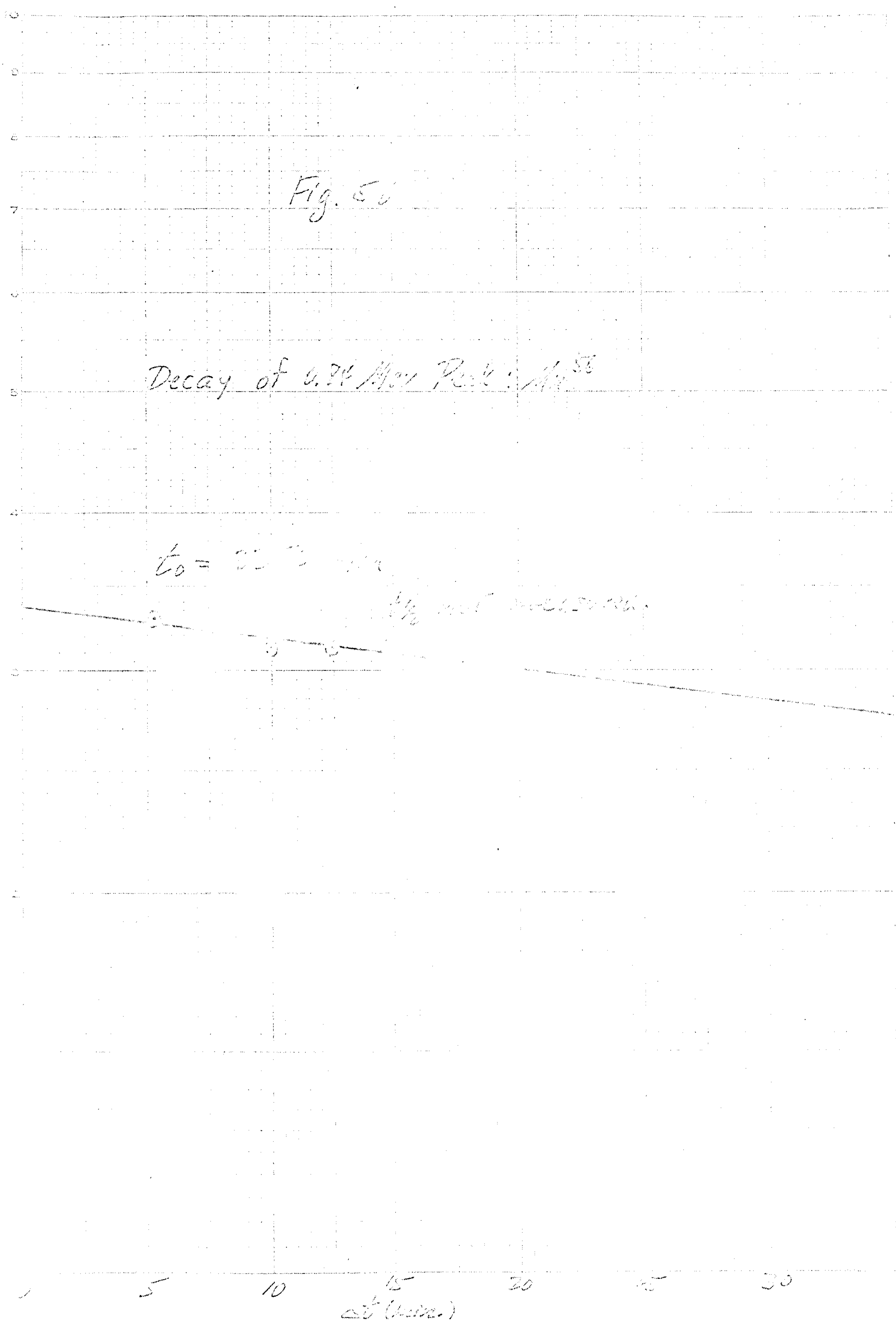
Decay of
5
10
15
20
25
30
Δt (min.)

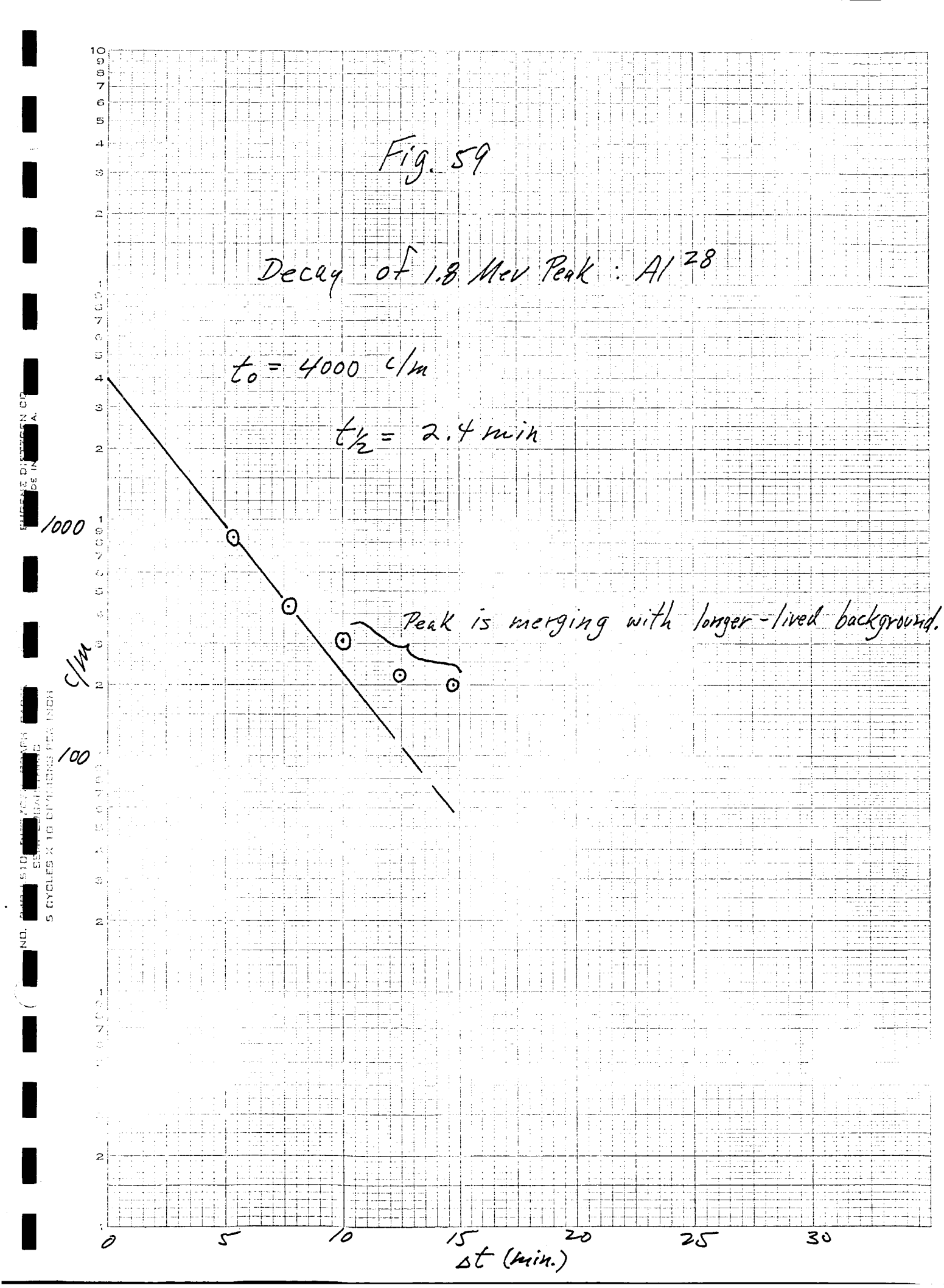
Fig. 59
Decay of 1.8 Mev Peak : Al 28
t_0 = 4000 c/m
$t_{1/2}$ = 2.4 min
Peak is merging with longer-lived background.
1000
100
c/m
0
5
10
15
20
25
30
Δt (min.)

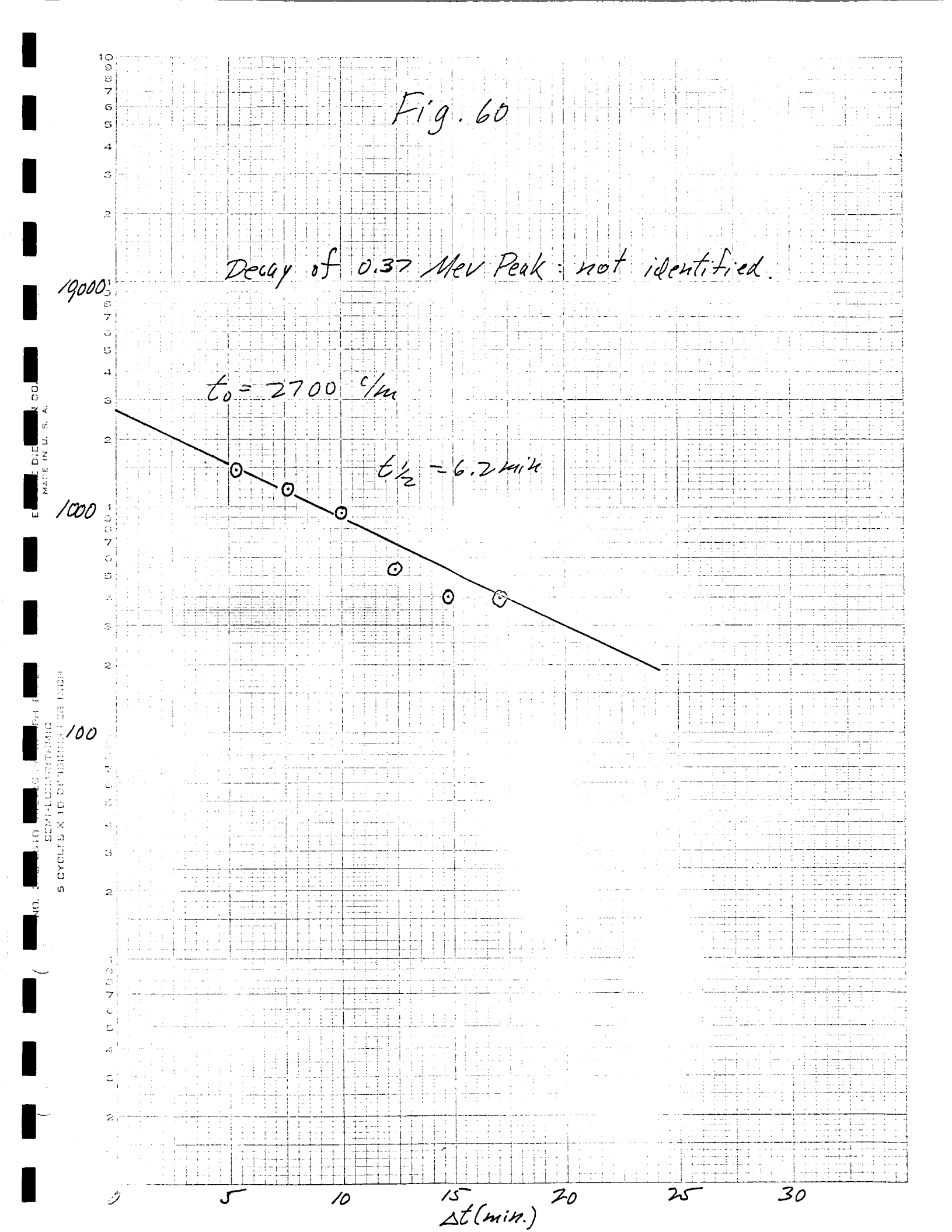
Fig. 60
Decay of 0.37 Mev Peak : not identified.
19000
t_0 = 2700 c/m
$t_{1/2}$ = 6.2 min
1000
100
5
10
15
20
25
30
Δt (min.)

Fig. 61 Spherule of unknown origin PN 4 collected in plankton net at ocean surface. Black, magnetic spherule 300 μ diam. 10 sec irradiation, one-minute count. Δt=6m30s. Identifiable peaks at 0.84 Mev channel 29 (Mn^{56}); 1.4 Mev channel 49 (V^{52}). The 1.8 Mev channel 61 peak may be Al^{28}. The 0.37 Mev channel 10 peak is unidentified.

Fig. 62 PN 4 decay curve, V^{52}

Fig. 63 PN 4 decay curve, Al^{28}(?)

Fig. 64 PN 4 decay curve, 0.37 Mev peak

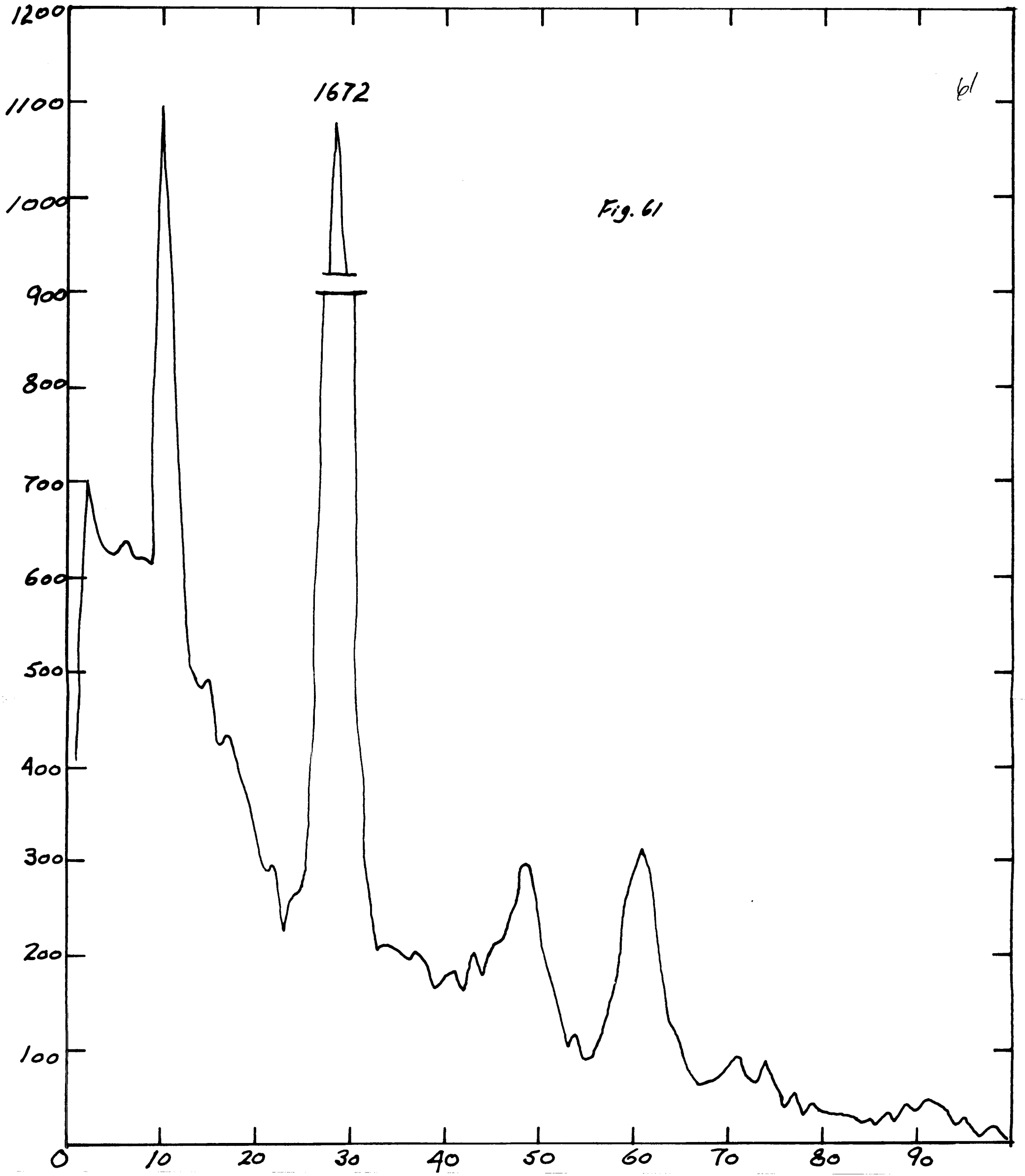
1672
1200
1100
1000
900
800
700
600
500
400
300
200
100
0
10
20
30
40
50
60
70
80
90

Fig. 61

Fig. 62

Decay of 1.4 Mev Peak : V^{52}

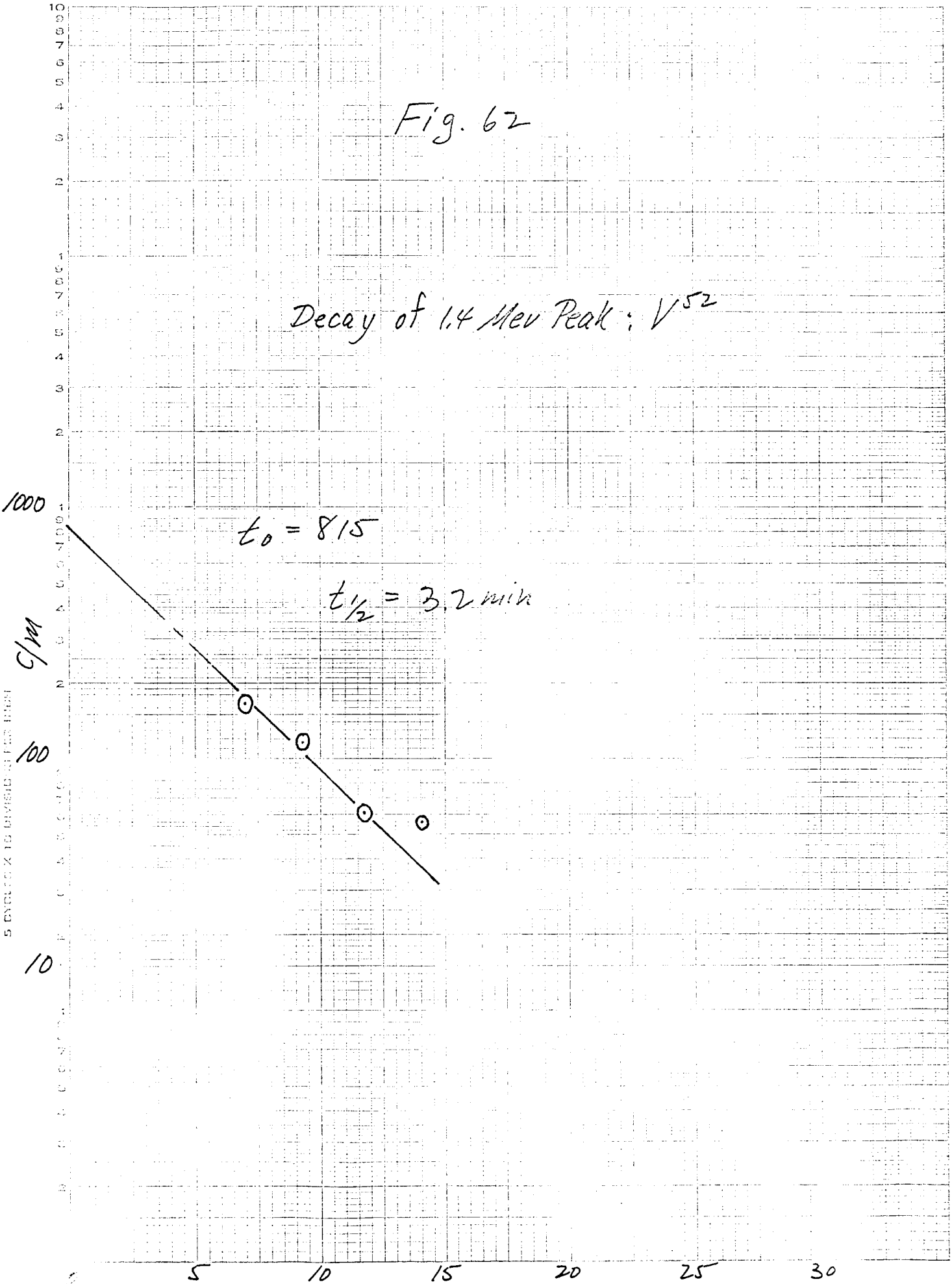

Fig. 63

Decay of 1.8 Mev Peak: Al^{28} (?)

$t_0 = 950$ c/m

$t_{1/2} = 3.4$ min (vs 2.4 min for Al^{28})

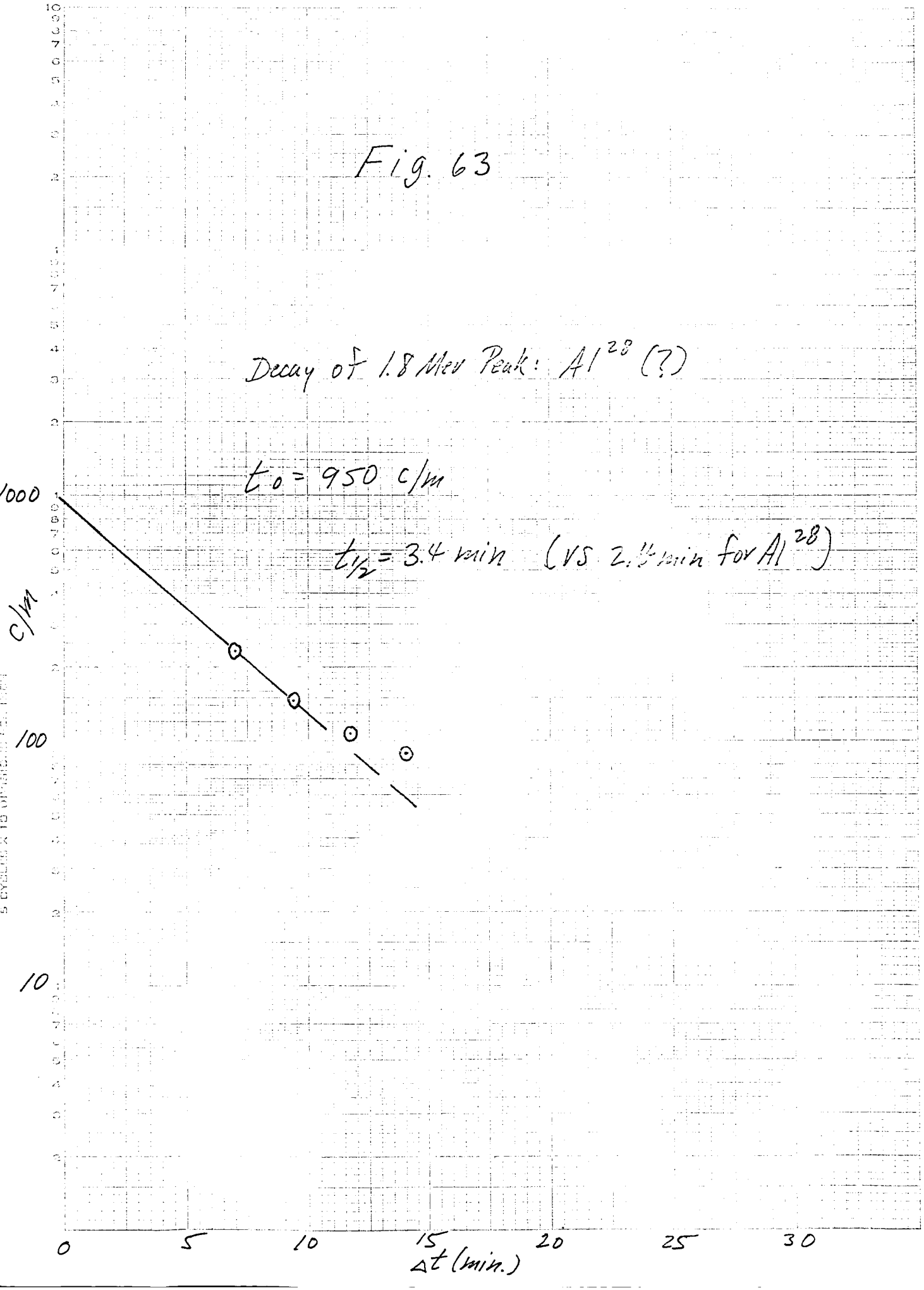

Fig. 64

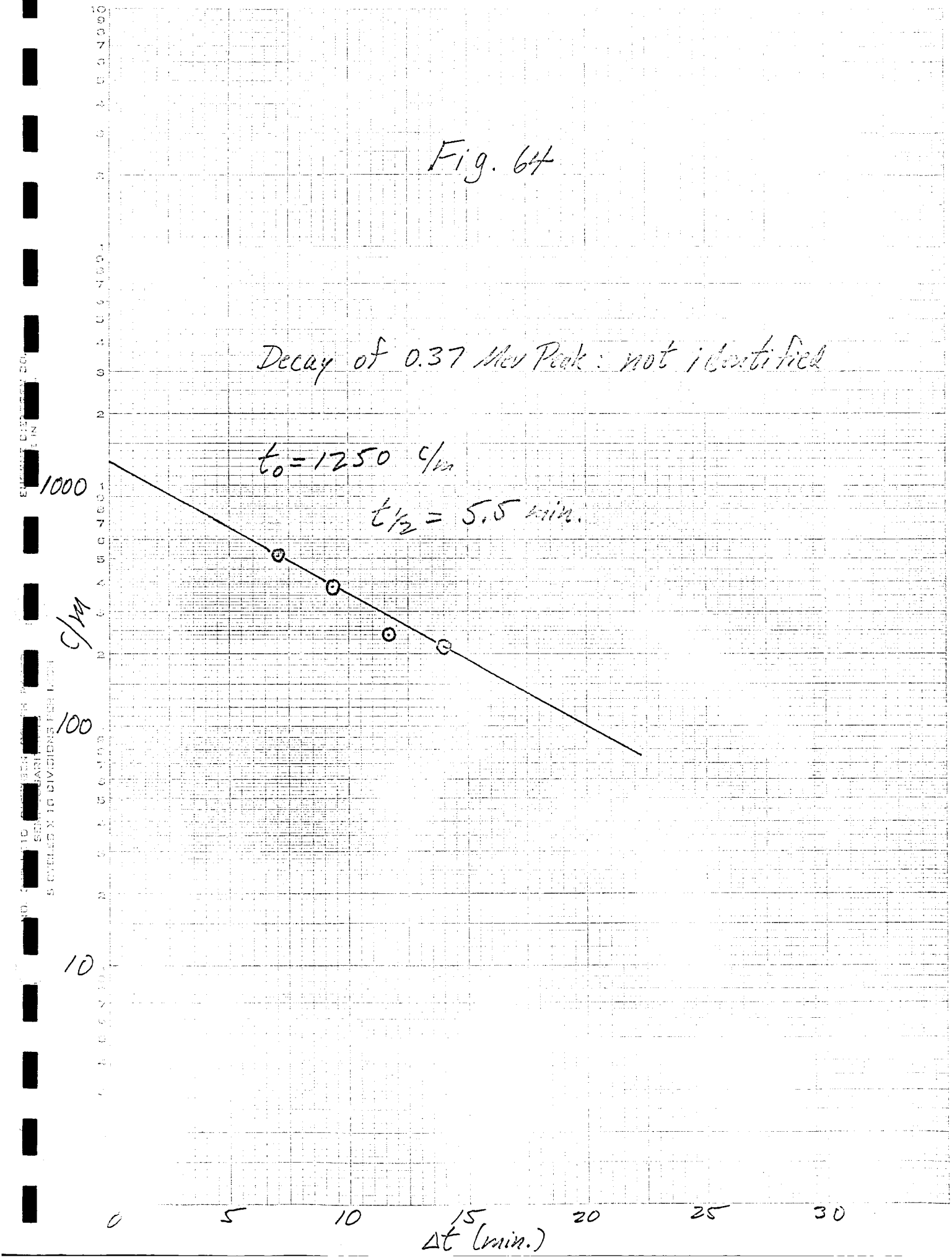
Decay of 0.37 Mev Peak : not identified
$t_0 = 1250$ c/m
$t_{1/2} = 5.5$ min.
1000
100
10
c/m
0
5
10
15
20
25
30
Δt (min.)

Fig. 65 Spherule of unknown origin PN 5 collected in plankton net at ocean surface. Shiny, black, magnetic spherule 400 μ diam. 30 sec irradiation, one-minute count. Δt approximately 6m5s. Indetifiable peaks are at 0.84 Mev channel 29 (Mn^{56}); 1.4 Mev channel 49 (V^{52}); 1.8 Mev channel 60 (Al^{28}). The peak at 0.35 Mev channel 11 is unidentified.

Fig. 66 PN 5 decay curve, Mn^{56}

Fig. 67 PN 5 decay curve, V^{52}

Fig. 68 PN 5 decay curve, Al^{28}

Fig. 69 PN 5 decay curve, 0.35 Mev peak

Fig 65

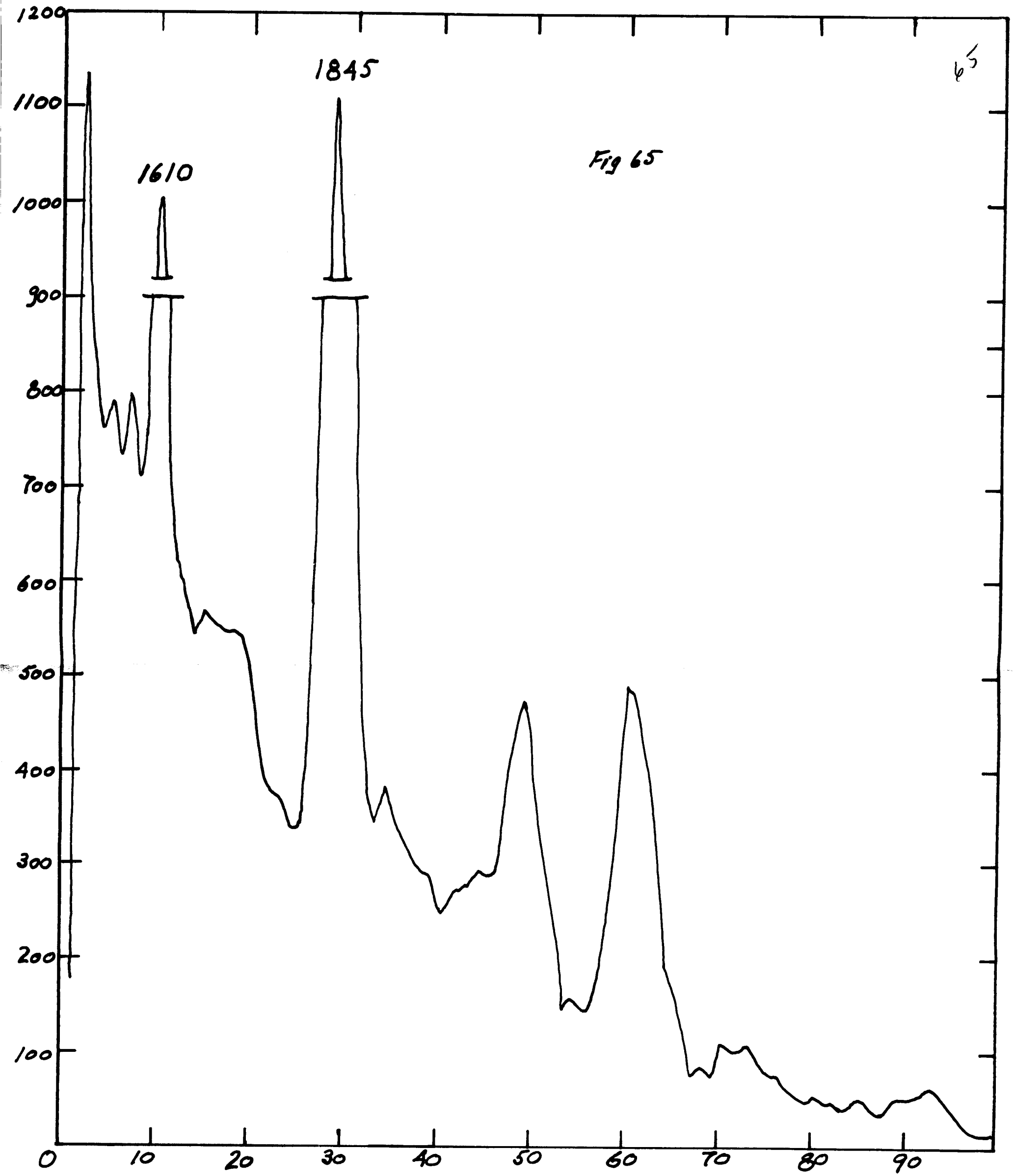
1200
1100
1000
900
800
700
600
500
400
300
200
100
1610
1845
0
10
20
30
40
50
60
70
80
90

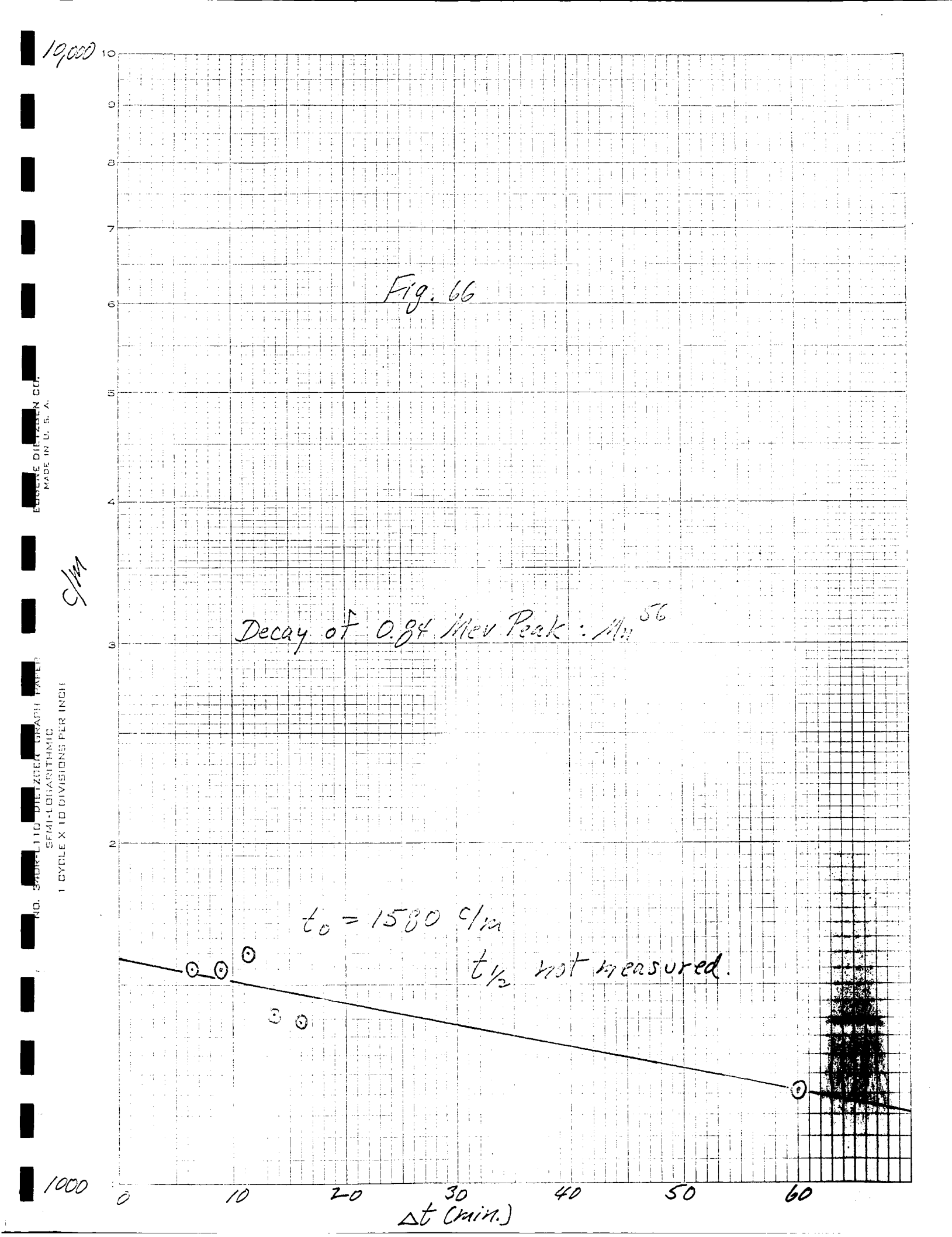
10,000
1000
c/m
Fig. 66
Decay of 0.84 Mev Peak : Mn^{56}
t_o = 1580 c/m
$t_{1/2}$ not measured.
0
10
20
30
40
50
60
Δt (min.)
EUGENE DIETZGEN CO.
MADE IN U. S. A.
NO. 340R-110 DIETZGEN GRAPH PAPER
SEMI-LOGARITHMIC
1 CYCLE X 10 DIVISIONS PER INCH

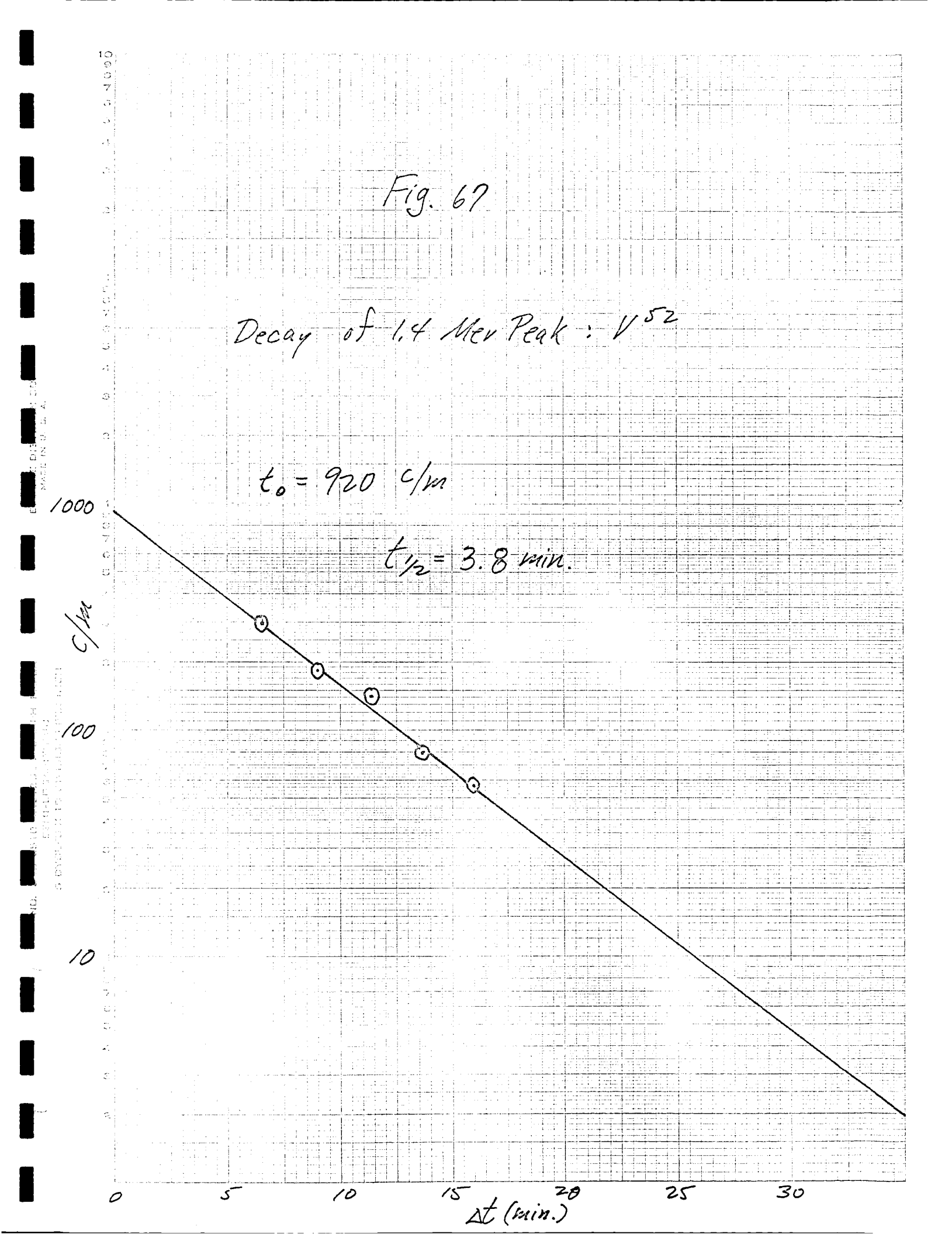
Fig. 67
Decay of 1.4 Mev Peak : V^{52}
$t_0 = 920$ c/m
$t_{1/2} = 3.8$ min.
1000
100
10
c/m
0
5
10
15
20
25
30
Δt (min.)

Fig 68

Decay of 1.8 Mev Peak : Al^{28}

$t_0 = 1700$ c/m

$t_{1/2} = 3$ min.

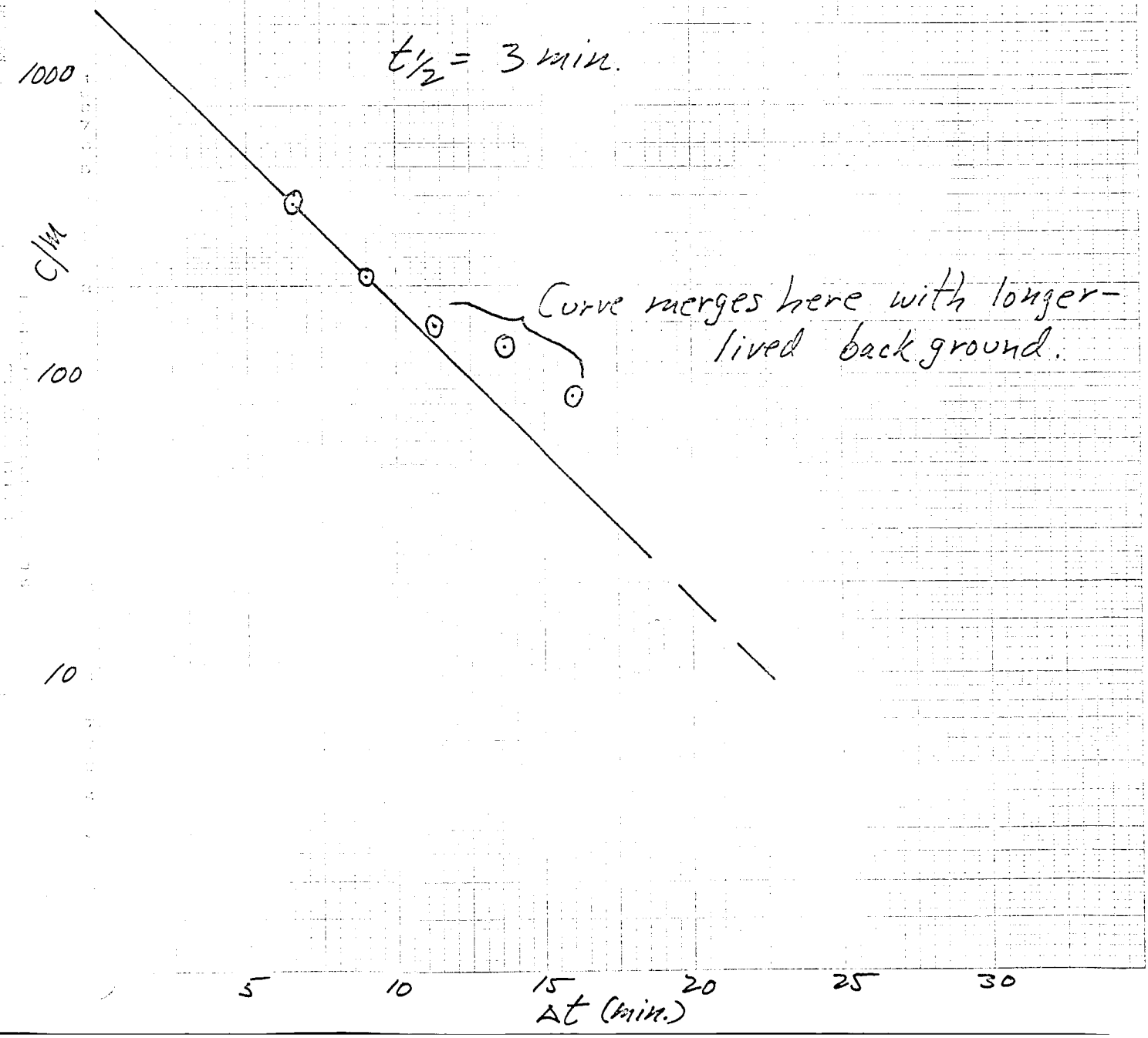

Fig. 69

Decay of 0.35 Mev Peak: not identified.

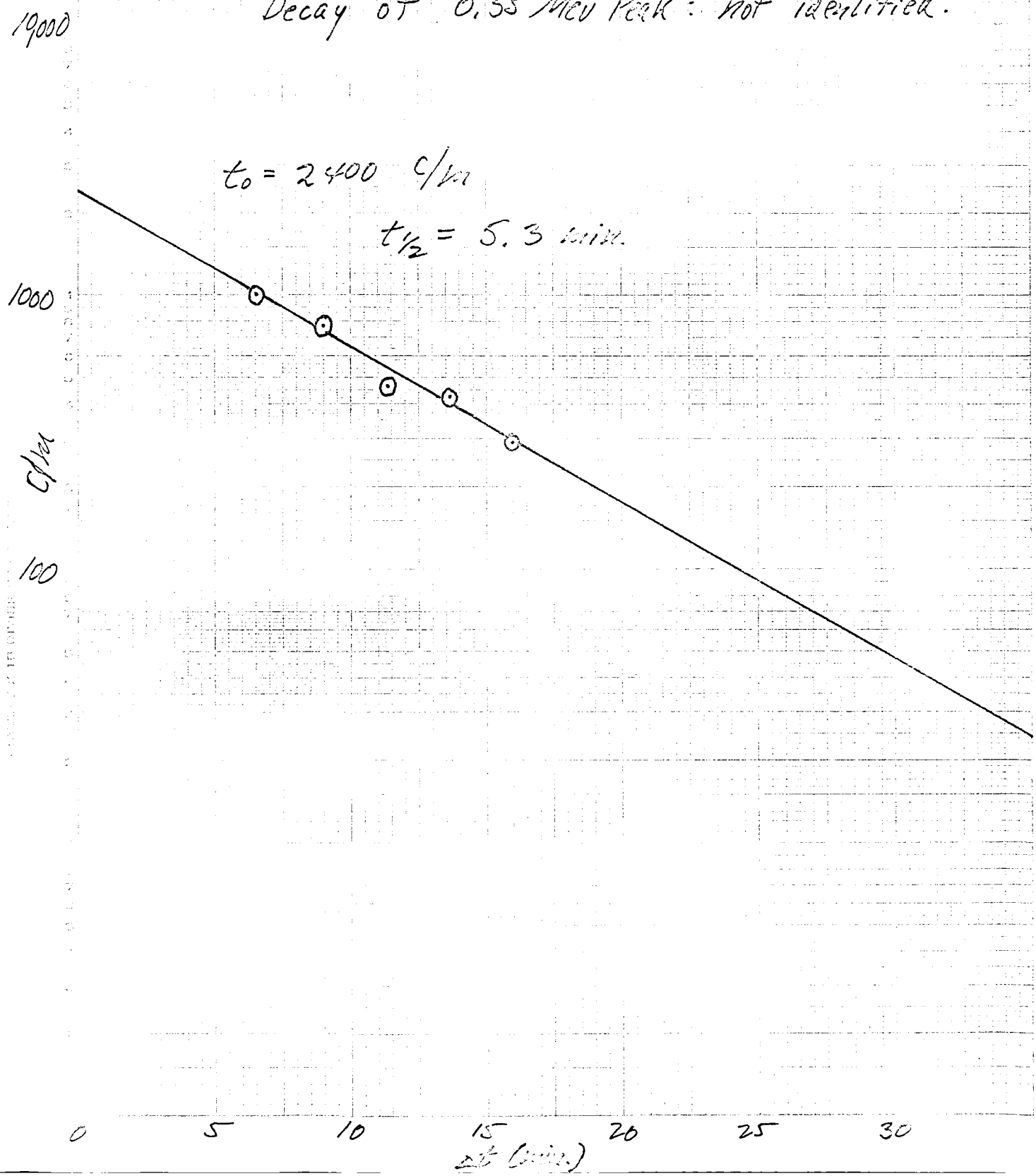

Fig. 70 Spherule of unknown origin PN 6 collected in plankton net at ocean surface. Black, shiny magnetic spherule, 360 μ diam. 10 sec irradiation, one-minute count. Δt=4m58s. Identifiable peaks are 0.84 Mev channel 29 (Mn^{56}) and 1.8 Mev channel 62 (Mn^{56}), plus two other minor Mn^{56} peaks. The peak at 1.30 Mev channel 44 may be Si^{29}, although its presence would be hard to explain in the absence of Al^{28} at 1.8 Mev.

Fig. 71 PN 6 decay curve, Mn^{56}

Fig. 72 PN 6 decay curve, Si^{29}(?)

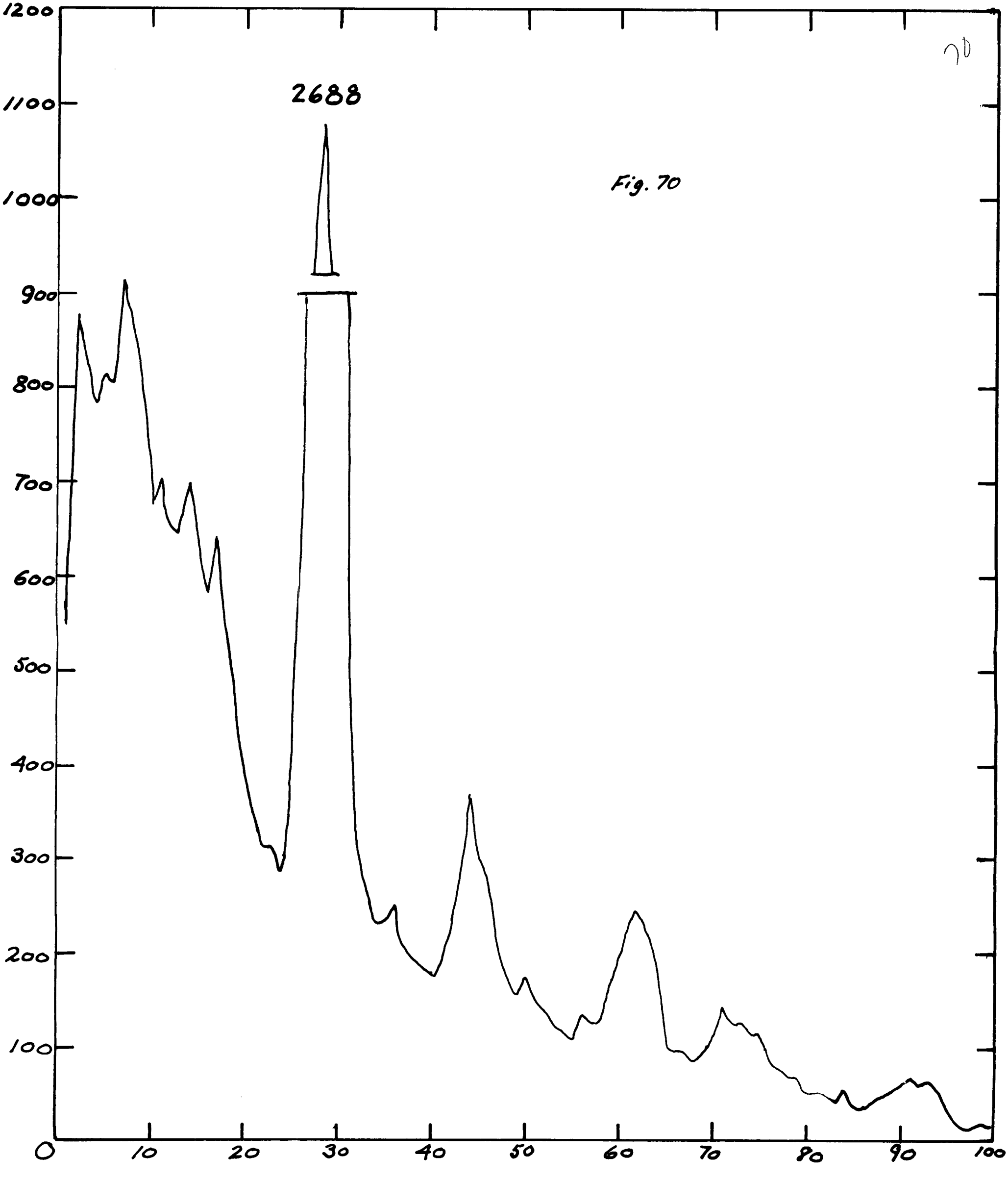
2688
1200
1100
1000
900
800
700
600
500
400
300
200
100
0
10
20
30
40
50
60
70
80
90
100

Fig. 70

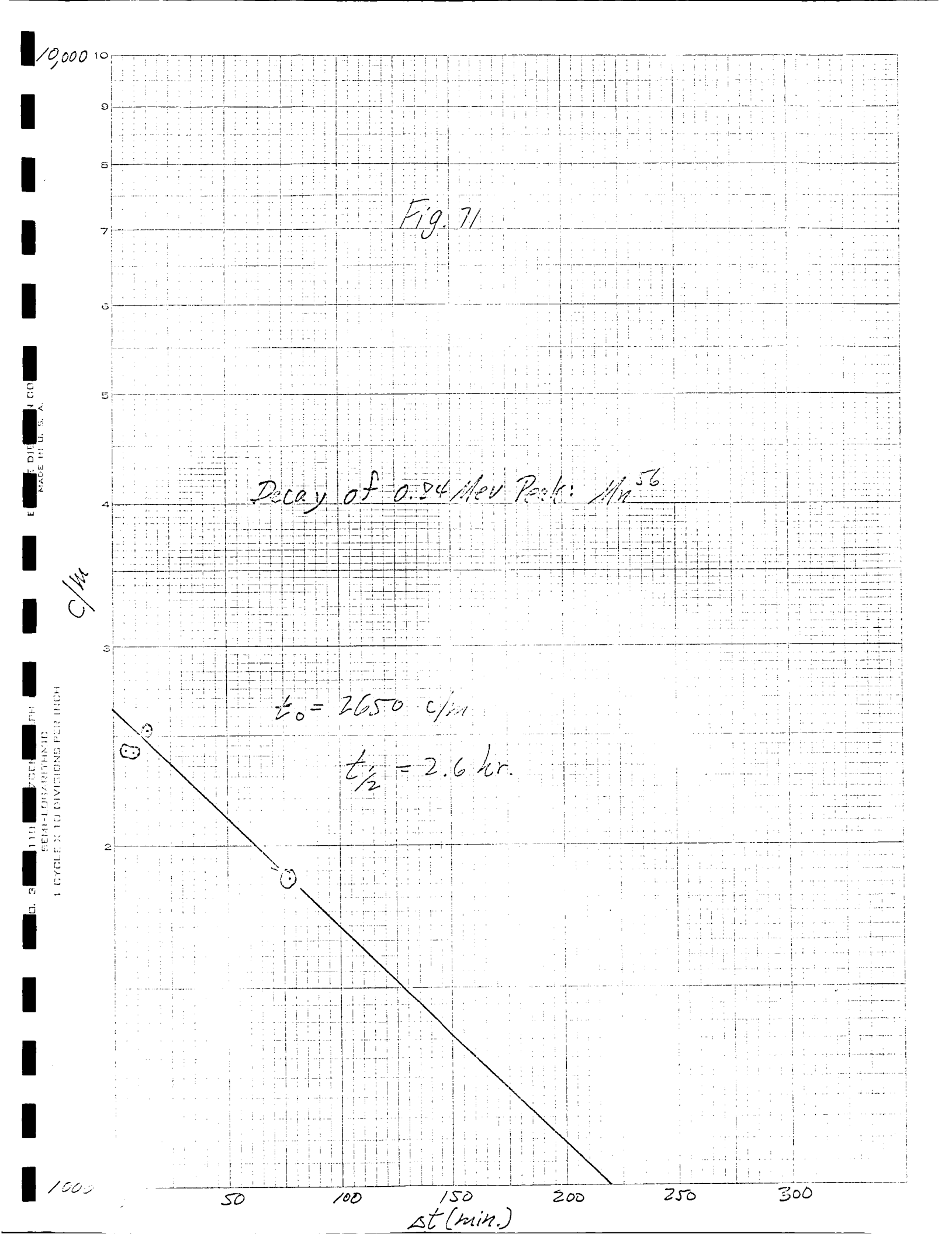
10,000
10
9
8
7
6
5
4
3
2
1000
C/m
Fig. 71
Decay of 0.84 Mev Peak: Mn 56
t_0 = 2650 c/m
$t_{1/2}$ = 2.6 hr.
50
100
150
200
250
300
Δt (min.)
SEMI-LOGARITHMIC
1 CYCLE X 10 DIVISIONS PER INCH

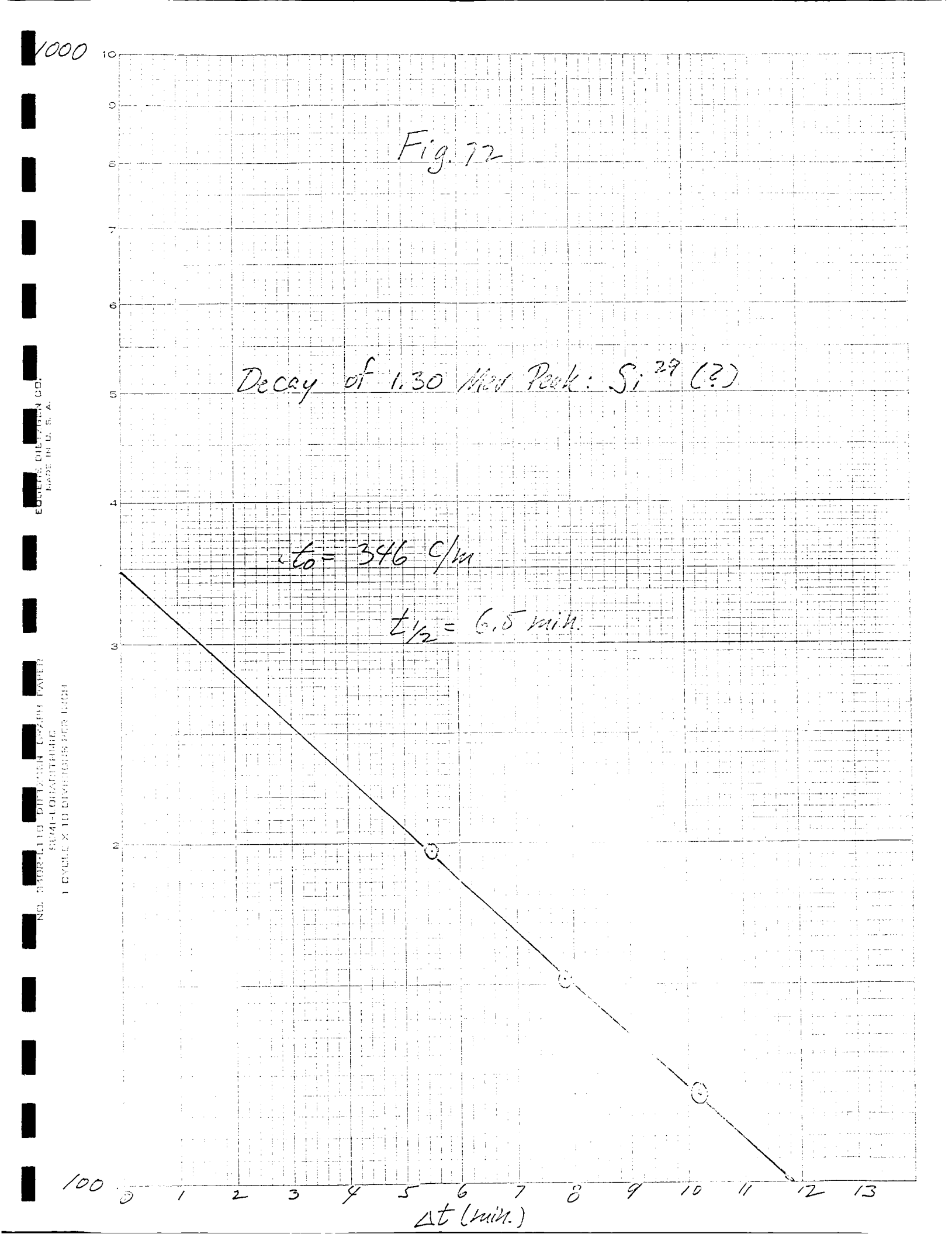
1000
Fig. 72
Decay of 1.30 Mev Peak: Si^{29} (?)
t_0 = 346 c/m
$t_{1/2}$ = 6.5 min.
100
0 1 2 3 4 5 6 7 8 9 10 11 12 13
Δt (min.)

Fig. 73 Spherule of unknown origin PN 7 collected in plankton net at ocean surface. Black, magnetic spherule 350 μ diam. 30 sec irradiation, one-minute count. Δ t=4m26s. Identifiable peaks are at 0.84 Mev channel 29 (Mn^{56}) and 1.4 Mev channel 48 (V^{52}).

Fig. 74 PN 7 decay curve, Mn^{56}

Fig. 75 PN 7 decay curve, V^{52}

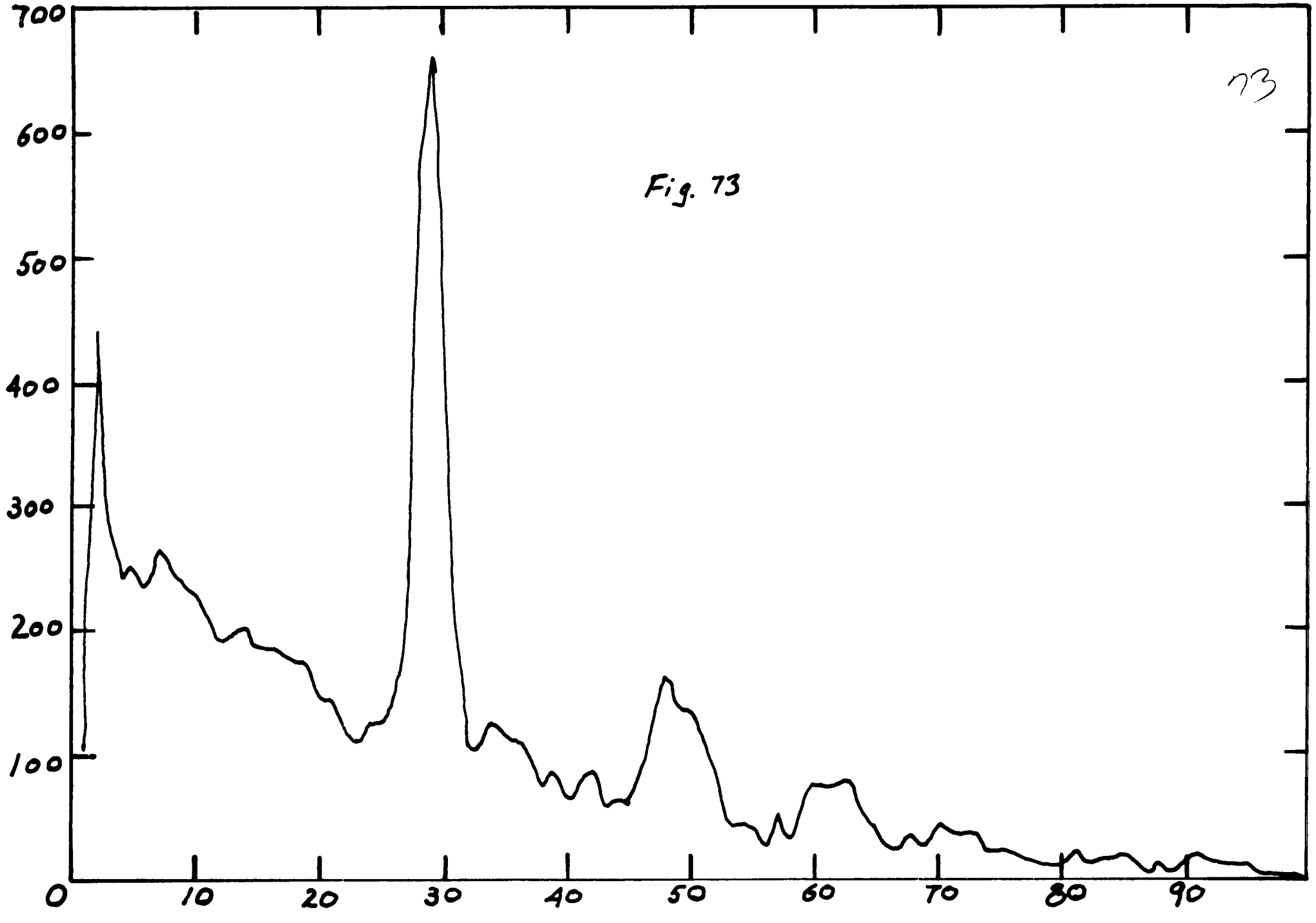

Fig. 73

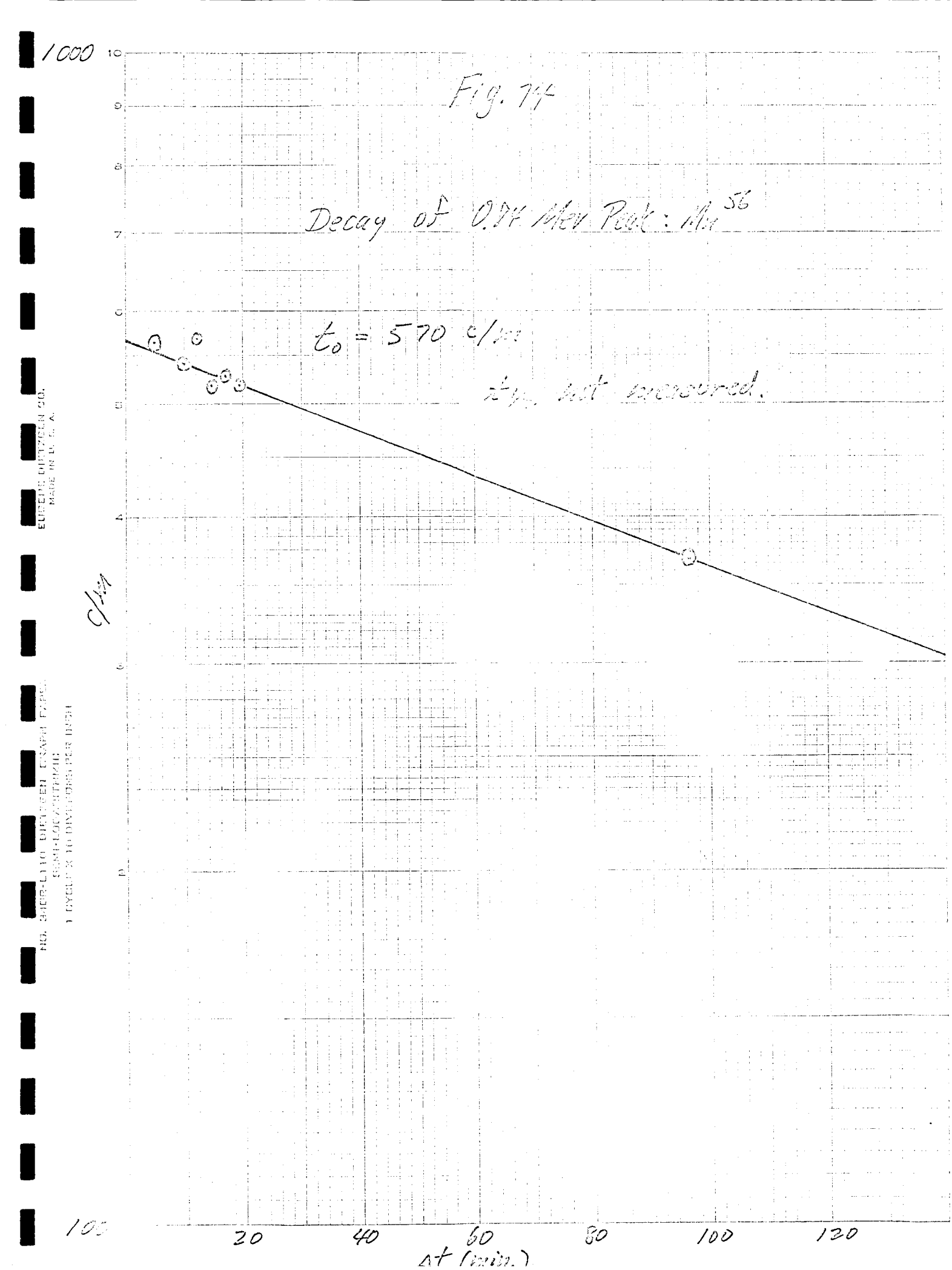
1000
10
9
8
7
6
5
4
3
2
100
Fig. 7f
Decay of 0.84 Mev Peak : Mn^{56}
t_0 = 570 c/m
$t_{\frac{1}{2}}$ not corrected.
c/m
20
40
60
80
100
120
Δt (min.)

Fig. 75

Decay of 1.4 Mev Peak : V^{52} (?)

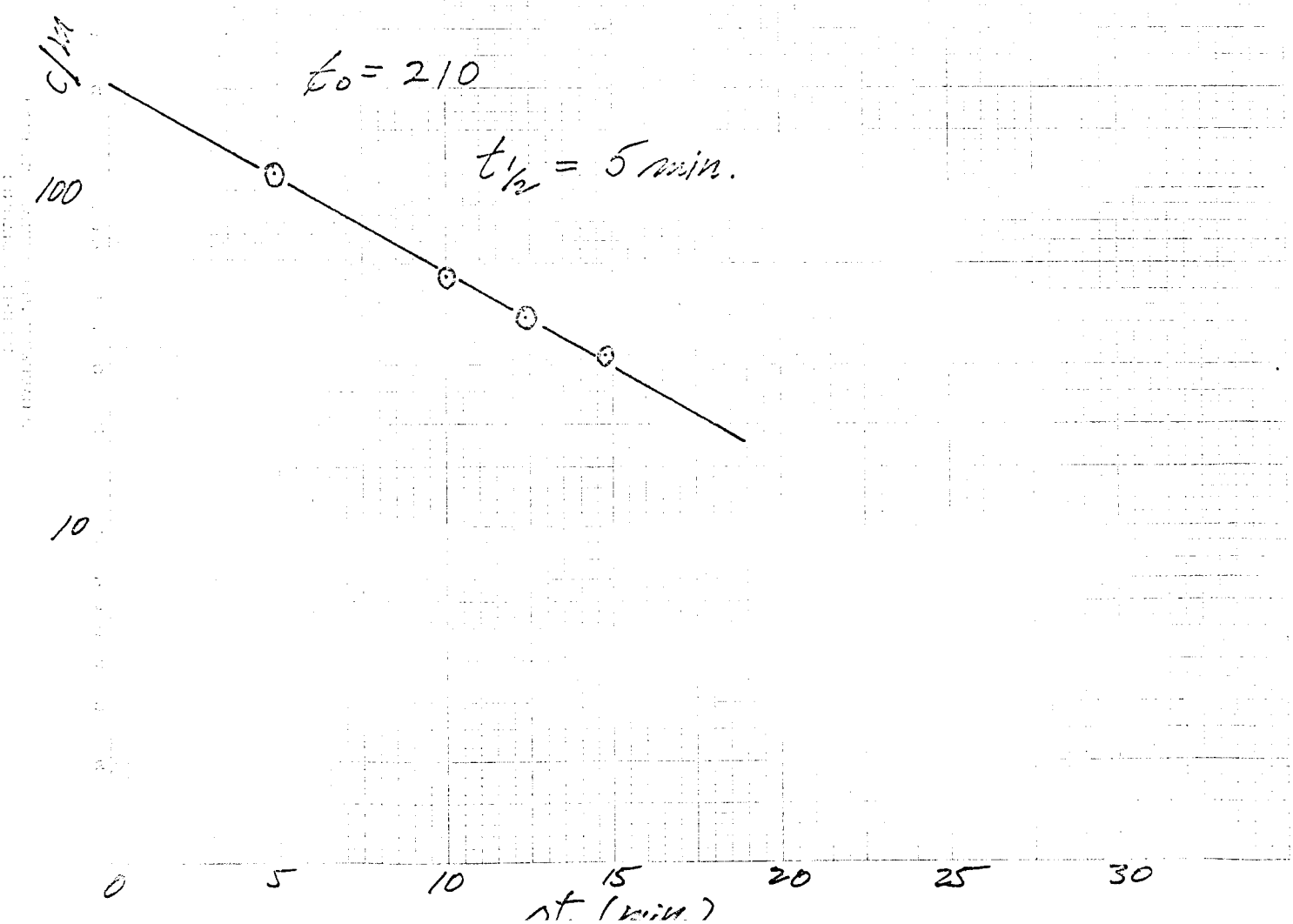

Fig. 76 Spherule of unknown origin BT 1 collected from the modern ocean floor with a Lamont biotrawl. Bright, shiny, magnetic oblate spheroid 100μ diam. 30 sec irradiation, one-minute count. Δt=7mls. Identifiable peak is at 0.84 Mev channel 29 (Mn^{56}). Two few spectra were taken to warrant plotting the decay curve of such a relatively long-lived nuclide.

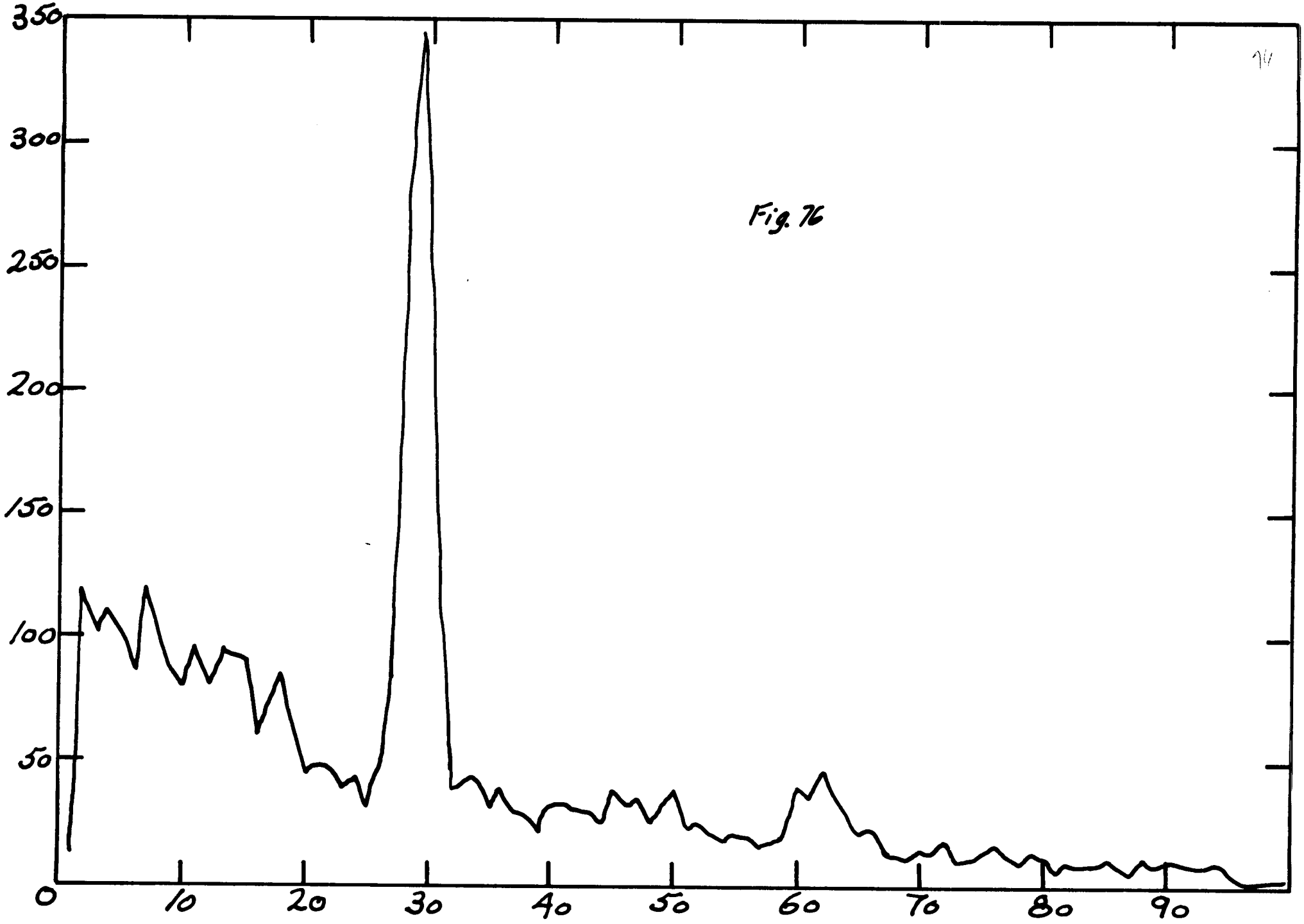

Fig. 76

Fig. 77 Spherule of unknown origin BT 2 collected on the modern ocean floor with a Lamont biotrawl. Shiny, black magnetic spherule 100 μ diam. 30 sec irradiation, one-minute count. Δ t=5m2s. Identifiable peak is at 0.84 Mev channel 29 (Mn^{56}).

Fig. 78 BT 2 decay curve, Mn^{56}

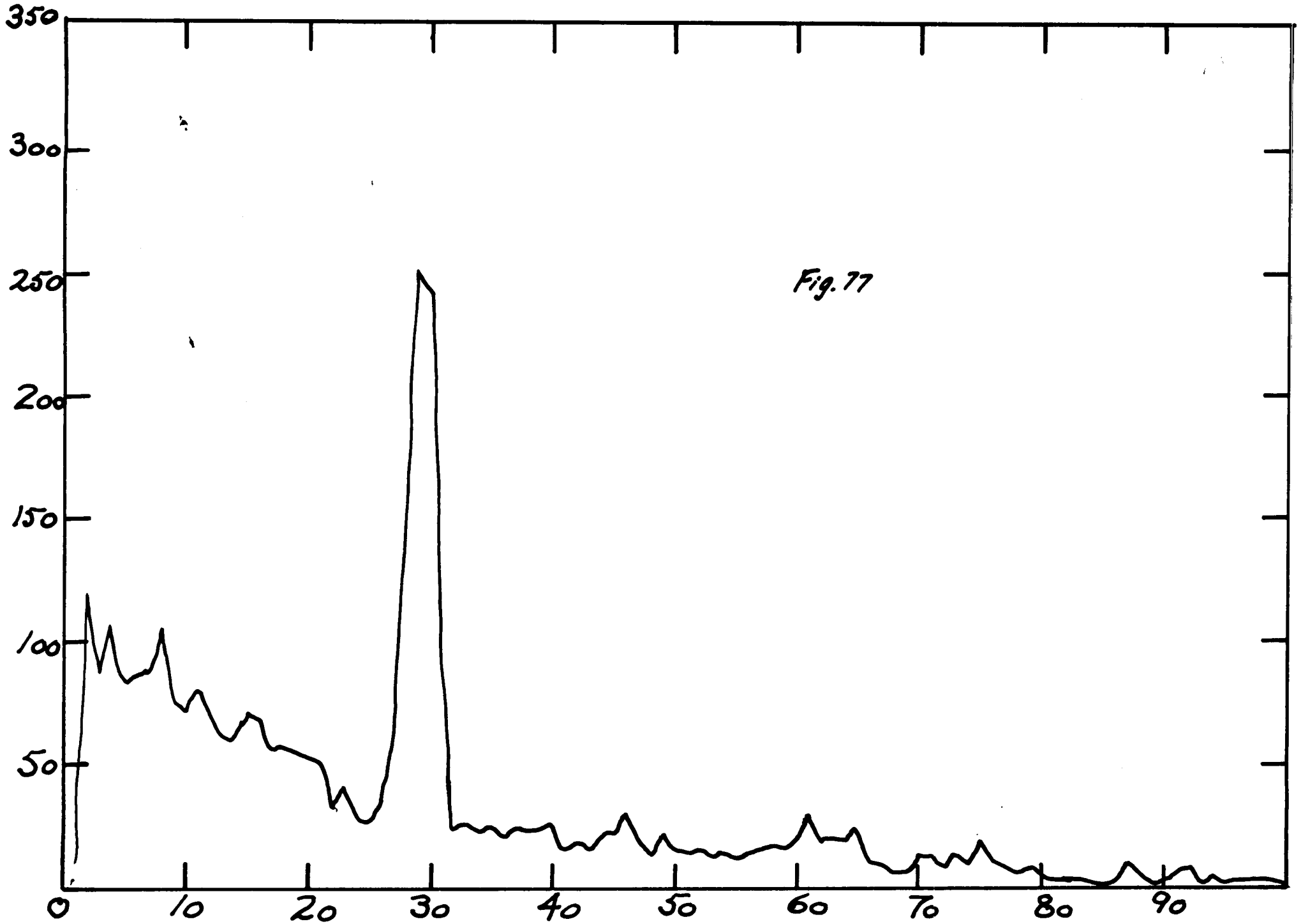

Fig. 77

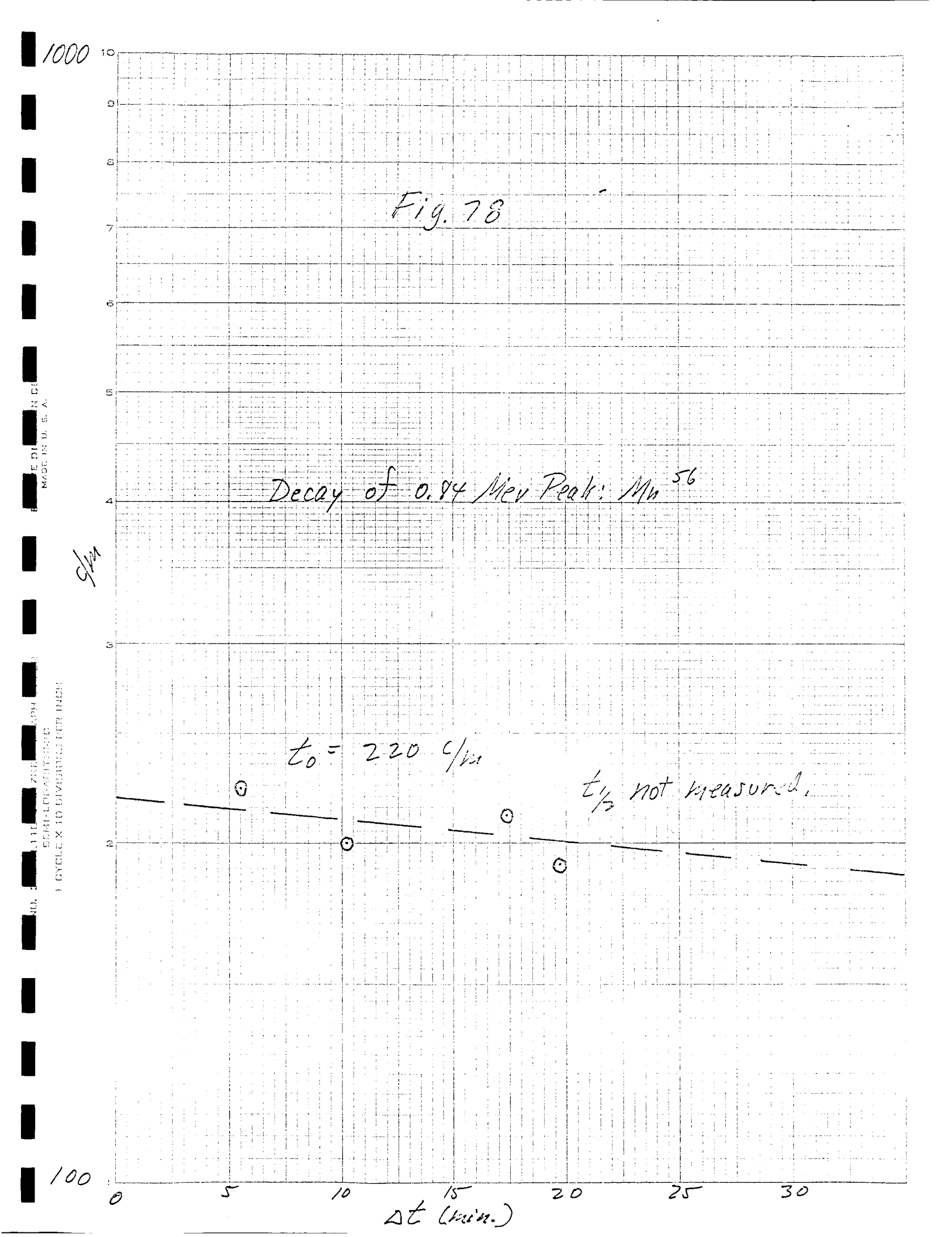
Fig. 78
Decay of 0.84 Mev Peak: Mn^{56}
t_0 = 220 c/m
$t_{1/2}$ not measured.
c/m
1000
100
10
9
8
7
6
5
4
3
2
0
5
10
15
20
25
30
Δt (min.)

Summary and Conclusions

A large majority of the natural spherules gave a very simple energy spectrum in which the only identifiable peaks were those of Mn^{56}, presumably from the reaction $Fe^{56}(n,p)\ Mn^{56}$. An example of this is the spectrum of a magnetic half-spherule 450μ in diameter recovered from flow-in muds in Lamont core V 16-79.(See fig. 25) This is a three-minute count, made in order to show better the minor peaks, which with the normal one-minute count would be less obvious. The count was made during a period after the end of irradiation ($_{\Delta}t$)=4m40s to 7m40s. Peaks are seen at channels 29, 62, 72, and 93. These correspond to gamma energies of 0.85, 1.80, 2.1, and 2.65, respectively. These peaks are the normal ones produced by decay of Mn^{56}(3), so the sample can be said to consist principally of iron (or iron oxide, since oxygen is not detectable with these procedures).

Fig. 26 shows the decay of the major peak of Mn^{56}, seen at channel 29 in Fig. 25. Plotted points represent peak heights, in counts/minute, corrected for background and block time, and plotted at the midpoints of a series of one-minute counts. The first point is plotted at the midpoint of the three-minute count shown in Fig. 8, and one-third total peak height has been plotted for this count in

order to be comparable. The curve shows an activity at the time of the end of irradiation (to) of 66,000 counts/minute, and the slope of the curve, if extrapolated to 33,000 counts/minute, gives a measured half-life ($t_{1/2}$) quite close to the known $t_{1/2}$ of 2.6 hrs. for Mn^{56}. More points, over a greater time, would be necessary before using the data in a strict quantitative sense, however.

A more interesting natural spherule, in many respects is a transparent, green, apparently glossy spherule 300μ in diameter. This nonmagnetic spherule, collected by D. Ericson from Lamont core A 153-156, is highly charged with bubbles and contains dark inclusions. This specimen received the usual thirty-second irradiation in the rabbit-tube facility and was counted periodically for one to ten minute intervals during a five-hour period after irradiation. Figures 27-34 show energy spectra obtained during decay of the induced radiation in this specimen. Figure 27 shows the gamma-decay spectrum during the interval Δt=6m15sec - 7m15sec. The prominent peak, at channel 60, is the 1.78 Mev peak of Al^{28}. Figures 28 through 30 show the further progressive decay of the Al^{28} peak with a 2.4 minute half-life (note that the scale is not the same for each figure) and the emergence from the background of two peaks at channels 28-29 and 47-48. These have energies of 0.85 and 1.35 Mev, respectively, and are the major peaks of 2.6 hour Mn^{56} and 15 hour Na^{24}.

Figures 32-34 show the faster decay of Mn^{56} relative to the longer-lived Na^{24}. Figure 32 is a five-minute count at Δt=107.5 minutes; Figures 33 and 34 are ten-minute counts at Δt=288 minutes and 422 minutes, respectively.

A refractive index determination on this spherule was very difficult because it was so highly charged with bubbles, but a tentative value of 1.486 was determined. O'Keefe (4) has pointed out that if this is the true value the spherule contains substantially more SiO_2 than a normal igneous rock, but is within the range of the most siliceous tektites. To investigate the SiO_2 content of the spherule further its spectrum and decay history can be compared with those of two other samples whose compositions are shown in Table II.

Table II (Composition in weight percent)

Sample No.	Si	Al	Fe	Mg	Ca	Na	K	O
6	34.8	6.5	3.6	1.3	1.8	1.0	1.9	49.3
11	29.0	4.8	9.7	6.5	3.0	0.7	1.0	45.2

Sample 6 is the average composition of sixty tektite analyses compiled and published by Barnes (5). Sample 11 is a less siliceous, less aluminous composition containing more iron and magnesium than Sample 6 (in other words, a more basic composition).

A series of decay spectra are given for Sample 6 in Figures 79, 80, and 81. For comparison, a spectrum of

sample 11 is given in Figure 82. Note the initial high Al^{28} peak in Figure 79. Its decay can be followed in the next figure, but in Figure 81 it has disappeared completely, leaving only the secondary peak of Mn^{56}. Repeating the same sequence it is possible to follow the emergence of the longer-lived Mn^{56} and Na^{24} peaks from the background. No scale is given, since these plots were made on an x-y plotter. Figure 79, with $_{\Delta}t$=12m28s, corresponds remarkably well to Figure 29, of the transparent green spherule, with $_{\Delta}t$=11m29s. An equally good comparison can be made between the upper curve of Figure 80, with $_{\Delta}t$=16m58s and Figure 31, of the green spherule, with $_{\Delta}t$=16m13s. Figure 81, with $_{\Delta}t$=27m35s, looks much like Figure 32, with $_{\Delta}t$=107.5m. The difference in Δt between comparable spectra is interesting: apparently the Al^{28} peak was relatively stronger in the spherule, and the high background associated with this peak obscured the Mn^{56} and Na^{24} peaks for a longer time. When they finally did emerge, however, they had the same relative height as in the earlier spectrum of Sample 6 (tektite composition). This could indicate two things: (a) relatively more Al + Si in the spherule than in the sample of tektite composition and (b) a slightly higher Fe/Mg ratio in the spherule than is the sample of tektite composition, because the 2.6-hour Mn^{56} apparently persisted for a longer time, in the spherule spectra relative to the 15-hour Na^{24} than was the case with the average tektite composition.

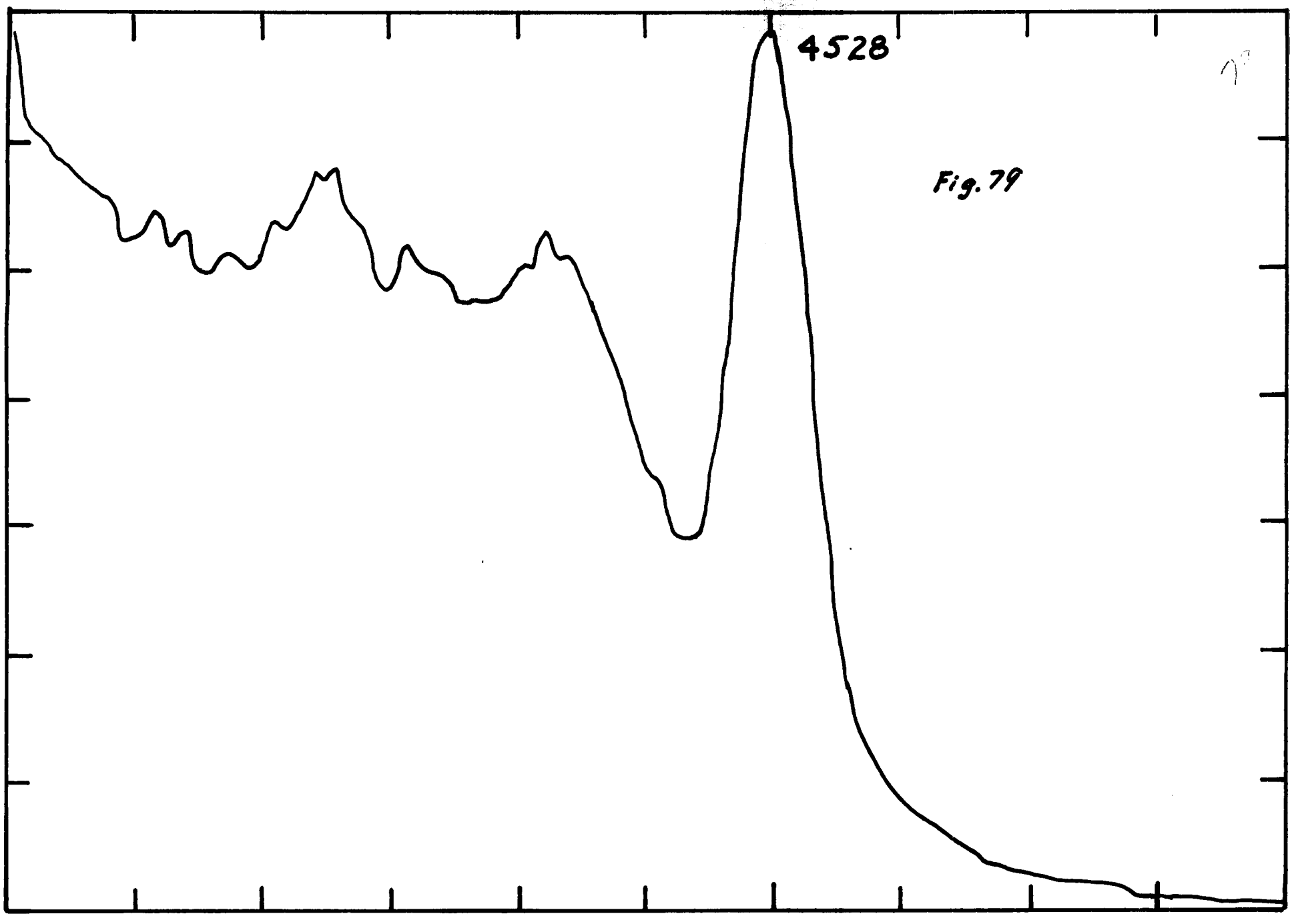

Fig. 79

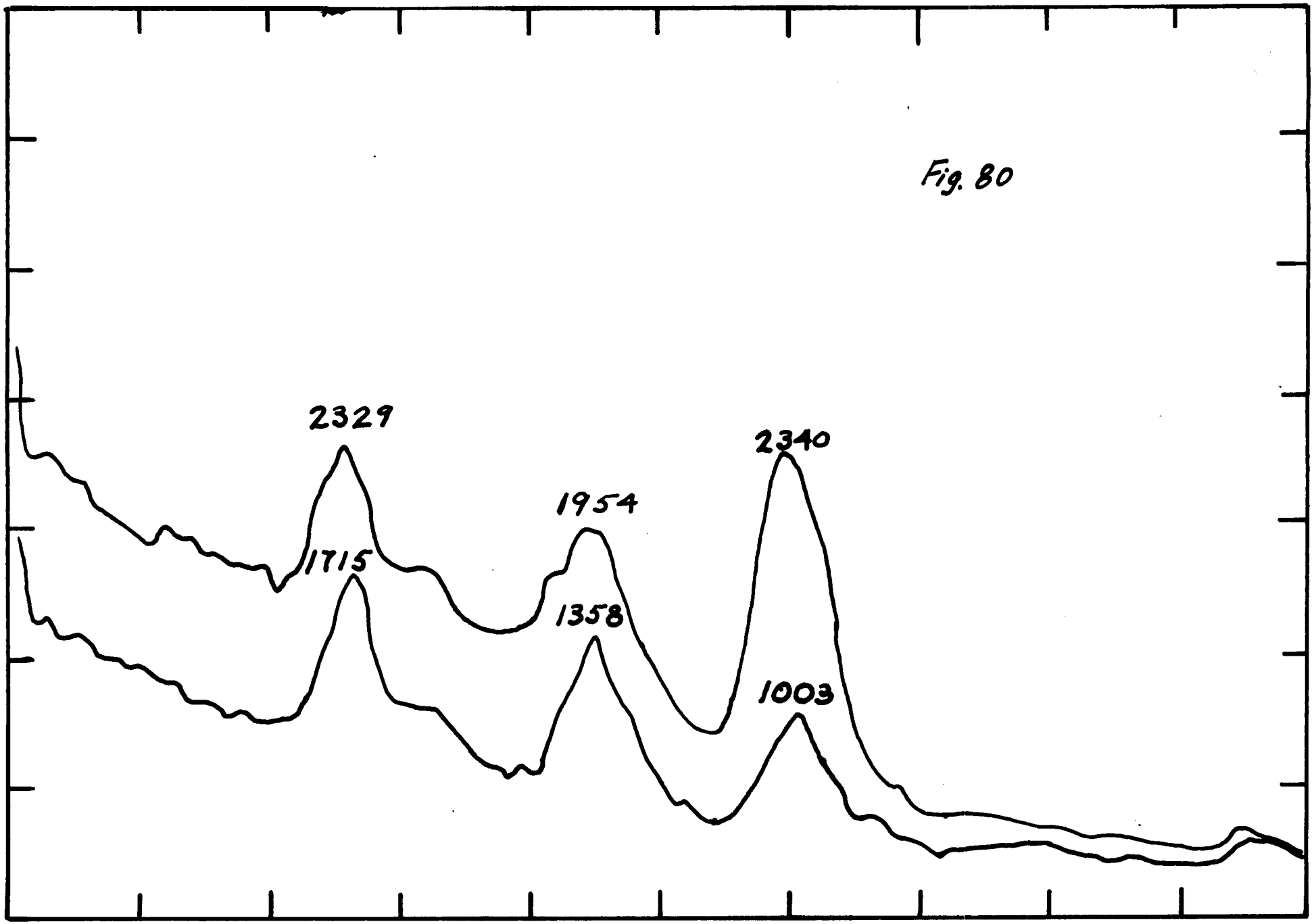

Fig. 80

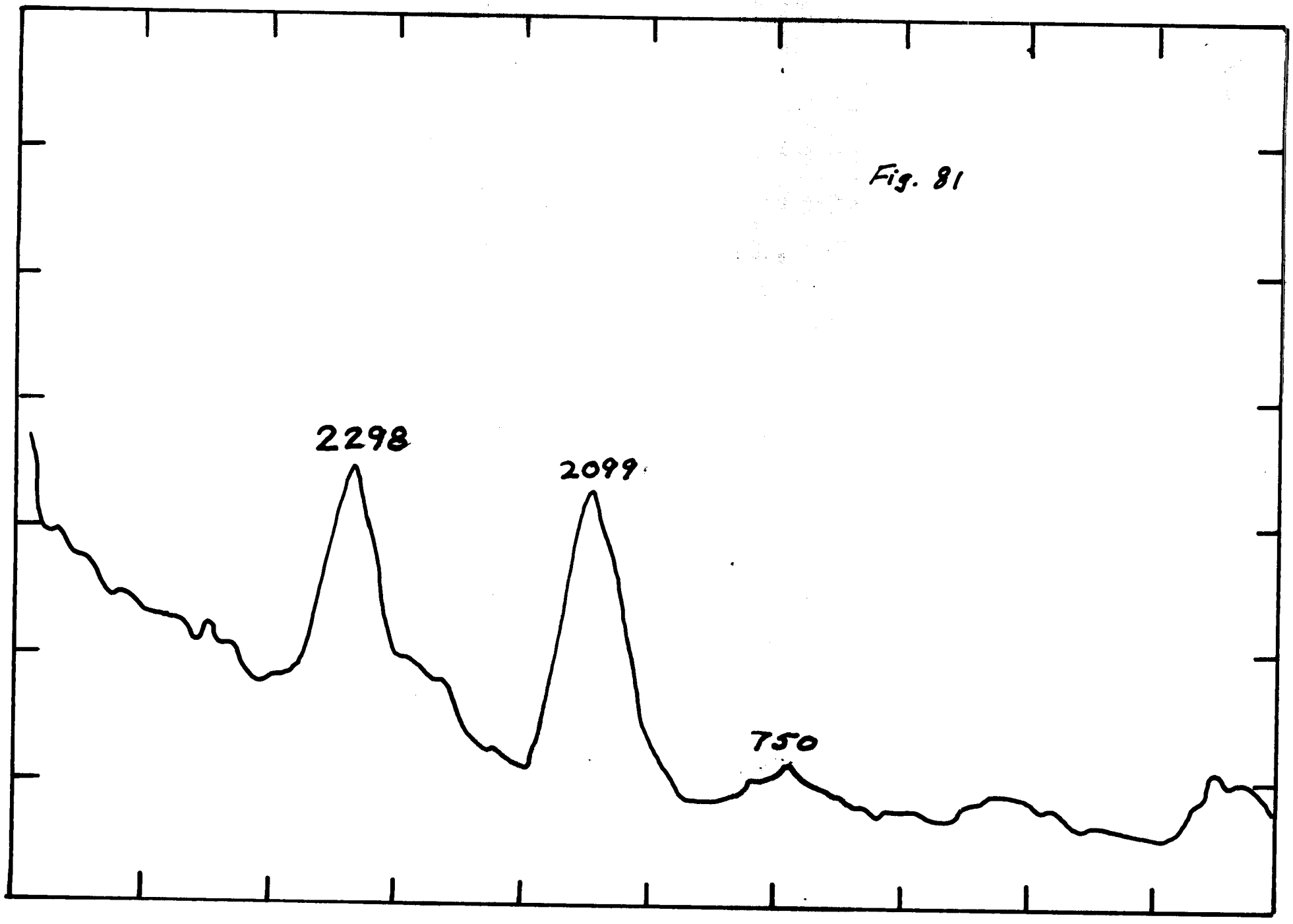

Fig. 81

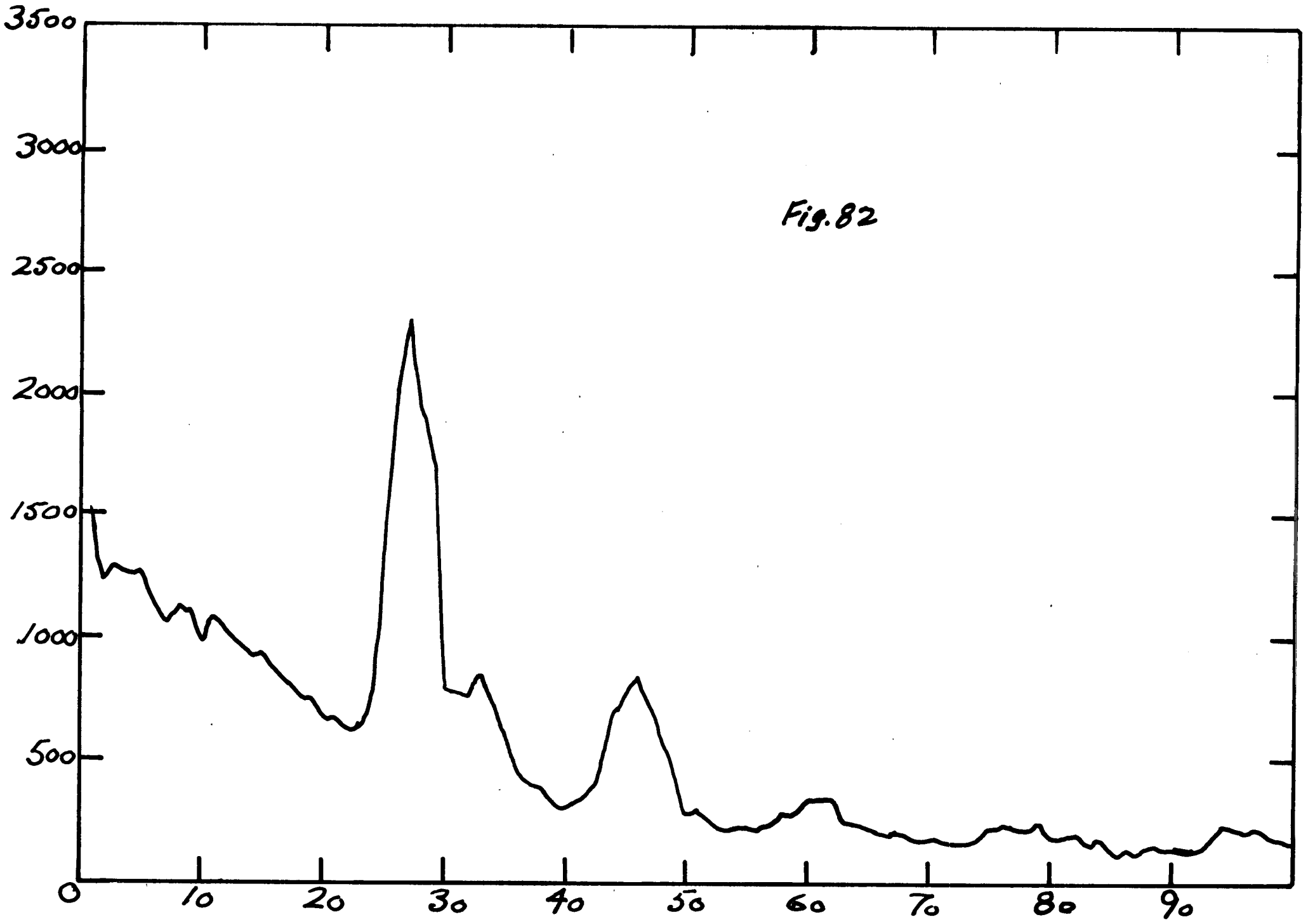

Fig. 82

Figure 82, a spectrum of Standard Sample 11, with Δt=26m36s, looks much different from any of the spectra either of average tektite or the transparent green spherule in having a much greater Mn^{56}/Na^{24} value, and therefore probably a much greater Fe/Mg value. (It should be mentioned that other spectra were taken for Sample 11, but these were only partial spectra and not useful for comparison purposes.)

It can be concluded from the foregoing that there are great similarities between the decay characteristics of a sample of average tektite composition and of the transparent green spherule. Furthermore, these spectra had demonstrable differences from the single spectrum given for the more basic composition of Standard Sample 11. Apparently, then, the green spherule has a composition similar to that of a tektite and may be even more siliceous than the average tektite. These conclusions are in agreement with the tentative refractive index determination made on the green spherule.

Concerning the problem of differentiating between different types of spherules on the basis of composition, the preceding discussion has illustrated the criteria that may be applied. That the method of nondestructive neutron-activation analysis is a useful tool is shown by the fact that the spherule still exists and can be used for other types of investigations. On the other hand, the method is

not a perfect answer to a difficult problem. Referring to the catalogue, it can be seen that most of the natural spherules gave only the Mn^{56} peaks, which suggest that they consist predominantly of iron or iron oxide. Thus, by this method there is no way to differentiate them from iron spherules of artificial origin. That such artificial spherules are common can be seen by reference to the spectra of welding beads WB 1 - WB 4 in the catalogue. Some of the welding beads had peaks other than Mn^{56}. The most prominent of these was an unidentified one around channel 11 in the spectra. Since this peak was not always present it could not be relied upon, however. This leaves a question as to whether or not the spherules collected in plankton nets (PN 1 - PN 7) and spherules collected on the modern ocean floor (BT 1 and BT 2) are natural or artificial in origin. This is an important question because the plankton nets, in particular, seem to be able to supply large numbers of the larger-sized spherules, and in addition they have no bias toward magnetic spherules.

There is a possibility of resolving the question by resorting to longer irradiations. These would produce larger fractions of the longer-lived nuclides which do not appear in noticeable amounts during a thirty-second irradiation. Several possible reactions of this

type are listed in Table III.

Table III (Data from Ross and Bailey)

Isotope Reaction	(Barns) Thermal	Fast	$t_{1/2}$	Abundance of Stable Isotope(%)	Gamma Decay(Mev)
$Cu^{63}(n,\gamma)Cu^{64}$	4.1		12.8hr	69.1	1.35
$K^{41}(n,\gamma)K^{42}$	1.17		12.47hr	6.9	1.53, 0.32
$Mo^{92}(n,\gamma)Mo^{93m}$	0.3		6.8hr	15.8	0.26, 0.68

Until this possibility can be investigated the question of natural vs artificial origin of a modern spherule will remain in doubt, and only data obtained from ancient spherules such as those from flow-in muds can be considered relevant. These data indicate that among the following five most abundant rock-forming elements, Si, Al, Fe, Mg and Na, the majority of spherules of natural origin contain only Fe. It would be of great interest in this connection to compare the analyses reported here with neutron-activation analyses of natural spherules from other sources such as volcanoes, ancient ice, and ancient terrestrial sediments. It is hoped that this will be possible in the future, and that a more complete catalogue of spherule spectra will result.

Difficulties with the nondestructive neutron-activation method have been mentioned earlier. One of these is the coincidence of peaks from different nuclides, such as that

of the primary peak of Al^{28} and the secondary peak of Mn^{56}, which both occur around 1.80 Mev. In most such cases the results obtained have not suffered from this difficulty because the coincident peaks have different half-lives, and the method of successive short-period counting used in this work has shown clearly which part of the decay curve was due to each peak.

The other main difficulty is the production of the same daughter nuclide from two different parent nuclides. An example of this is the production of Al^{28} from both Si^{28} and Al^{27} (See Table I). In such cases it is hoped that advantage can be taken of the fact that the Si^{28} reaction is produced by fast neutrons and the Al^{27} reaction by thermal neutrons. Three methods have been tried to obtain irradiation-energy spectra of limited range in order to favor one of the converging reactions over the other. The first method tried was irradiation in the thermal column, under conditions where the fast-neutron flux was extremely diffuse. In this work the samples were irradiated four feet inside the reactor face, where even the thermal-neutron flux density was rather low. Due to small sample size only negligible activity was obtained, even after thirty-minute irradiations. Recently this facility has been redesigned and changed to permit easier access to positions in the

thermal column closer to the core, and future work may show better results.

The second method tried was shielding from thermal neutrons by surrounding the sample with Cadmium sheet .064" thick. This produced a reduction in total flux sensity to a point where the small sample size became critical. It is possible, however, that the method would work better if the shielded sample were irradiated in a vertical tube inside the core, instead of in the rabbit tube outside the core. This should be tried in future work.

The third method tried was irradiation of the sample in the vertical tube facility at varying distances from the core, so that the sample received varying relative amounts of moderated neutrons and fast neutrons. In this survey the goal was to find effective threshold distances from the core beyond which a particular fast-neutron reaction became unimportant. The mass of data obtained in this survey has not yet been completely reduced, but this may be the most promising method yet tried.

A summary of results of these methods will be presented in the next report, which will also contain a series of photographs of the spherules analyzed, with some photographs of polished sections.

A paper titled "Nondestructive Neutron-Activation Analysis of Microscopic Spherules," based on this work, will be presented at the forthcoming Conference on Cosmic Dust to be held November 21 and 22, 1963. This Conference is being sponsored by the New York Academy of Sciences, and is being organized by the author of this report, who will be conference chairman.

Some of the spherules collected in the course of this NASA-sponsored project have been sent to Professor R. Castaing for analysis with his newly developed secondary ion-emission mass spectrograph. If his results are available in time they will be reported at the Conference on Cosmic Dust.

This is the first report in depth to be submitted on the present NASA-sponsored work, but it is felt that its value is greater than if reports of completed research had been presented in small increments. In its present form, a good perspective on the problem can be gained.

Grateful acknowledgement to the National Aeronautics and Space Administration is given here for the opportunity to pursue this line of investigation to its present stage of development.

Respectfully submitted,

William A. Cassidy
(Principal Investigatpr)

WAC:vgj

Reference List

(1) Ross, D. A. & R. F. Bailey. 1960. Neutron Activation Chart. R.C.A. Pub. Princeton, N.J.

(2) No author. Reaction cross sections for 14-mev neutrons. compilation by AEC Neutron Cross Section Advisory Group, U.S. Atomic Energy Commission Document AECU - 2040 and its first three supplements.

(3) Heath, R. L. 1957. Scintillation Spectrometry Gamma-Ray Spectrum Catalogue. Office of Technical Services, U.S. Dept. of Commerce. Washington, D.C.

(4) O'Keefe, J. A. 1963. personal communication.

(5) Barnes, V. E. 1939. Univ. Tex. Pub: 3945, 525-32.